UNIVERSITY OF CAPE COAST

INVESTIGATION OF THERMOELECTRIC PROPERTIES OF GRAPHENE SUPERLATTICE

FESTUS NONGNENUOR

2023

UNIVERSITY OF CAPE COAST

INVESTIGATION OF THERMOELECTRIC PROPERTIES OF GRAPHENE SUPERLATTICE

BY

FESTUS NONGNENUOR

Thesis submitted to the Department of Physics of the School of Physical Sciences, College of Agriculture and Natural Sciences, University of Cape Coast, in partial fulfillment of the requirements for the award of Master of Philosophy degree in Physics

JANUARY 2023

DECLARATION

Candidate's Declaration

I hereby declare that this thesis is the result of my own original research and that no part of it has been presented for another degree in this university or elsewhere.

Candidate's Signature:…….. Date:…….

Name: Festus Nongnenuor

Supervisor's Declaration

I hereby declare that the preparation and presentation of the thesis were supervised in accordance with guidelines on supervision of thesis laid down by the University of Cape Coast.

Supervisor's Signature:…….. Date:…….…….

Name: Prof. Raymond Edziah

ABSTRACT

Graphene and its derivatives have attracted significant attention due to their unique electronic, thermal, and mechanical properties which make it a promising material for device applications. This work theoretically investigated the thermoelectric properties of graphene superlattice which was subjected to a combined direct and alternative field. This was done by solving the Boltzmann's kinetic equation within the semiclassical regime with the energy dispersion relation of graphene superlattice obtained using tight-binding approximation. The expressions for the resistivity, thermo-power as well as thermoelectric power factor of this novel material were derived analytical as a function of temperature, material parameters, and amplitudes of the external applied field. The findings suggest that graphene superlattice exhibits a metallic property, and as expected, its resistivity generally rises with temperature. Due to its low resistivity and high figure of merit at room temperature, graphene superlattice could be served as a suitable material for thermoelectric device applications.

KEYWORDS

Boltzmann transport equation

Figure of Merit

Graphene

Superlattice

Thermoelectrical Materials

Thermoelectricity

ACKNOWLEDGEMENTS

First and foremost, I am most grateful to God Almighty for his endless protection and mercies through my life. I would like to express my profound gratitude to Prof. (Mrs.) Alfredina Zepto Penn Kuupole for her advice, counseling, encouragement, and financial support for my education.

Special thanks go to my supervisor, Prof. Raymond Edziah, who has been a father and a mentor and whose support, guidance, and encouragement enable me to finish this thesis on time. This thesis would not have been feasible without his guidance, patience, and meticulous proofreading. Not forgotten Dr. Samuel Sonko Sackey whose advice and support have brought me this far. I would also want to take this opportunity to thank the Department Head and all lecturers in the Department of Physics for their support and guidance throughout my time at this university.

Last but not least, I would want to convey my profound appreciation to my family, especially Rev. Fr. Nicodemus Nongnenuor, for their unending prayers, support, and love. Final thanks go to each and every one who supported me in diverse ways. God bless you all.

DEDICATION

To my belove mother Hellen Nongnenuor

TABLE OF CONTENTS

LIST OF FIGURES

LIST OF PHYSICAL CONSTANTS

Boltzmann's constant	$k_B = 8.617 \times 10^{-5}$ eVK^{-1}
Carrier concentration	$n_o = 10^{12}$ cm^{-3}
Electronic charge	$e = 1.6 \times 10^{-19}$ J
Frequency	$\omega = 10^{12}$ s^{-1}
Graphene sheet width	$a_o = 0.345$ n m
Planck's constant	$\hbar = 6582 \times 10^{-16}$ eVs
Relaxation time	$\tau = 10^{-12}$ s

LIST OF ABBREVIATIONS

1D	One-Dimensional
2D	Two-Dimensional
3D	Three-Dimensional
ac	Alternative Current
BTE	Boltzmann Transport Equation
BZ	Brillouin Zone
CVD	Chemical Vapor Deposition
dc	Direct Current
GSL	Graphene Superlattice
h-BN	Hexagonal Boron Nitrate
PLV	Pulsed Laser Vaporization
SL	Superlattice
SiO_2	Silicon Dioxide
T	Temperature
TE	Thermoelectric
ZT	Normalized Figure of Merit

CHAPTER ONE

INTRODUCTION

Energy crisis and heat management are the two major problems in this twenty-first century. The ability to manage waste heat is a major challenge, which currently impedes the performance of information technology devices. The need to use energy resources more efficiently has become a critical concern on a worldwide scale. To solve this problem, there is a need to develop new materials and devices, innovative device architectures, and smart integration techniques, coupled with new strategies for managing and recycling on-chip waste heat. Researchers and industry are devoting significant time and their resources to finding solutions to this increasing energy crisis as well as the threat of global warming. One approach to addressing these concerns is to develop more effective thermal management systems, which can simultaneously solve multiple other issues. Since the introduction of semiconductor materials in the application of thermoelectricity, there has been a great deal of effort to help improve their normalized figure of merit (ZT) to be close to 3 in order to make them commercially feasible [1]. Understanding carbon-based materials' transport and thermoelectric properties can help reduce the amount of energy wasted as waste heat.

A thermoelectric power system tends to transform heat energy into electrical energy without using harmful chemicals like chlorofluorocarbons (CFCs). However, their inclusion in functional thermoelements has been hampered because semiconductor materials are chemically unstable at higher temperatures. The use of carbon-based compounds as possible thermoelectric

materials has a lot of potential for solving the problems mentioned above provided their thermal conductivities can be reduced.

Background to the Study

Thermoelectric devices are made up of materials that employ the Seebeck effect to convert heat directly into electricity through thermal gradient [2]. When electric current is conducted between two different wires, the Peltier effect cools the junction, resulting in similar energy conversion processes. Thermoelectric effects are caused by the transport of phonons and electrons over a temperature gradient in thermoelectric materials. The thermal fluctuation of carriers in the material's hot region is greater than those in the cold region. Therefore, the temperature difference causes the charged carriers (i.e. electrons or holes) in the thermoelectric material to flow from the high temperature region to a low temperature region, analogues to how classical gas expands [3]. The concentration of these particles defines the diffusion currents. The thermoelectric transport parameters are basically expressed using simple physical parameters. These are Seebeck coefficient, electrical conductivity as well as the thermal conductivity. It is preferable to enhance electronic diffusion while minimizing phonon diffusion when applying thermoelectricity to power generation [4].

The semiclassical Boltzmann Transport Equation (BTE) is proposed as a technique for exploring thermoelectric metrics in two-dimensional graphene superlattices, taking into consideration the impacts of carrier dispersion and intraminiband transition in producing the best normalized ZT. The ZT is a dimensionless parameter that measures the efficiency of a thermoelectric device

and it depends on the square of the Seebeck coefficient, the material electrical conductivity, the absolute temperature as well as the material thermal conductivity which is a contribution of both electrons and phonons. In addition to exploring thermoelectric transport at the nanoscale, the semiclassical BTE serves as a basis for analyzing other novel technologies in the field of condensed matter physics, where temperature effects on electrons and holes transport are particularly severe. Due to the growing importance of nanotechnology in industries like medical imaging, microelectronics, and nanocomposite materials, the demand for mesoscopic modeling has never been higher. As a result, employing the semiclassical approach to investigate carrier and phonon transport in nanoscale devices requires a paradigm shift in charge carrier transport modeling [5].

Graphene

Graphene is the only true two-dimensional material in the universe [6]. It has outstanding anisotropy properties such as thermal and electrical conductivities. These characteristics of graphene have significantly changed the face of materials science research for many years. Graphene has become a valuable nanomaterial due to its high tensile strength, exceptional electrical conductivity, transparency, as well as being the thinnest two-dimensional (2D) material in the world [7]. The single atomic layer of carbon shows varieties of unusual two-dimensional Dirac fermions. As a result, graphene presents some unique electronic and 2D transport properties such as an ambipolar field effect, quantum Hall effect, breakdown of the Born-Oppenheimer approximation, Klein reflectionless tunneling, etc. [8–13].

To be an effective thermoelectric material, its thermal conductivity must be low in order to maintain the temperature gradient. On the other hand, to obtain a high normalized ZT, a high-power factor is required. In spite of the fact that graphene has high electrical conductivity, its application in thermoelectricity has not been considered because of its high thermal conductivity. Prior to this research, the Seebeck coefficient of graphene was investigated by other researchers [12]. The objective for such efforts was primarily to study the physics of the carrier's dynamiacs in graphene, with little focus on its thermoelectric (TE) applications. However, graphene has some outstanding properties which could be used for TE applications. Due to its planar structure, a million of graphene-based TE devices can be cascaded to produce a compact TE device. The one-atomic thick layer of carbon makes it flexible to be integrated almost everywhere. Again, the carrier density of graphene can be tuned through electrostatic gating rather than chemical doping because of its large surface area.

Graphene is known to have numerous applications in electronic systems because of its outstanding electrical characteristics such as high carrier mobility and high Fermi velocity. However, the zero gap in graphene inhibits its full capacity in electronics [14, 15]. The gapless graphene has a charge neutral point (CNP) call the Dirac point. The Dirac point is a point of zero density of state at which the characters of graphene shift from electrons to holes. Graphene therefore, requires a bandgap to improve its applicability. One way of addressing this problem is to use graphene superlattice for electronic device applications. This is possible by patterning the graphene sheet into superlattices. Several researches have shown that forming a graphene superlattice can open

up a bandgap in graphene and by converting semi-metallic graphene into a semiconductor [15].

A superlattice structure was first explained in a workshop by Harman, Dresselhaus, and Venkatasubramanian [16] to have composed of alternating layers of different materials which exhibit many interesting transport and optical properties that are related to the quantum size effect. The thickness of these layers is normally measured in nanometers, and the average superlattice is exceedingly tiny. These architectures are used to create new types of semiconductors with characteristics that are different from the individual materials. As this technology becomes more widely available, scientists believe it will enable them to design materials with vastly diverse characteristics while maintaining their appearance. The structure is made up of layers of different materials placed on top of one another. When such small materials are stacked on top of one another, their properties combine in unexpected ways.

There are two main reasons for making superlattice structures. The first is to make the material more resistant to shearing effects. The process of creating a superlattice improves shear resistant far beyond the resistance of the constituent materials. This resistance allows the material to withstand larger stresses under higher temperature than traditional materials. The other major reason for the construction of a superlattice is to produce new varieties of semiconductors. These materials conduct electricity more efficiently than insulators, but not as efficiently as conductors. Superlattices are used in almost every kind of modern electronics, most often as integrated circuits or microchips. Most semiconductors are composed of silicon, superlattice

semiconductors can be made of a variety of materials. Figure 1 depicts the structure of a superlattice composed of alternate layers.

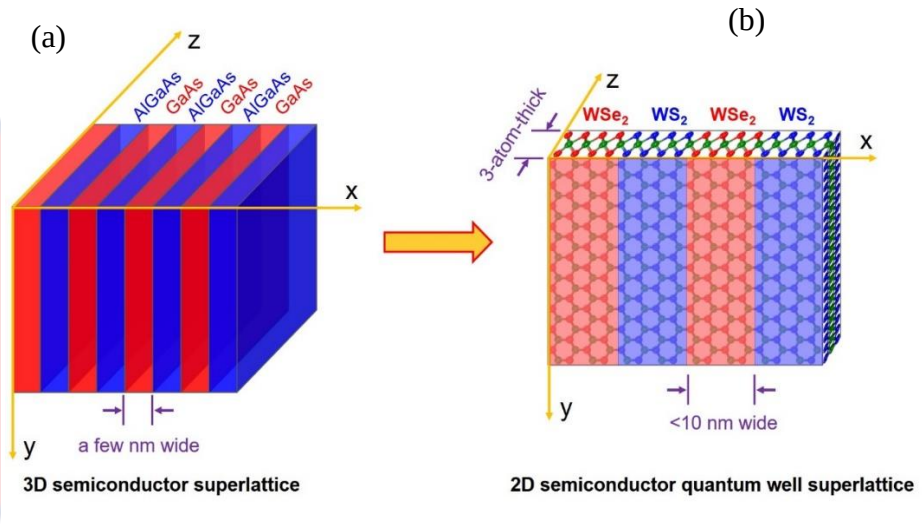

Figure 1: A schematic representation of: (a) superlattice structure. (b) how a superlattice is made of alternating crystals [17].

Wang and Zhu have investigated the electronic band structure and the transmission of carriers in graphene based one-dimensional (1D) superlattice with periodic-potential of square barriers. According to their findings, a new Dirac point is formed at the energy level which corresponded to the zero averaged wave number in the system. Such new Dirac point location does not depend on the lattice, but rather on the ratio of widths of the potential barriers [18]. Graphene has exceptional band structure at this Dirac point which gives an excellent conductivity. Electrons in graphene pass through the barrier with a hundred percent probability. This is because, the strong force between the carbon molecules has no effect on the motion of the electrons.

Statement of the Problem

Due to global warming, emission of greenhouse gases, and the depletion of non-renewable energy (i.e. fossil fuels) sources, there has been a growing trend toward greener energy. The subject of thermoelectricity has been regarded long time as a potential disruptive power-generating technology, and the field is presently expanding widely because of its capacity to directly convert thermal energy to electricity by producing cost-effective and pollutant-free forms of energy. Various types of semiconductors and superlattice materials have been investigated. Thorough studies were done on Bi_2Te_3 and PbTe semiconductor materials due to their outstanding efficiency [19]. Even though these materials improve the TE normalized ZT, superlattices of semiconductors and semimetals are very expensive, scarce, toxic, and unstable for mass production, necessitating the need to search for novel materials. Nanostructured materials have demonstrated significant potential for commercial use due to their high remarkable thermoelectric performance. As a result, this research is to theoretically study the thermoelectric properties of graphene superlattice.

Purpose of the Study

The purpose of the research is to find the thermoelectric power factor of GSL for nano-electric applications.

Research Objectives

The general objective of the study is to theoretically study thermo-optical properties of GSL for possible TE applications.

The research is guided by the following specific objectives, to determine the

i. Electrical conductivity of GSL.

ii. TE power in GSL.

iii. TE power factor of GSL

Significance of the Study

The results obtained from the research will guide in the synthesis of GSL materials for possible TE applications by providing the necessary additional theoretical basis for further thermoelectric research in order to promote the physics of this material for better understanding of its TE properties.

Depending on the nature of the variation of the electrical resistivity with electric fields and other material parameters of the GSL, high-performance thermoelectric devices could be fabricated for practical applications.

Delimitations

The fundamental goal of this research is to theoretically study the TE properties of GSL under the influence of applied electric field. The scope of this research will include the analytical derivation of expressions for the TE metrics of GSL, such as carrier current density, electrical resistivity, thermopower as well as thermoelectric power factor. The variation of these TE metrics with temperature, the material parameters such as the real overlapping integrals for jumps, and carrier concentration as well as dc-ac field intensities will be investigated.

Limitations

The BTE is solved using a semiclassical technique to get the TE metrics of the GSL for constant relaxation time. For the sake of mathematical simplicity, time constrain and computational limitations, quantum mechanical phenomena such as interband transition, quantum mechanical correction to intraband motion, correlation energy, Coulombic correction, and Coulombic interaction

will be excluded from this work, as seen in Mensah [20]. In other words, the study will be entirely semi-classical.

Organization of the Study

The thesis is composed of five main chapters: Chapter one provides the general background to the study with a brief introduction that states the problem under study, its relevance, how this research is related to earlier studies, and both theoretical and practical implications of the study. This chapter also highlighted the purpose of the research as well as its objectives. The chapter also covers the scope of work as well as the organization of the thesis. Chapter two reviews the literature on TE materials, BTE, electron-phonon interactions, electronic transport, and the principles underlying the theories used in this work. Chapter three deals with the theoretical formulations and techniques used in achieving the results in the research. The BTE together with the energy dispersion relation of graphene superlattice will be used to determine the electrical current density, electrical conductivity, thermoelectric power, and power factor for the GSL. Analysis and discussion of the analytical results are provided graphically in chapter four. In chapter five, conclusions are drawn and recommendations are provided to help future study in this field.

CHAPTER TWO

LITERATURE REVIEW

Introduction

This chapter reviews the thermoelectric effect and the basic physical properties of two-dimensional (2D) materials. The dynamics and mechanisms of electron transport in the semiclassical region leading to the derivation of thermoelectric metrics of graphene superlattice are reviewed. In addition to this, the carrier-phonon interactions are also discussed.

Thermoelectricity

Thermoelectricity is the direct conversion of temperature gradient to electricity and vice versa. A TE device creates a potential difference when there is a temperature different between its two terminals of the device. In the atomic scale, the different in temperature causes the charged carriers (electrons or holes) in a TE material to move from high temperature region to a low temperature region which is analogues to the expansion of classical gases when heated. TE materials employed in waste heat recycling and power generation are required to have good thermal and mechanical properties. Traditionally, thermoelectricity includes three distinct identified effects. These are the Seebeck effect, the Peltier effect and the Thomson effect.

Thomas J. Seebeck discovered in 1821 that when two different wires are joined together to form a circuit, a potential difference is created if there is a temperature different between these two wires. The potential difference created is directly proportional to the temperature gradient between these two junctions,

with the proportionality constant given as the Seebeck coefficient α, which is derived from the ratio of the potential difference ∇V produced to the temperature gradient ∇T between the cold and the hot sides of the TE device. The strength of the effect is described by the Seebeck coefficient which is given by

$$\alpha = -\left(\frac{\nabla V}{\nabla T}\right) \tag{2.1}$$

The negative sign of α is determined by whether the dominant carriers are holes or electrons. The Seebeck coefficient could be negative or positive depending on which direction the current is flowing and it is expressed in μV/K. In the semiconductor industry, thermoelectricity has numerous uses such as chip-level carrier cooling, remote telecommunication power generation, temperature control technologies in solid-state lasers, and so on. Due to their low efficiencies and performances, commercial applications of thermoelectric devices are limited. However, the advent of low-cost, high-efficiency thermopower generators has helped reduce dependency on non-renewable energy sources.

The Seebeck coefficient is also affected by two material properties such as carrier diffusion and phonon diffusion. The magnitude of the Seebeck voltage is determined by the entropy transmitted by carrier's diffusion through a material. Phonon drag reduces the ∇V created by raising the effective mass of the charge carriers. The contributions of phonon drag to the Seebeck coefficient is thought to be significant for particular materials [21], but has not been rigorously explored [22]. The Seebeck coefficient is limited near a material's

melting point due to increasing phonon drag and extremely low temperatures due to reduction in carrier's diffusion [8, 9].

The Peltier effect is the direct reverse to the Seebeck effect. When an electrical current is pass through a junction connecting two wires, it will either absorb or release heat per unit of time at the junction in order to balance the potential difference between the two materials. As a result of this effect, an electric refrigerator known as the Peltier Cooler is created. The heat generated per unit time per unit the flow of current from conductor 1 to conductor 2 is defined as the Peltier coefficient Π_{12}. As previously stated, this heat generated is directly proportional to the current flowing through the junction as described by Eqn. (2.1).

Years later, William Thomson published a paper which explained the details of Seebeck and Peltier phenomena, as well as their interaction. The Peltier coefficient is just the product of absolute temperature and the Seebeck coefficient. Based on this thermodynamic reasoning, Thomson predicted a third thermoelectric effect, now known as the Thomson effect. When current flows through a conductor with a different temperatures, heat is created or absorbed [23]. The heat created is proportional to the temperature gradient and the electric current. The constant of proportionality is the Thomson coefficient, and it is related to the Seebeck coefficient through thermodynamics. The Thomson coefficient is positive when a positive current flows from a higher temperature region [24].

Figure of Merit

To examine the efficiency of a TE device in the practical applications of converting waste heat directly into electricity, the most used parameter is the normalized figure of merit, ZT. The normalized ZT is a dimensionless parameter that uses the Seebeck coefficient together with other important physical properties to define a material's energy conversion efficiency and it is expressed as:

$$ZT = \frac{\alpha^2}{\kappa}\sigma T \qquad (2.2)$$

Where α denotes the Seebeck coefficient, σ is the material's electrical conductivity, T represents thermodynamic temperature, and k is the thermal conductivity of the material [25]. Thermal conductivity of a material comprises two terms, i.e. electron thermal conductivity and phonon thermal conductivity. The electrical thermal conductivity is dominant for metals while the phonon thermal conductivity is dominant for semiconductors.

The figure of merit is a significant metric used in engineering and materials science to compare the efficiency of TE materials. It is anticipated that ZT must be about 3 for TE devices to compete with other existing technologies [26]. At 300 K, materials such as GaAs and Si have very low ZT values which is less than 0.01 [27]. Bi_2Te_3 and PbTe are the two most prevalent TE materials nowadays [28]. Recently, nanostructure materials, such as silicon nanowires with ZT ≈ 0.6 at 300 K have been developed [29].

Again, the Seebeck coefficient and the conductivity of the carriers are controlled by the material's carrier properties. However, thermal conductivity

is affected by both carrier and lattice vibrations. The best initially available TE device has ZT ≈ 0.99 [22]. Extensive TE research has sought materials with higher thermoelectric power but lower heat conductivity, resulting in a higher ZT. The difficulty here is that, the parameters that define ZT are interdependent of each other, thus changing one changes the others. High atomic weight semiconductors are employed to minimize the thermal conductivity in bulk materials such as Bi_2Te_3 and its alloys with Sb, Sn, and Pb without altering the Seebeck coefficient and the electrical conductivity. Although it is theoretically conceivable to build bulk semiconductors with ZT >3, no promising materials are on the horizon [30].

Based on these benefits, the introduction of nanofilm and superlattice (SL) nanowire structures in the 1970's dramatically enhanced the ZT of thermoelectric devices, redirecting the attention away from bulk materials toward understanding the dynamics of carrier transport in nanodevices. The confinement of carriers in quantum nanostructures increases the carrier local density of state close to the Fermi level [31]. Phonon confinement and the scattering phonon in material interfaces in SLs boost thermoelectricity [32] but decreases thermal conductivity. This is because the large bandgap and the differences between the phonon and carrier-free mean paths in the semiconductors have little effect on the electrical conductivity [30, 31].

Thermoelectric materials

Thermoelectric processes are caused by the movement of phonons and electrons over a temperature gradient in electrically conducting materials. The concentration of these particles defines the diffusion currents. The basic TE

transport parameters are expressed using simple physical parameters such as electrical and thermal conductivities and the Seebeck coefficient. It is preferable to enhance electronic diffusion while minimizing phonon diffusion when applying thermoelectricity to power generation.

Thermoelectricity is a method which is widely used for sensing and cooling to ensure thermal management. This applies to materials and structures which have sustainable chemical potential difference between their cold and hot ends. Although, semiconductors are widely used in optoelectronics and microelectronics, it is difficult to imagine that the initial excitement was as the result of their promise in refrigeration, but not in electronics [35]. It was the discovery in the 1950s that semiconductor materials can act as efficient heat pumps which leads to the premature expectations of environmentally friendly solid-state home refrigeration and power generators that contains no moving parts.

In semiconductors, holes and electrons are charge carriers, while lattice phonons or vibrations dominate heat transport. Phonons and electrons (or holes) have two lengths associated with their transport which, are free mean path, l and wavelength, λ. Nanostructure semiconductors which have sizes comparable to the wavelength λ, have sharp edges and peaks at their electronic density of state, whose location in energy space depends on their sizes. By matching the locations peaks with their shapes to the Fermi energy, one can modify the thermopower. Such quantum confinement increases electron mobility, which could lead to high values of conductivity. Hence, quantum confinement allows

manipulation of electrical power factor $\alpha^2\sigma$ that is hard to achieve in bulk materials [36].

Majority of thermoelectric materials are alloys. This is because alloys scatter through short-wavelength acoustic phonons and this reduces thermal conductivity without substantially altering $\alpha^2\sigma$. It is possible that increasing ZT may be less dependent on quantum confinement of holes and electrons, but depends more on phonon dynamics and transport. For example, if the semiconductor size is smaller and the mean free path of the phonons is larger than that of the electrons or holes, one can reduce thermal conductivity by boundary scattering without affecting electrical transport.

Several questions about quantum effects have received increasing attention and their answers hold promise in increasing ZT [25, 26]. Hicks et al. in [35,36] proposed that it may be possible to increase ZT of certain materials by preparing them in quantum-well SL structures. In their paper, calculations were carried out to investigate the potential for this approach, and authors also evaluated the effect of anisotropy on ZT. Their calculations showed that layering has the potential to increase significantly the ZT of a highly anisotropic material such as Bi_2Te_3, provided that the SL multilayers are made in a particular orientation. This result opens the possibility of using quantum-well SLs structures to enhance the performance of TE coolers.

Mensah et al. in [39] also investigated the TE effect in a semiconductor SL placed in a non-quantized electric field. These researchers obtained analytical expressions for thermopower and the heat conductivity coefficient as functions of the SL's parameters such as its bandwidth, period, temperature,

carrier concentration, and electric field. Their results confirmed the fact that depending on the relationship between the bandwidth and the other energies characteristics of the charge carriers, the charge carriers can behave either as a quasi 2D particle or as a 3D electron gas. They proposed the prospect of using a SL as a quality and highly efficient thermoelement.

Graphene and two-dimensional materials

The study of the physical properties of 2D materials has emerged as one of the most effective and relevant fields in condensed matter physics. The interest in these materials started with the isolation of graphene in 2004 by Novoselov and Geim [40]. In recent years, attention has switched to various 2D materials and, more significantly, their combinations [41, 42]. Multiple layers of various 2D materials can be piled on top of one another to produce complex structures. These layers are kept together by Van der Waals forces. As a result, these structures are known as Van der Waals structures (VdW) [43].

Carbon allotropes form a unique hybridization structure of sp^3, sp^2 and sp networks which are more stable than any other element. The most common allotropic form of carbon known since antiquity is graphite and diamond which are naturally abundant. Graphite is made up of sp^2 hybridization of carbon atomic layers that are held together by weak Van der Waals forces. The basic unit of graphite is graphene which is a single atomic layer of graphite sheet densely packed into a 2D honeycomb-like crystal structure [10].

A 2D quantum wire is created from a three-dimensional (3D) crystal in such a way that the length of the wire is very long and its diameter is small enough to achieve quantum confinement. Graphene, the mother of all graphite

which is composed of weakly coupled layers, can be wrapped in all directions into a zero-dimensional Bucky ball (0D). When a 2D crystal structure is rolled at its longitudinal ends, it forms a one-dimensional (1D) structure, known as carbon nanotube, and when stacked into a (3D) structure it is as known as diamond and other carbon compounds [44, 45], as shown in Figure 2.

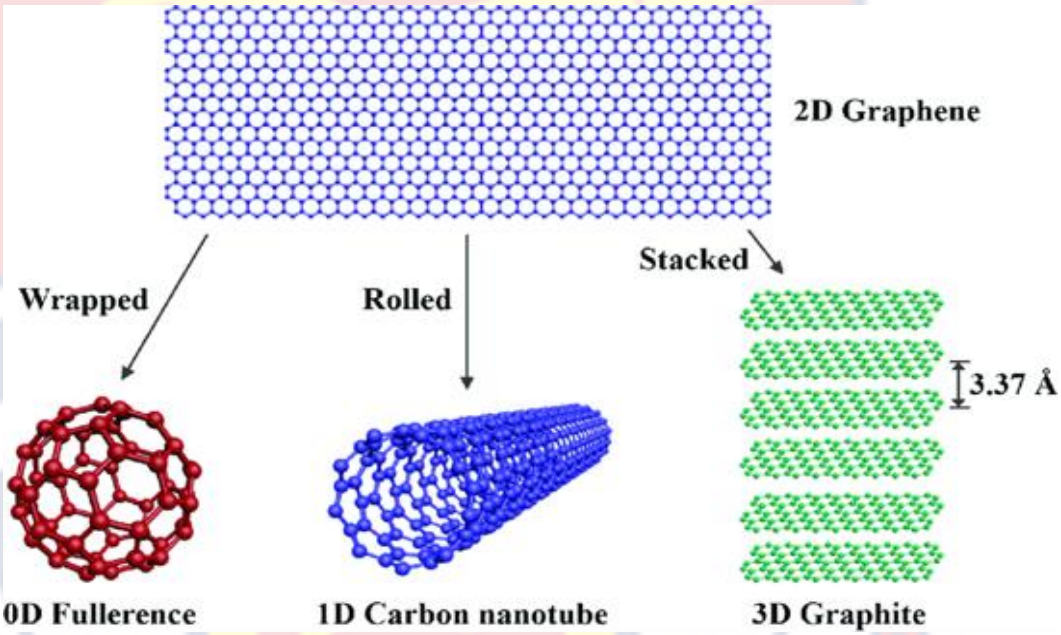

Figure 2: Some allotropes of Carbon: Fullerenes (0D) Carbon Nanotubes (1D), Graphene (2D) and Graphite (3D) [46].

Graphene as a material was scientifically proved not to exist due to thermal expansion [47]. These scientists argued that, strictly 2D crystals were thermodynamically unstable. This is as a result of thermal fluctuations in low-dimensional crystal structures which will lead to displacements of the atoms interatomic distances at finite temperature [13]. This hypothesis was disproved in 2004 [44] by a Manchester group led by Andre Geim and Novoselovs who reported a method by creating a single layer graphene on a silicon oxide

substrate by mechanical exfoliation [12, 45]. The quasiparticles behave as non-relativistic electron charge carriers with zero mass.

The unique band structure of graphene is the results of touching of valance and conduction bands at the Dirac point (k and k') on the edge of the first Brillouin zone. Near these crossing points, the electron's energy is linearly dependent on the wave vector. This linear dispersion produces massless excitons, which are described by the Dirac equation. The Dirac fermions (electrons or holes) exhibit unusual characteristics as compared to the ordinary electrons which leads to new phenomena such as linear energy dispersion, , ballistic conduction, chiral behavior and quantum Hall effect [48], frequency dependent conductivity [49], gate-tunable optical transitions, [50] and so on.

Methods of Fabricating Graphene

Graphene is currently synthesized using different methods. Depending on the desired size, purity, and crystallinity of the finished products, four basic methods currently exist in the synthesis of graphene. These are mechanical exfoliation, liquid phase exfoliation of graphite, pulse laser deposition, and chemical vapor deposition.

Mechanical Exfoliation

Mechanical exfoliation was the first and most widely used method of producing graphene for research purposes [51]. This common method uses adhesive scotch tape to peel off single layers of graphene by breaking the weak Van der Waals forces. The sample may contain mixture of layers, which are then peeled off repeatedly to produce predominant single layer of graphene.

This method produces high-quality graphene with no grain impurities. However, the graphene coverage on the substrate is minimal and uncontrollable. As a result, mechanical exfoliation is unsuitable for large-scale production.

Liquid Phase Exfoliation of Graphite

Liquid Phase Exfoliation (LPE) process uses solvent sulfuric acid and acetic acid, or hydrogen peroxide to produce graphene materials from graphite by ultrasonication [52]. Sonication is a method used in LPE to produce graphene from graphite material, since it involves different layers of graphene which are held together by Van der Waals forces. This approach, shown in Figure 3, is used to produce graphene nanoribbons. However, large-scale graphene growth is problematic in this technique.

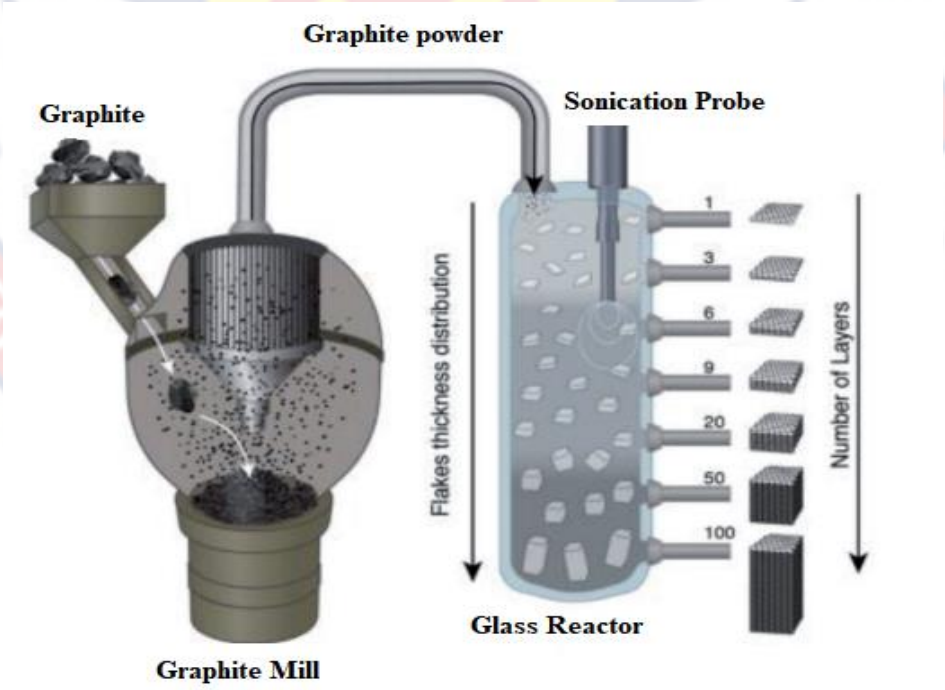

Figure 3: Schematic diagram of production of graphene using LPE [50]

Pulsed Laser Deposition

Pulsed Laser Deposition **(**PLD) is a commonly used method for producing graphene materials for practical application and its schematic is shown in Figure 4. During the PLD techniques, the laser source is positioned outside the chamber, and the chamber is kept at an ultrahigh vacuum. In this approach, the material is deposited at an angle of 45° through stoichiometry transfer between the ablated target and substrate material in this technique. Throughout this process, substrates are added to the surfaces parallel to the target at a distance of (2-10) mm. The main advantage of the PLD process is the low temperature growth rate observed, which allows for the production of high-quality graphene with no flaws [41, 44].

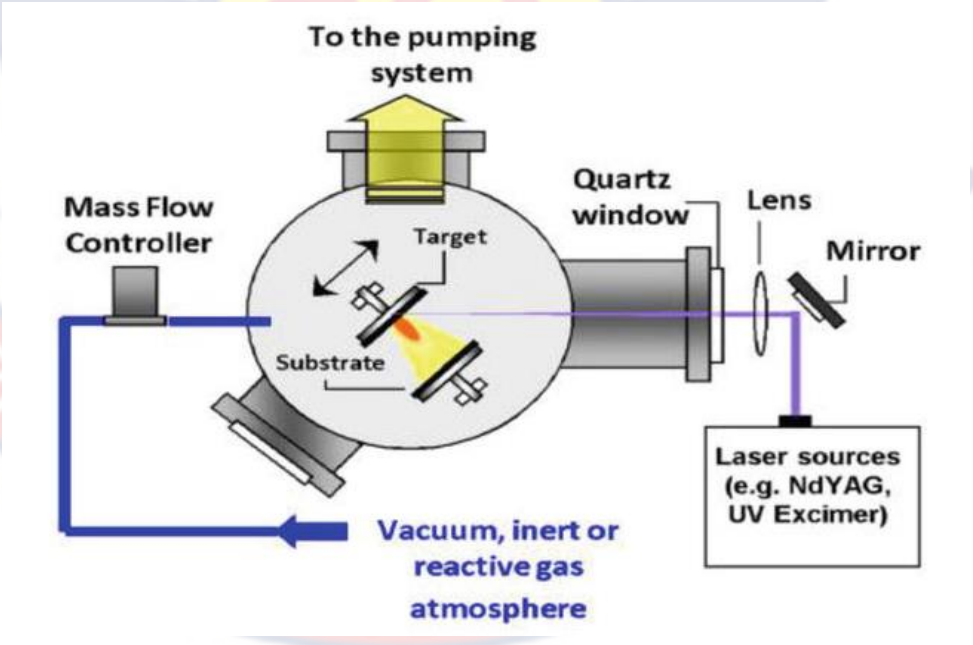

Figure 4: Schematic representative of pulsed Laser deposition of graphene [53].

Chemical Vapor Deposition

As illustrated in Figure 5, Chemical Vapor Deposition (CVD) works by depositing volatile gas molecules onto a substrate. This process occurs in the reaction chamber, where the substrate is formed on the material surface and the waste gases are released. Temperature dependence plays an important role and can affect the kind of reaction that will occur. CVD produces high-quality and pure graphene films, however, the by-products formed in the process may be toxic due to the volatile nature of the precursor gases [54].

The graphene sheet produced by the CVD technique is divided into two phases. The first method includes pyrolysis of a precursor substance in order to produce carbon atoms on the substrate material. Pyrolyzing the substrate on the material prevents the formation of carbon clusters. Due to the amount of energy needed for breaking the carbon bonds, a high temperature may be required, necessitating the use of a metal catalyst during the process. The second phase is heat-intensive one in which fragmented carbon atoms assembled onto a substrate in the presence of a catalyst to form a single layer structure [55]. Depending on the arrangement of the atoms in the film, CVD graphene films are expected to have strong electrical, chemical, and magnetic characteristics. Due to the five-order-of-magnitude disparity between grains and atoms at grain boundaries, only a few experiments have been undertaken to examine these interactions. Copper is one of the recognized substrates that is used to produce high-quality graphene. Copper serves as both a catalyst and a substrate. The copper bonds to the carbon atoms which creates strong carbon-substrate interactions, that allow a single graphene sheet to grow on the surface. Copper

oxide can also be placed between graphene sheets to help facilitate the removal of a single layer.

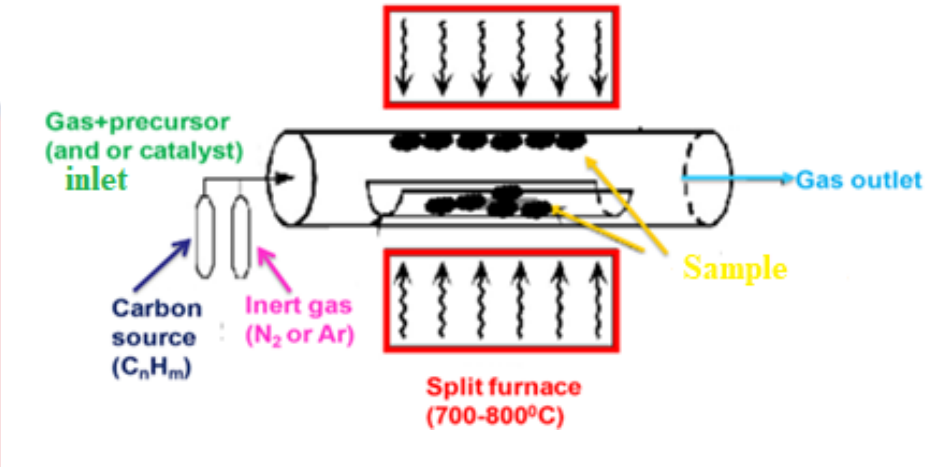

Figure 5: Schematic diagram of chemical vapor deposition Setup [56].

Graphene Superlattice

GSL is widely known for its ability to control the electrical structures of several common semiconducting materials [57]. Extensive studies on the basic characteristics of SLs, such as carrier transport and energy band structures have been widely studied. Novel devices such as infrared detectors, semiconductor lasers, modulators and light-emitting diodes (LEDs) have been developed using quantum SL structures. A SL structures are said to be formed when thin layers ($d \leq 25$ nm) of a larger band gap semiconductor (AlGaAs) and a smaller band gap semiconductor (GaAs) are grown alternately on a conducting or a semi-insulating substrate. The periodic structures are formed by alternately depositing thin epitaxial layers of two different band gap materials to produce a periodic potential similar to the 1D Kronig–Penney model.

Both experimental and theoretical investigations have demonstrated that SL structures have significant influence on the characteristics of charge carriers in graphene [53, 56, 57]. This suggests a possible approach for building electrical devices on graphene without the requirement for cutting or etching. Among the several approaches for producing GSL [59, 60], partial hydrogenation seems very fascinating. Theoretically, a 1D GSL formed by partial hydrogenation is expected to have surprising electrical characteristics that might be highly beneficial in real-world applications [60, 61]. Figure 6 shows the schematic arrangement of 2D GSL substrate (SiO_2/h-BN) relating to graphene sheet.

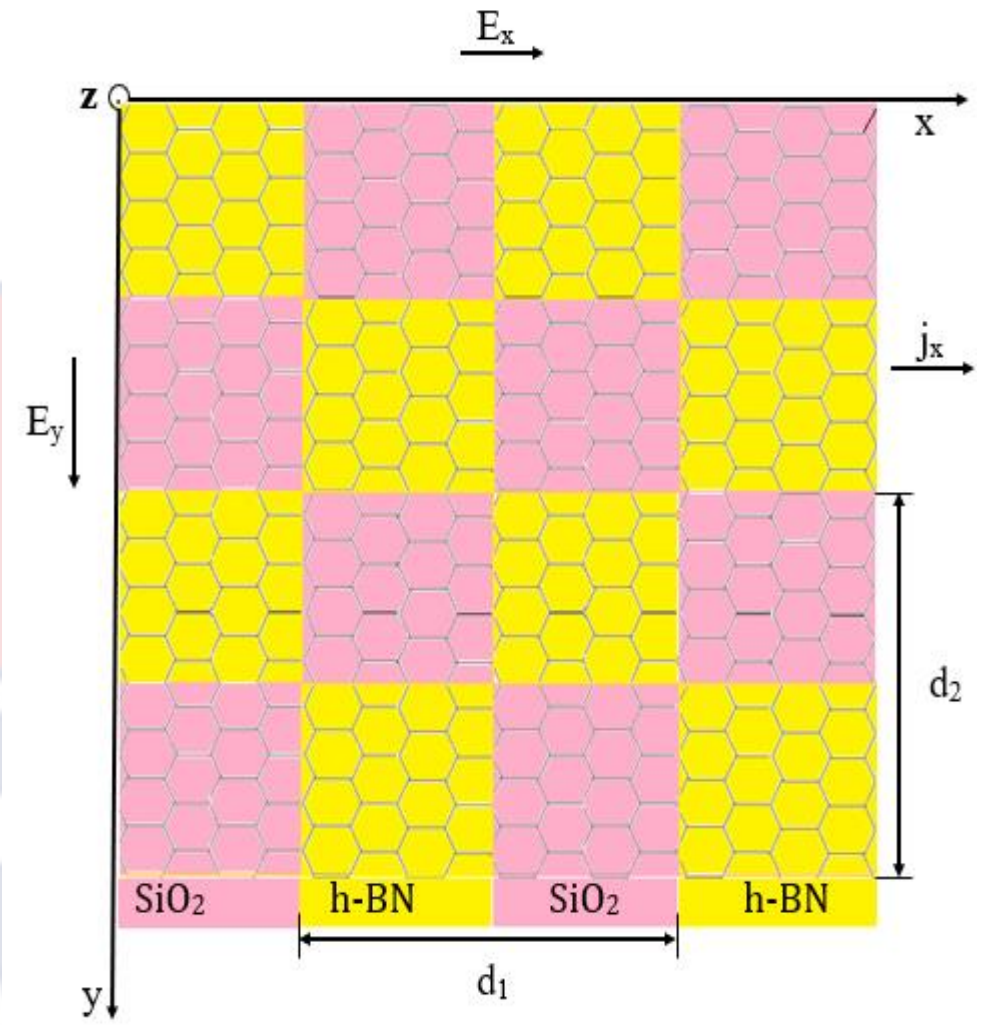

Figure 6: Schematic representation of 2D GSL showing the arrangement of the substrate (SiO_2/h-BN) relative to Graphene sheet (adapted from Ref. [62]). The alternate regions provide a periodic structure in the graphene sheet with a period of d_1 along one axis (the x-axis in this case) and a period of d_2 along the y-axis.

Two-Dimensional Graphene Nanomaterials

The isolation of graphene monolayer experimentally has prompted numerous attentions in condensed matter physics to investigate its exceptional properties, especially with its linear dispersion and massless Dirac fermions. In

addition, due to graphene's high electron mobility at ambient temperature (>50,000 cm2/Vs), it has natural uses in high-speed electrical devices [63]. However, the zero bandgap of graphene presents significant challenges in most electronic applications, prompting subsequent efforts to modify graphene by opening a bandgap. For example, a bandgap can be formed in graphene by breaking the symmetry of (k and k') points in the first Brillouin zone, which could lead to research into graphene-related materials like graphene oxide and hexagonal boron nitride (h-BN). In this context, h-BN is an extreme case in which carbon atoms in the (k and k') locations are replaced with boron and nitrogen resulting in a broad bandgap (~6 eV) insulator.

Real Space Lattice of Graphene

Graphene is a two-dimensional (2D) single atomic layer of carbon allotropes which serves as the fundamental building block for graphite, carbon nanotubes, fullerenes, and other carbon-based compounds with hexagonal structure which consist of a bi-particle lattice of two triangular sublattice. Figure 7 shows the hexagonal honeycomb lattice structure, as well as the primitive cell denoted by the basis vectors $\mathbf{a}_1$ and $\mathbf{a}_2$ respectively. The interatomic distance is sometimes indicated as a_o [52, 53]. To determine the lattice vectors, the structure of a graphene sheet with two carbon atoms per unit cell forms two sublattices. Sublattices a and b atoms are represented by blue and grey dots, respectively (see Figure 7).

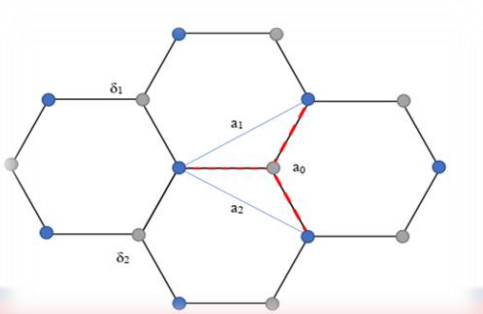

Figure 7: A representation of graphene honeycomb lattice basic structure in real space. The sublattices a and b are represented in blue and grey, respectively. The interatomic spacing is shown in red, while the primitive cell is shown in blue. Adapted from Ref. [64]

The primitive lattice vectors $\vec{a}_1$ and $\vec{a}_2$ with primitive unit cell a_o can be derived using plane geometry as specified as follows:

$$\vec{a}_1 = a_o\left[\frac{3}{2}, \frac{\sqrt{3}}{2}\right], \qquad \vec{a}_2 = a_o\left[\frac{3}{2}, \frac{\sqrt{3}}{2}\right] \tag{2.2}$$

From Pythagorean theorem, the magnitude of the basic lattice vectors is given by;

$$\left|\vec{a}_1\right| = \left|\vec{a}_2\right| = a_o\sqrt{3} \tag{2.3}$$

where the interatomic spacing is indicated by a_o and the magnitude of the associated lattice vectors $\vec{a}_1$ and $\vec{a}_2$ is 2.46 Å.

It is noted that the hexagonal honeycomb lattice of Bravais lattice is defined by the next-to-nearest neighbors rather than the basis vectors linking the nearest adjacent vectors. The Bravais lattice is hexagonal, with its unit cell shown in blue (see Figure 7).

Due to the periodicity of the lattice, it follows that any physical characteristic *f* (r) of the lattice will inherit this periodicity, which implies that *f* (r) is translationally symmetric [64].

Reciprocal Lattice of Graphene

According to periodic lattice theory, the periodicity of a lattice is inherited by each lattice's physical characteristic *f* (r). To support this, every function in space which is periodic may be characterized by a wavelength (λ). Ionic cores in an atomic lattices can alternatively be conceived as two-dimensional periodic waves [65]. The primitive lattice vectors $\vec{a}_1$ and $\vec{a}_2$ establish the crystal planes inside the lattice. The wavelengths λ_i of the lattice are simply the distance between crystallographic planes calculated from primitive lattice vectors.

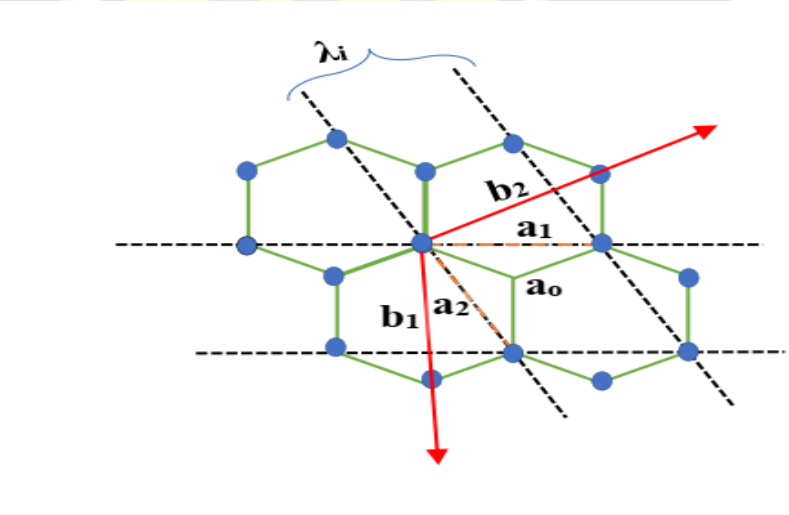

Figure 8: A representation of the primitive (yellow) and reciprocal (red) lattice vectors in real space. Lattice planes (dashed) are also illustrated so that the reciprocal lattice vectors' directions are intuitive. Adapted from Ref. [65].

Figure 8 shows the primitive and the reciprocal lattice of graphene. A wave theory describes the lattice based on its crystal planes which is equally justifiable as described by the primitive lattice vectors.

This is done by identifying the spatial frequency in the lattice planes given by the lattice vectors $\boldsymbol{b_i}$. These vectors point to the direction of the wave propagation, and their magnitude $|\boldsymbol{b_i}|$ is the wavenumber. The wavenumbers and wavelengths of the lattice are related as:

$$b_i = \frac{2\pi}{\lambda_i} \tag{2.4}$$

where λ_i is the space between the crystal planes and the lattice wavelength. Using plane geometry, the wavenumbers as well as the wavelengths relating to the primitive lattice vectors in the graphene sheet can then be calculated as:

$$\lambda_i = \left|\hat{a}_i \times \hat{a}_j\right| \tag{2.5}$$

Thus, for graphene lattice, we obtain

$$\lambda_i = \left|\hat{a}_i \times \hat{a}_j\right|$$

$$\left|\vec{b}_1\right| = \left|\vec{b}_2\right| = \frac{4\pi}{3a_o} \tag{2.6}$$

The reciprocal vectors of lattice are vectors $\vec{b}_1$ and $\vec{b}_2$. The direction of the wavevector is perpendicular to the lines or planes of constant phase. The crystal planes are also defined to be surfaces of constant phase in lattice. This is because the vectors $\vec{a}_1$ and $\vec{a}_2$ define the lines in the planes through which their corresponding wavevectors should be normal. In that way, the primitive unit vectors are expressed as:

$$\hat{a}_1 = a_o\left[\frac{\sqrt{3}}{2}, \frac{1}{2}\right], \qquad \hat{a}_2 = a_o\left[\frac{\sqrt{3}}{2}, \frac{1}{2}\right] \tag{2.7}$$

Rotating Eqn. (2.7) by 90^0 and then multiply it by the wavenumber gives the vectors corresponding to the primitive lattice vectors as:

$$\hat{b}_1 = \frac{4\pi}{3a_o}\left[\frac{1}{2}, \frac{\sqrt{3}}{2}\right], \qquad \hat{b}_2 = \frac{4\pi}{3a_o}\left[\frac{1}{2}, -\frac{-\sqrt{3}}{2}\right] \tag{2.8}$$

The reciprocal lattice vector is symmetric under translation for any physical property in k-space, g (**k**) [59, 65].

$$\text{g}(\mathbf{k}) = \text{g}(\mathbf{k} + \mathbf{G}) \tag{2.9}$$

where **G** is the translational vector which is the integral sum of the reciprocal lattice vectors

$$G = \sum_i n_i b_i \tag{2.10}$$

Figure 9 indicates the points of constructing a graphene reciprocal lattice and its reciprocal lattice vectors. The reciprocal primitive lattice cell (red) and its first Brillouin zone (light blue) are also shown and the irreducible path (purple) in the Brillouin zone. The diagram is considered to exist in k-space, where k_x and k_y serve as unit vectors. In k-space, two points are regarded as comparable if and only if they can be reached by a reciprocal lattice vector translation. From a mathematical point of view, the Fourier transform of the reciprocal lattice is the primitive lattice [66, 67].

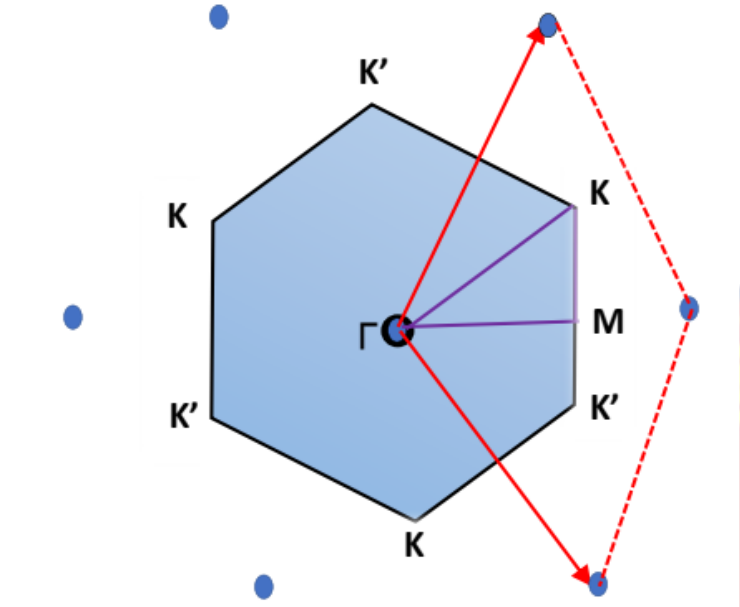

Figure 9: A diagram showing the reciprocal lattice in graphene along with the first Brillouin zone (red) in momentum space. Adapted from Ref. [65].

The Brillouin zone becomes relevant when the wave's reflection from a periodic structure is elastic. According to the de-Broglie theory, this wave may be a phonon or an electron. As reported by Bragg's reflection theory, periodic reflection happens if and only if the incident k wave and the reflected k' wave constructively interact. Constructive interference occurs if the difference between the incident and reflected waves is equal to the reciprocal lattice vector G.

$$\Delta k = k - k' = \mathbf{G} \qquad (2.11)$$

The above relationship holds if **G** is a reciprocal lattice vector. It denotes the wavevectors related to the periodicity of the lattice planes. On the other hand, an elastic scattering causes the direction momentum to change while keeping the magnitude unchanged.

$$|k| = |k'| \tag{2.12}$$

By combining Eqn. (2.11) and Eqn. (2.12), the elastic condition that applies to the reflection of a wave from a periodic structure is obtained as:

$$\mathbf{k}.\mathbf{G} = \frac{1}{2}|G|^2 \tag{2.13}$$

Equation (2.13) above is a vector representation of the well-known 1D Bragg condition, $n\lambda_i = 2dcos\theta$, where λ is the wavelength of the incident beam, n is an integer, d is the lattice spacing, and θ is the incident angle. The aforementioned geometrically specifies the limits of volumes in k-space. These volumes are the Brillouin zones BZ, with the lowest volume being the first BZ and so on. Although knowledge of the BZ initially appears in the study of Bragg's reflections, it is applicable to the physical theory of solids [68, 69]. The graphene BZ is of particular importance in the investigation of the band structure, its acoustic and electrical characteristics. This is because the location of the k-points in the BZ are considered equivalent and can be accessed by reciprocal lattice vector **G** through translation. The physical properties of every lattice structure will be approximately the same at the k-points. In other words, the Physics at the k-point is the same. However, it is impossible to translate the reciprocal lattice vector, **G** through k and k'. This is because these points are inequivalent, resulting in different Physics at the k and k'. This discrepancy between the vertices eventually leads to a two-fold valley degeneracy in the graphene band structure known as valley isospin or valley degeneracy.

Electronic Band Structure of Graphene

In 1947, Wallace theoretically investigated the band structure of graphene and found that it behaves as a semimetal due to lack of band gap between the valence and conduction bands [70]. The material transport properties are intrinsically linked to its energy band structure. The GSL allows carriers to move freely in two dimensions. The carriers near the Dirac points are important in graphene carrier transport.

Graphene's single layer has a honeycomb crystal structure made up of two quasi sublattices. This gives a unique band structure for restless-electrons that act like massless Dirac fermions close to the Fermi energy. At two separate Dirac points known as k and k' points, the valence and conduction bands join together conically by generating a time-reversed pair with opposing polarity. The chirality and Berry phase at these points enable uncommon and exciting 2D electronic phenomena such as the half-integer quantum Hall effect, the lack of backward scattering and phase shift of the Shubnikov–de Haas oscillations [70, 71].

The hexagonal lattice of graphene consists of carbon atoms. Each of these carbon atoms has six electrons' pair in $1s^2$, $2s^2$ and $2p^2$ orbitals. The orbitals of different carbon atoms can make bonds by lowering their total energy in the valence electrons. The energy band structure of a graphene sheet is obtained by first characterizing the basal planes with the tight-binding approximation and then superimposing the periodic boundary conditions. The electronic structure is determined within these approximations by distinguishing interactions within each basal plane (covalent) from in-plane interactions [53, 72]. The graphene unit cell in real space is generally known to contain two

carbon atoms. Each carbon atom is also known to have four valence electrons. According to hybridization theory, each of these three electrons forms a strong sp^2 σ-bond with its three nearest neighbours who are in the same plane, with a bond angle of 120^0 and energies of -2.5eV, which is significantly below the Fermi level. These bonds have no effect on the conductivity of the graphene sheet [73]. The fourth valence electron is positioned somewhat below the Fermi level in the π-orbitals which is perpendicular to the plane of the graphene sheet. This π-electron is thought to be in control of the graphene sheet's electrical conductivity and transport properties [49, 58]. The Fermi level is slightly below the anti-bonding π^*-orbital, and it corresponds to the conduction band in the energy band diagram as shown in Figure 10. In other words, the electronic properties of graphene are best explained by considering simply the electron energy dispersion [74].

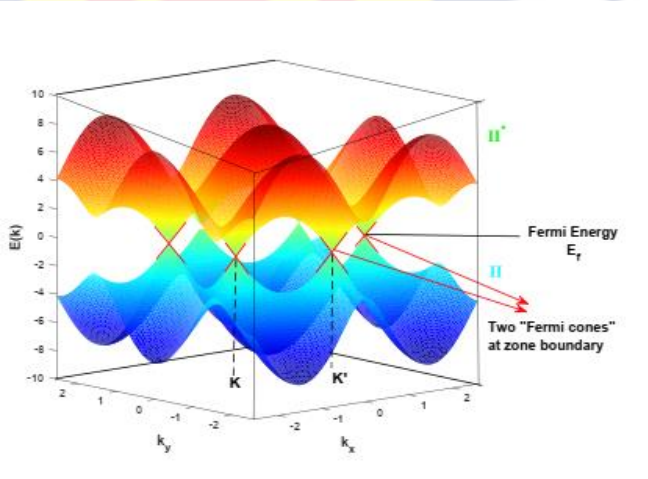

Figure 10: Electronic dispersion relation (plot of electron energy as a function of wavevector k in the xy plane) for single-layer graphene. The single-layer graphene conduction band touches the valence band at k and k' points in the reciprocal space. Adapted from Ref. [65].

When Wannier functions are combined with the second quantization formalism, an intuitive description of the band structure is obtained [75]. The creation operators $\alpha_i^\dagger$ and $\beta_i^\dagger$ are in the sublattices a and b. The sublattices are obtained in the vacuum state as:

$$\alpha_i^\dagger |0\rangle = |R_i^\alpha\rangle \;\; ; \;\; \beta_i^\dagger |0\rangle = |R_i^\beta\rangle \tag{2.14}$$

These relations are interpreted as creating an electron on the $\alpha_i^\dagger$ or $\beta_i^\dagger$ atom of the unit cell indexed with position vector R_i. The tight-binding Hamiltonian $\hat{H}$ will take the form:

$$\hat{H} = -\gamma \sum_{\langle i,j \rangle} \beta_j^\dagger \alpha_i + \alpha_j^\dagger \beta \tag{2.15}$$

The exact solution of Eqn. (2.15) is obtained by summing over all $i \neq j$, since the analytic solution of such a problem is tedious. For first approximation, the sum will be taken only over the nearest neighbours. The first term in the sum indicates that an electron is annihilated at position R_i^α and subsequently created at a nearest neighbor R_i^β [64, 65], which is known as α/β hopping. Similarly, the second term denotes the hopping from β sublattice to sublattice α. By symmetry, the hopping energy is approximately the same in both cases of the problem. Experimental measurements have revealed that γ =2.65 eV [76]. In analogy with quantum mechanics, the eigenvalues of the Hamiltonian are of much concern, with special interest in the energy dispersion relation, $\varepsilon(k)$ such that a change of basis to momentum space is required. So, the creation operators are written as:

$$\alpha_i^{\dagger} = \sum_k e^{-iR_i^{\alpha}.k}\alpha_k^{\dagger}$$
$$\beta_i^{\dagger} = \sum_k e^{-iR_i^{\beta}.k}\beta_k^{\dagger} \tag{2.16}$$

The hopping term β/α is found from the complex conjugate (α/β) term [67]. This means $\vec{H}$ is Hermitian, and performing a change of basis for $\vec{H}$ then yields

$$\vec{H} = -\gamma\sum_k\sum_{\langle i,j\rangle} e^{-i(R_j^{\alpha}-R_i^{\beta}).k}\beta_k^{\dagger}\alpha_k$$
$$= -\gamma\sum_k\left\{\sum_n e^{-i\delta_n.k}\right\}\beta_k^{\dagger}\alpha_k \tag{2.17}$$

where k is sum over all the k'-values within the first BZ. The result for β/α is shown [75] as:

$$f(k) = -\gamma\sum_n e^{-i\delta_n.k}\; f^*(k) = -\gamma\sum_n e^{-i\delta_n.k} \tag{2.18}$$

This is summed over the nearest neighbour vectors to get the overall Hamiltonian in k-space. A 2×2 anti-diagonal matrix represents this Hamiltonian. This matrix results from working on the sublattices' basis. The interaction that takes place is only between the α and β sublattices, which are off-diagonal elements. That is,

$$f(k) = -\gamma\sum_n f(k)\beta_k^{\dagger}\alpha_k + f^*(k)\alpha_k^{\dagger}\beta_k \tag{2.19}$$

$$\begin{bmatrix} 0 & f(k) \\ f^*(k) & 0 \end{bmatrix} = 0 \tag{2.20}$$

Solving the secular equation gives the energy relations

$$\left|\vec{H} - \varepsilon_k I\right| = 0 \tag{2.21}$$

$$\varepsilon_k = \pm \left| f(k) \right| \tag{2.22}$$

Substituting for the nearest neighbor vectors δ_n yields for $f(k)$ and $\varepsilon(k)$ [76].

$$f(k) = -\gamma \left[e^{ik.\delta_n} + 2e^{ik.(\delta_1+\delta_2)/2} \cos\left(\frac{k.(\delta_1+\delta_2)}{2} \right) \right]$$

$$= -\gamma \left[e^{ik_x.a_o} + 2e^{ik_x.a_o/2} \cos\left(\frac{\sqrt{3}a_o k_y}{2} \right) \right] \tag{2.23}$$

Substituting Eqn. (2.23) into Eqn. (2.22) and simplify to obtain

$$\varepsilon(k) = \pm \sqrt{3 + 2\cos(\sqrt{3}a_o k_y) + 4\cos\left(\frac{\sqrt{3}a_o k_x}{2} \right) \cos\left(\frac{\sqrt{3}a_o k_y}{2} \right)} \tag{2.24}$$

The eigenvalues of the Hamiltonian, $\varepsilon(k)$ yields the electronic band structure. The corresponding normalized eigenvectors are [77]

$$\left| + \right\rangle = \frac{1}{\sqrt{2}} \begin{pmatrix} 1 \\ +e^{-i\theta(k)} \end{pmatrix}, \quad \left| - \right\rangle = \frac{1}{\sqrt{2}} \begin{pmatrix} 1 \\ -e^{-i\theta(k)} \end{pmatrix} \tag{2.25}$$

As shown in Eqn. (2.26), the Hamiltonian can be written in terms of $\varepsilon(k)$ by identifying that $f(k) = \left| \varepsilon(k) \right| e^{i\theta(k)}.\theta(k)$ describes the phase associated with the Bloch eigenstate that is composed of the wavefunction.

$$\hat{H} = \left| \varepsilon(k) \right| \begin{bmatrix} 0 & e^{i\theta(k)} \\ e^{-i\theta(k)} & 0 \end{bmatrix} \tag{2.26}$$

The k and k' points in the neighborhood of the BZ and have the energy $\varepsilon(k + \delta k) = \varepsilon(k' + \delta k)$ such that measuring the electron energy close to k or k' will not indicate whether it is in the creation $\left| + \right\rangle$ or destruction $\left| - \right\rangle$ states [66, 75].The phonon spectrum and band structure of graphene are derived by summing the nearest neighbor vectors. The results in both situations are the

consequence of considering the coupling between the sublattices. The coupling in the former (phonon spectrum) is derived from a harmonic restoring force between the nearest neighbors, whereas the coupling in the latter (band structure) originates from the assumption that a tightly-bound electron has some finite coupling with its nearest neighbors. The physics underlying the quantized theory of phonons and band structure is ultimately linked to the periodicity of the arrangement of the carbon atoms that constitute the lattice. Any hexagonal honeycomb lattice has the same phonon characteristics except the magnitudes of the force components. The band structure is as a result of the hexagonal arrangement of sp^2 carbon atoms.

Similarly, solving for the off-diagonal element yields the dispersion relation

$$\varepsilon(k) = \exp(-ik_y a) + \exp(-ik_x \frac{\sqrt{3a}}{2}) \exp(-ik_y \frac{a}{2}) + \exp(-ik_x \frac{\sqrt{3a}}{2}) \exp(-ik_y \frac{a}{2})$$

$$\varepsilon(k) = \exp(-ik_y a) + 2\exp(ik_y \frac{a}{2}) \cos(k_x \frac{\sqrt{3a}}{2}) \tag{2.27}$$

Simplifying further gives the magnitude of $\varepsilon(k)$

$$\varepsilon(k) = \left\{ (\exp(-ik_y a) + 2\exp(ik_y \frac{a}{2}) \cos(k_x \frac{\sqrt{3a}}{2})) \times (\exp(ik_y a) + 2\exp(-ik_y \frac{a}{2}) \cos(k_x \frac{\sqrt{3a}}{2})) \right\}^{1/2}$$

$$\varepsilon(k) = \left\{1 + 2\exp(-k_x \frac{3a}{2})\cos(k_x \frac{\sqrt{3a}}{2}) + 2\exp(ik_y \frac{3a}{2})\cos(k_x \frac{\sqrt{3a}}{2}) + 4\cos^2(k_x \frac{\sqrt{3a}}{2})\right\}^{1/2}$$

$$\pm\gamma_o \sqrt{\begin{matrix}1 + 2\exp(-k_x \frac{3a}{2})\cos(k_x \frac{\sqrt{3a}}{2}) + 2\exp(ik_y \frac{3a}{2})\cos(k_x \frac{\sqrt{3a}}{2}) \\ +4\cos^2(k_x \frac{\sqrt{3a}}{2})\end{matrix}} \quad (2.28)$$

of which $\varepsilon(k) = \pm\sqrt{|f(k)|^2}$ has been employed in the derivation of the band structure.

Visualizing Band Structure of Graphene

The study of the energy band structure of graphene yields several unique physical characteristics, which are particularly helpful in visualizing its band structure. The energy $\varepsilon(k)$ associated with each of these vectors is obtained by the tight-binding model. Figure 11(a and b) depict the band of graphene structure visualized in three dimensions. The solution to $\varepsilon(k)$ comprises of each two values of k. The magnitude of the values is the same but opposite in sign. In such a scenario, the 3D plot of the band structure of graphene is symmetric about the plane $\varepsilon(k) = 0$. This direct result is obtained by considering the energy to be equal to zero in the tight-binding approximation [77, 78]. The band structure around the k and k' in the first Brillouin zone is roughly conical. Geometrically, $\varepsilon(k)$ is flat in this region and therefore, its second derivatives are zero. As a result, the most important property of an ideal graphene is obtained. That is, the effective mass of a Bloch state is zero at k and k' locations. This is because in k and k' valleys, electrons are massless fermions and require

a relativistic quantum mechanical model (Dirac equation) to be solved. For this purpose, electrons near the Dirac point (k and k') are referred to as massless Dirac fermions [78].

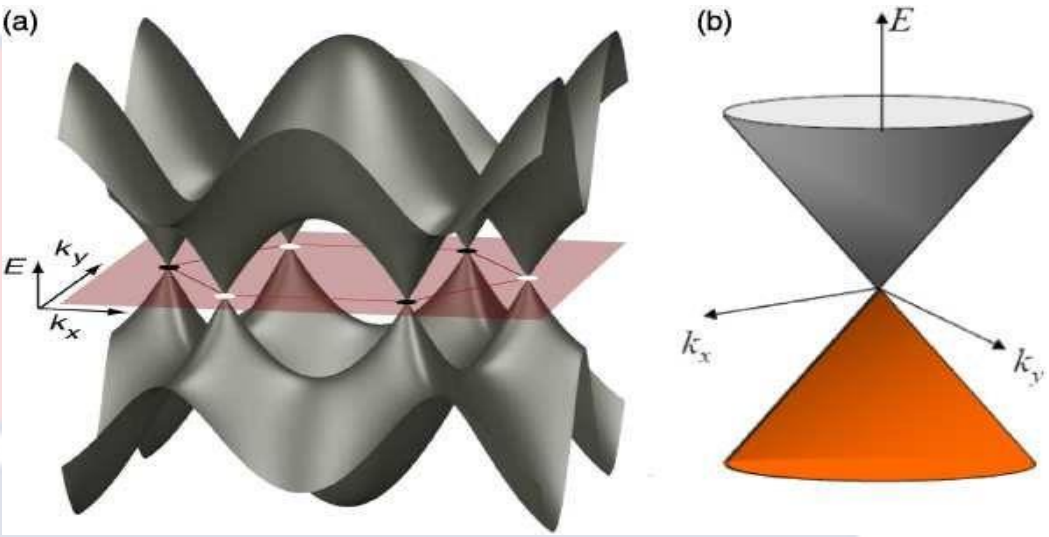

Figure 11: (a) A three-dimensional plot of the band structure of graphene [79]. (b) A three-dimensional visualization of the band structure as it approaches $E = 0$ at special points k and k' [79].

Applications of Graphene

Graphene is a promising material for electronics and photonics applications as well as for gas sensors. When gas molecules collide with graphene, their electrical characteristics are altered in a detectable way, allowing for gas detection [78]. As a result of its large surface area, graphene has potential uses as a support material in catalysis [79], as electrode material in electrochemical applications such as batteries and supercapacitors. Graphene layer structures act as a barrier to nanoparticle aggregation in the catalyst or electrode material. This is because of the enormous surface-to-volume ratio and highly conductive nature of graphene. The use of reduced graphene oxide

(RGO) or chemically derived graphene (CDG) based materials as anode or cathode in Li-ion battery technology stimulates the recent advancement in the sector. The development of nanopores and defects in the CDG by chemical synthesis promotes lithium insertion active sites, which are critical in Li battery technology.

The Boltzmann Transport Equation

The semi-classical theories of transport processes are founded on the Boltzmann Transport Equation (BTE). The BTE governs the statistical distribution of particles in liquid, solid, or gas, and it is the most fundamental equations in non-equilibrium statistical mechanics. It is frequently used to study heat, mass, charge, and spin transport processes, as well as to derive electrical conductivity, thermal conductivity, spin conductivity, and Hall conductivity in materials. The BTE is obtained by first defining a parameter known as the distribution function and then analyzing its variation over time. The distribution function describes how the particles of interest are distributed in real and momentum spaces, as well as how the distribution changes over time. The basic principle underlying the BTE is charge conservation. Each particle (such as phonon or an electron) is assumed to have momentum and space coordinates. A distribution function $f(r,k,t)$ counts the number of particles occupying each set of coordinates in momentum and space, as defined by either Bose-Einstein statistic for bosons (phonons) or Fermi-Dirac statistics for fermions (electrons). However, in momentum and space the particles are conserved by equating the total rate of change in time to the change in the distribution function caused by various scattering mechanisms [80].

Using the product rule, and expanding the gradient as in [81] yields;

$$\frac{df(r,k,t)}{dt} = \frac{\partial f}{\partial t} + \frac{\partial f}{\partial x}\frac{\partial x}{\partial t} + \frac{\partial f}{\partial k}\frac{\partial k}{\partial t} = \left(\frac{\partial f}{\partial t}\right)|_{scat} \quad (2.29)$$

The velocity of the electron is given by the time derivative of the position. i.e., $\frac{dx}{dt} = v(k)$. The velocity is determined by the gradient of the electron band structure.

$$\vec{v}(k) = \frac{1}{\hbar}\frac{d\vec{E}(k)}{dk} \quad (2.30)$$

The momentum derivative is identified with the effect of the electric field as:

$$\frac{dk}{dt} = \frac{eF(x)}{\hbar} \quad (2.31)$$

where e is the charge of the electron, $F(x)$ is the applied electric field at a given position.

The exact solution of the general BTE in Eqn. (2.29) BTE, which can be derived by considering more details on electron conservation [82].

$$\frac{\partial f}{\partial t} + v(k)\frac{\partial f}{\partial x} + \frac{eF(x)}{\hbar}\frac{\partial f}{\partial k} = \delta f|_{scat} \quad (2.32)$$

The BTE in Eqn. (2.29) represents a first-order partial differential equations in space, momentum and time dimensions. One advantage of using this formulation to solve for the distribution function is that the total charge along the transverse direction of the sheet is obtained by simply multiplying the electronic charge, *e* by distribution function and integrate over momentum.

$$\rho(x,t) = e\int f(x,k,t)dk \quad (2.33)$$

The electric field strength along the sheet can now be obtained using the charge density. Similarly, the current density is calculated by integrating all of the momentum states' velocities, weighted by their distribution.

$$j(x,t) = e\int v(k)f(x,k,t)dk \qquad (2.34)$$

Once the equilibrium state distribution function $f(r,k,t)$ is known, Eqn. (2.29) can be used to calculate the current. The Poisson equation below is used to achieve the coupling between externally applied potentials and electronic transport as:

$$\nabla^2 v(x) = \frac{d^2 v(x)}{\partial x^2} = \frac{\rho(x)}{\varepsilon} \qquad (2.35)$$

Electron Scattering Rates

The force term in Eqn. (2.30) i.e. $\frac{\partial k}{\partial t}$ is the change in the distribution function as a result of collisions. Electron interacts with quantized physical vibration as of harmonic nature (phonons), as well as other excitations and other electrons. For ballistic transport, the distribution occurs or advert in momentum and space under the influence of the velocity of the electron and amplified field [80]. The scattering process brings the distribution function to a stable state after some initial transient time. The collision integral is then calculated by considering the probability of transitions from one momentum state k to another state k', given by $S(k,k')$ and the reverse is $S(k',k)$. The probability of occupation of these states is dictated by the distribution functions $f(k)$ and $f(k')$. The scattering-out of a state k term is $S(k,k')f(k)$ and the scattering-into a state k is $S(k',k)f(k')$. Integrating the difference over all the states k' gives the total change in the distribution function due to the collision [83] as:

$$\frac{df(x,k,t)}{dt} = \int dk'[S(k,k')f(x,k,t) - S(k',k)f(x,k',t)] \quad (2.36)$$

The probabilities scattering states such as $S(k,k')$ and $S(k',k)$ are obtained using perturbation the in the quantum approach, by including the appropriate probabilities or scattering statistics [84]. This calculation can also be extended to include Pauli's exclusion principle, which states that not more than one electron can occupy the same quantum mechanical state. This principle translates into an additional factor which counts the probability of a final state not being available, denoted by $(1-f(k))$. Substituting this term complicates the expression for the scattering integral.

$$\delta|_{scat} = \int dk'[S(k,k')f(k)(1-f(k')) - S(k',k)(1-f(k))(f(k')] \quad (2.37)$$

A tractable form can be derived from Eqn. (2.38) by assuming that the distribution function perturbed slightly from its equilibrium position by a small factor, denoted by $\delta f(x,k,t)$ is

$$\frac{d}{dt}(f_{eq}+\delta f) = \int dk'[S(k,k')(f_{eq}+\delta f) - S(k',k)(f_{eq}+\delta f')] \quad (2.38)$$

The equilibrium distribution function, given by Fermi-Dirac statistics in a steady state is expressed as:

$$f_{eq}(x,k,t) = \left[\exp\left(\frac{E(k)-E_F(x)}{k_BT}\right)+1\right]^{-1} \quad (2.39)$$

However, the overall scattering integral in equilibrium is zero as expressed in [85] as:

$$\frac{df_{eq}(x,k,t)}{dt} = \int dk'[S(k,k')f_{eq}(x,k,t) - S(k',k)f_{eq}(x,k't)] = 0 \quad (2.40)$$

This is known as the principle of detailed balance, as each process is exactly balanced out by an opposite but equal component, causing no net change to the distribution function.

$$\frac{d\delta f_{eq}(x,k,t)}{dt} = \int dk'[S(k,k')\delta f_{eq}(x,k,t) - S(k',k)\delta f_{eq}(x,k',t) \tag{2.41}$$

where $f_{eq}(x,k,t) = \delta f_{eq}(x,k,t)$

The perturbed term δf, is predominantly an odd function in term of momentum i.e. $\delta f(x,k,t) = \delta f(x,-k,t)$, but the scattering probabilities $S(k,k')$ and $S(-k,k')$ are even functions i.e. $S(k,k') = S(-k,k')$. This gives an equal simplified expression for scattering out and into a state.

$$\frac{d\delta f(x,k,t)}{dt} = \delta f(x,k,t)\int S(k,k')dk' \tag{2.42}$$

The integral taken over all the scattering probabilities produces the total scattering rate

$$\Gamma(k) = \frac{1}{\tau_m(k)} = \int S(k,k')dk' \tag{2.43}$$

This probability is calculated to first order from Fermi Golden Rule [83, 84] as:

$$S(k,k')dk' = \frac{2\pi}{\hbar}|H(k,k')|^2\,\delta(E(k) - E(k') \pm \hbar\omega(q)) \tag{2.44}$$

where H is the matrix element, and $\omega(q)$ is the phonon frequency. The plus and minus signs $(\pm)$ denotes absorption and emission respectively.

Using the rigid pseudo-ion approximation [86] for the matrix element, Eqn. (2.44) is simplified as:

$$\begin{aligned} S(k,k')dk' = {} & \frac{2\pi}{\hbar}\frac{|D(q)|^2 I^2(q)}{\rho\omega(q)} \\ & \times \left(N(x,q.t) + \frac{1}{2} \pm \frac{1}{2}\right)\delta(E(k) - E(k') \pm \hbar\omega(q)) \end{aligned} \tag{2.45}$$

where $|D(q)|^2$ is the result of matrix element calculation from the Fermi golden rule. The application of this formula requires numerical integration over the whole momentum space and the inclusion of complete electron and phonon dispersion laws [85, 86]. This gives the probability of scattering from each position in momentum space.

From Eqn. (2.46), the slightest perturbation to the equilibrium distribution function relaxes the system back to equilibrium state with a time-constant approximately equal to the relaxation time, τ such that

$$\frac{df(x,k,t)}{dt} = \frac{\delta f(x,k,t)}{\tau_m(k)} = \frac{f(x,k,t) - f_{eq}(x,k,t)}{\tau_m(k)} \tag{2.46}$$

This time dependent solution of the BTE in Eqn. (2.46) denotes a balance between drift and diffusion which acts to displace the distribution function from equilibrium, and the scattering again acts to return the system back to its equilibrium position through the relaxation time [85, 88, 89].

Electron-Phonon Interaction

Phonons are the principal medium of energy and momentum exchange between electrons and their surrounding excitations in nanostructured materials. The exchange of energy and momentum depends on the relaxation time approximation τ [90, 91], where the net transfer rate is determined by the rate at which energy flows out of the electron gas by phonon emission [86] and the rate at which energy flows into the electron gas by phonon [66, 92] from the lattice vibrations. The energy exchange between electrons and longitudinal acoustic phonons may lead to two major conditions namely: (1) deformation

potential scattering [93, 94] in the material which is a result of the charge carriers undergoing inelastic scattering, and (2) piezoelectric interaction [93].

The electron distribution of a system is affected, when phonons impart momentum to electrons. Thus, the electron tends to carry energy as they are dragged along the axis of the phonon stream which results in a phonon called drag. In the case of phonon drag, the BTE for the phonon and electron distribution are solved simultaneously coupled by the phonon drag term in [95]. The reverse is also true when the electron impacts momentum to the phonons. This results in electron emitting phonons which leads to amplification of the phonons when the drift electrons velocity exceeds the sound velocity of the material [96]. The fundamental Hamiltonian for the electron-lattice system is given as:

$$H = \sum \frac{p_k^{\,2}}{2M} + \frac{1}{2}\sum_{kk'} \frac{e^2}{|k_k - k_{k'}|} + \sum_i \frac{p_i^{\,2}}{2M} + \frac{1}{2}\sum_{ii'}{}' v_{ion}(R_i - R_{i'}) + \sum_{ki} v_{el-ion}(r_k - R_i) \tag{2.47}$$

where the first two terms constitute $H_{electron}$, the third and fourth terms H_{ion} and the last term is $H_{electron-ion}$. The wavefunction is denoted by:

$$\Psi = \psi(r_1, r_2, r_3 \ldots)\varphi(R_1, R_2, R_3 \ldots) \tag{2.48}$$

The electron-ion interaction term can be separated into two parts: the interaction of electrons with ions in their equilibrium positions, and an additional term due to lattice vibrations:

$$H_{el-ion} = H^{o}_{el-ion} - H_{el-ph} \tag{2.49}$$

and

$$\sum_{ki} v_{el-ion}(r_k - R_i^o) = \sum_{ki} v_{el-ion}[k_k - (R_i + s_i)] \tag{2.50}$$

where R_i^o is the equilibrium lattice site position and s_i is the displacement of the atoms from their equilibrium positions in a lattice vibration so that;

$$H_{el-ion}^o = \sum_{ki} v_{el-ion}(r_k - R_i^o) \tag{2.51}$$

and

$$H_{el-ph} = -\sum_{ki} s_i . \nabla v_{el-ion}(r_k - R_i^o) \tag{2.52}$$

In solving the Hamiltonian, an adiabatic approximation, which solves the electronic part of the Hamiltonian, is required and considering an ion localized at a position R_i and at a displacement u_i from its equilibrium position R_i^o. Combining the interaction Hamiltonian of the electronic charge density with the ions, yields;

$$H_{\text{int}} = \sum_{i\vec{\sigma}} \int d^3 r \Psi_{\vec{\sigma}}^{\dagger}(r) \Psi_{\vec{\sigma}}(r) u_i v(r - R_i) \tag{2.53}$$

For small amplitude vibration, Eqn. (2.53) can be expressed in the power of u_i as,

$$\begin{aligned} H_{\text{int}} = & \sum_{i\vec{\sigma}} \int d^3 r \Psi_{\vec{\sigma}}^{\dagger}(r) \Psi_{\vec{\sigma}}(r) u_i v(r - R_i) \\ & + \sum_{i\vec{\sigma}} \int d^3 r \Psi_{\vec{\sigma}}^{\dagger}(r) \Psi_{\vec{\sigma}}(r) u_i . \nabla v_{R_i} v(r - R_i)_{R_i^o} + \ldots \end{aligned} \tag{2.54}$$

The field operators $\Psi_{\vec{\sigma}}$ expanded in terms of the Bloch waves by employing the Bloch theorem, yields;

$$\Psi(r) = \sum_{k} a_{\vec{k},\vec{\sigma}} \Psi_{\vec{\sigma}}(r) \tag{2.55}$$

where

$$\Psi_{\vec{k}\vec{\sigma}}(r) = e^{ik.R_i^o} \Psi_{\vec{k}}(r) \tag{2.56}$$

and $\Psi_k(r)$ has the same periodicity as the lattice. Employing the periodicity of $\nabla R_i^o v(r - R_i^o)$ and a shift by a Bravais lattice vector yield;

$$\begin{aligned} &\int d^3 r \Psi^*_{k'\vec{\sigma}}(r) \Psi_{k\vec{\sigma}}(r) \nabla R_i^o (r - R_i^o) \\ &\quad = \int d^3 r \Psi^*_{k'\vec{\sigma}}(r + R_i^o) \Psi_{k\vec{\sigma}}(r + R) \nabla R_i^o (r - R_i^o) \\ &\quad = e^{i(k-k'R_i^o)} \int d^3 r \Psi^*_{k'\vec{\sigma}}(r) \Psi_{k\vec{\sigma}}(r) \nabla R_i^o (r - R_i^o) \end{aligned} \tag{2.57}$$

$$W_{kk}' = \int d^3 r \Psi^*_{k'\vec{\sigma}}(r) \Psi_{\vec{k}\vec{\sigma}}(r) \nabla R_i^o (r - R_i^o) \tag{2.58}$$

In the second quantization formalism, the displacement u_i gives

$$u_i(t) = \frac{1}{\sqrt{NM}} \sum_{k\lambda} Q(k,t) e^{\lambda}(k) e^{ik.R_i^o}$$

with

$$Q\lambda(\tilde{q}) = \frac{1}{\sqrt{2\omega\lambda(q)}} (b_{\lambda}(q) + b^{\dagger}(-q)) \tag{2.59}$$

The interaction Hamiltonian can be written as;

$$
\begin{aligned}
H_{\text{int}} &= \sum_{kk'\sigma} a^{\dagger}{}_{k'\sigma} a_{k\sigma} \sum_{j} W_{kk'} e^{i(k-k').R_j^o} \frac{1}{\sqrt{NM}} \sum_{q\lambda} Q\lambda(q) e^{\lambda}(q) e^{iq.R_j^o} \\
&= \sum_{kk'\sigma} \sum_{\lambda} a^{\dagger}{}_{k'\sigma} a_{k\sigma} (W_{kk'} e^{\lambda}(q)) Q_{\lambda}(q) \sqrt{\frac{N}{M}} \qquad (2.60) \\
&= \sum_{kk'\sigma} gkk'\lambda a^{\dagger}{}_{k'\sigma} a_{k\sigma} (b_{\lambda}(q) + b_{\lambda}{}^{\dagger}(-q))
\end{aligned}
$$

where q is the momentum conservation interpreted as:

$$q = k - k' + G \qquad (2.61)$$

and k is the wave vector of the incident wave, k' is the wave vector of the reflected wave, with G being a vector of the reciprocal lattice [67,73]. The lattice coupling constant is

$$gkk'\lambda = (W_{kk'} e^{\lambda}(q)) \sqrt{\frac{N}{2M\omega_{pl}^{im}(q)}} \qquad (2.62)$$

Examining the Hamiltonian of the many-body particles and their mutual interactions, the interaction between two fields is introduced via minimal coupling, $\hat{p} \to \hat{p} - e/cA$. The carrier density Hamiltonian is given as:

$$
\begin{aligned}
\hat{H} &= \int d^3 r \Psi^{+}(r,t) \left[-\frac{\hbar^2}{2m} \nabla^2 + v(r) \right] \Psi^{\dagger}(r,t) \\
&= \int d^3 r \sum_{n} \hat{b}_n^{\dagger} \Psi_n^{\dagger}(r,t) \left[-\frac{\hbar^2}{2m} \nabla^2 + v(r) \right] \Psi(r,t) \sum_{n'} \hat{b}_{n'} \Psi_{n'}(r)
\end{aligned}
$$

$$\hat{H} = \hat{H}_{mp} + \hat{H}_{ion} + \hat{H}_{\text{int}} \qquad (2.63)$$

where $\hat{H}_{mp}$ is the many-particle Hamiltonian and equals $\hat{H}_{electron}$. The electronic states for free-particle Hamiltonian in the presence of a magnetic field $\hat{H}$ is described by the Schrödinger equation.

$$\frac{1}{2m}\left(p-\frac{e}{c}A\right)^2\Psi_r = E\Psi_r, \qquad A(0,H_x,0) \tag{2.64}$$

Ignoring the electron spin, the total Hamiltonian in momentum space is expressed as:

$$H=\sum_p \frac{\left(p-\frac{e}{c}A\right)^2}{2m} a_p^{\dagger}a_p + \sum \omega_k (b_k^{\dagger}b_k) + \sum_{p,k} g_{pk} a_{p+k}^{\dagger} a_k (b_{p,k} + b_{p,k}^{\dagger}) \tag{2.65}$$

Chapter Summary

The chapter reviewed the dynamics of electron-phonon transport in the semiclassical regime using the BTE. The phenomena of nanoscale transport were reviewed as well as the theoretical overview of graphene band structure using the tight-binding approach.

CHAPTER THREE

METHODOLOGY

Introduction

This chapter outlines the physical concepts, theories, and phenomena used in understanding electron transport in graphene superlattices. Electron transport in a material has been a major focus of experimental and theoretical research since Esaki-Tsu's seminal publication on electron transport in semiconductor superlattices. The Boltzmann Transport Equation is solved using momentum-independent relaxation time and the semiclassical approach. Moreover, the thermoelectric metrics such as the carrier current density $\vec{J}_x$, electrical charge conductivity σ_x, electrical resistivity ρ_x, thermoelectric power a_x, and electrical power factor p_x of a two-dimensional graphene superlattice exposed to combined dc and ac fields are derived analytically. The results of these derived quantities were calculated as a function of temperature T, carrier-phonon interaction Δ_1 and Δ_2, and the carrier concentration n_o. The calculation is done using the theoretical approach developed by Mensah et al. [97] based on the phenomenological model developed in Ref. [98]. The results of these calculations are analyzed in chapter four.

Carrier Current Density of GSL

Consider a GSL placed in an electric field $\vec{E}(t)$ parallel to the horizontal axis under a temperature gradient ∇T. The current density in the GSL is

calculated in the semiclassical approximation by starting with the BTE expressed as:

$$\frac{df}{dt}+\vec{v}(p)\frac{\partial f(\vec{r},\vec{p},t)}{\partial r}+e\vec{E}\frac{\partial f(\vec{r},\vec{p},t)}{dp}=-\frac{f(\vec{r},\vec{p},t)-f_o(\vec{p})}{\tau} \tag{3.1}$$

Here, $\vec{E}(t)=\vec{E}_o+\vec{E}_1 cos\omega t$ and $f(\vec{r},\vec{p},t)$ is the non-equilibrium distribution function, $f_o(\vec{p})$ is the distribution function at equilibrium, $\vec{v}(\vec{p})$ is the electron velocity, $\vec{E}_o(\vec{E}_{ox},\vec{E}_{oy})$ is the constant electric field, $\vec{E}_1(\vec{E}_x,\vec{E}_y)$, and ω are amplitude and frequency of the ac-field, respectively, t is time elapsed, $\vec{p}$ is the dynamical electron momentum, τ is the relaxation time of electron and e is the charge of an electron. The collision integral is taken in the τ approximation and further assumed to be constant. The direct solution of Equation (3.1) is difficult; therefore, it is solved using perturbation theory.

The solution to the BTE for an electron in the lowest miniband is given in the linear approximation of $\nabla\mu$ and ∇T as:

$$f(\vec{p})=\tau^{-1}\int_0^{\infty}dt\exp(-t/\tau)f_o\left(\vec{p}-e\int_{t-t'}^{t'}\left[\vec{E}_o+\vec{E}_1\cos(\omega t")\right]dt"\right)$$

$$+\tau^{-1}\int_0^{\infty}dt\exp(-t/\tau)\left\{\left[\varepsilon\left(\vec{p}-e\int_{t-t'}^{t'}\left[\vec{E}_o+\vec{E}_1\cos(\omega t")-\mu\right]dt"\right)\right]\frac{\nabla T}{T}+\nabla\mu\right\}$$

$$\times v\left(\vec{p}-e\int_0^{\infty}\left[\vec{E}_o+\vec{E}_1\cos(\omega t')\right]dt'\right)\frac{\partial f_o}{\partial\varepsilon}\left(\vec{p}-e\int_{t-t'}^{t'}\left[\vec{E}_o+\vec{E}_1\cos(\omega t")\right]dt"\right) \tag{3.2}$$

where $\varepsilon(k)$ is the electron energy obtained in the tight-binding approximation, and μ is the chemical potential.

(Refer to Appendix A).

The current density is defined as;

$$\vec{J} = -e\sum_{p} v(\vec{p}) f(\vec{p}) \tag{3.3}$$

When Eqn. (3.2) is substituted into Eqn. (3.3) it yields;

$$\vec{J} = e\tau^{-1}\sum_{p} v(\vec{p})\int_{0}^{\infty} dt \exp(-t/\tau) f_o\left(\vec{p} - e\int_{t-t'}^{t'}\left[\vec{E}_o + \vec{E}_1\cos(\omega t")\right]dt"\right)$$

$$+ e\tau^{-1}\int_{0}^{\infty} dt \exp(-t/\tau)\sum_{p} v(\vec{p})\left\{\left[\varepsilon\left(\vec{p} - e\int_{t-t'}^{t'}\left[\vec{E}_o + \vec{E}_1\cos(\omega t")\right]dt"\right)\right]\frac{\nabla T}{T} + \nabla\mu\right\}$$

$$\times v\left(\vec{p} - e\int_{t-t'}^{t'}\left[\vec{E}_o + \vec{E}_1\cos(\omega t")\right]dt"\right)\frac{\partial f_o}{\partial\varepsilon}\left(\vec{p} - e\int_{t-t'}^{t'}\left[\vec{E}_o + \vec{E}_1\cos(\omega t")\right]dt"\right) \tag{3.4}$$

Making the substitution $\left(\vec{p} - e\int_{t-t'}^{t'}\left[\vec{E}_o + \vec{E}_1\cos(\omega t")\right]dt"\right) \to \vec{p}$ the current density is obtained as:

$$\vec{J} = e\tau^{-1}\int_{0}^{\infty} dt \exp(-t/\tau)\sum_{p} v\left(\vec{p} - e\int_{t-t'}^{t'}\left[\vec{E}_o + \vec{E}_1\cos(\omega t")\right]dt"\right) f_o(\vec{p})$$

$$+ e\tau^{-1}\int_{0}^{\infty} dt \exp(-t/\tau)\sum_{p} v(\vec{p})\left\{\left[\varepsilon(\vec{p}) - \mu\right]\frac{\nabla T}{T} + \nabla\mu\right\}$$

$$\times v\left(\vec{p} - e\int_{t-t'}^{t'}\left[\vec{E}_o + \vec{E}_1\cos(\omega t")\right]dt"\right)\frac{\partial f_o}{\partial\varepsilon} v(\vec{p}) \tag{3.5}$$

where the integration is carried out over the first Brillouin zone (See Appendix A).

The dispersion relation of graphene superlattice obtained within the tight-binding is expressed as [62] :

$$\varepsilon(\vec{p}) = \sqrt{\Delta^2 + {\Delta_1}^2\left(1 - \cos\frac{p_x d_1}{\hbar}\right) + {\Delta_1}^2\left(1 - \cos\frac{p_y d_2}{\hbar}\right)} \tag{3.6}$$

Using the Binomial theorem of half-integers, Eqn. (3.6) is expressed as:

$$\varepsilon(\vec{p}) = D - \Delta_x \cos\frac{p_x d_1}{\hbar} - \Delta_y \cos\frac{p_y d_2}{\hbar} \tag{3.7}$$

where $D = \sqrt{\Delta^2 + \Delta_1^{\,2} + \Delta_2^{\,2}}$ is the outer-shell energy of the carrier in an isolated carbon atom, $\Delta_x = \frac{\Delta_1^{\,2}}{2D}$ and $\Delta_y = \frac{\Delta_2^{\,2}}{2D}$ are the real overlapping integral for jumps along the respective coordinate, p_x and p_y are the components of the momentum along the respective graphene superlattice axes. (See Appendix B).

The equilibrium distribution function of the carriers is given by the Fermi-Dirac statics as:

$$f_o(\vec{p}_x) = \frac{1}{1+\exp[(\varepsilon(\vec{p}_x) - \mu)/k_B T]} \tag{3.8}$$

where k_B is the Boltzmann's constant, and T is the absolute temperature in energy units. Substituting Eqn. (3.7) into Eqn. (3.8) yields an equation with the term $\xi_{1/2}$, representing Fermi Dirac integral, which is expressed as:

$$\xi_{1/2}(\eta_f) = \frac{1}{\Gamma(1/2)}\int_0^{\infty}\frac{\eta_f^{\,1/2}d\eta}{1+\exp(\eta-\eta_f)} \tag{3.9}$$

where $(\mu - \varepsilon_c)/k_B T \equiv \eta_f$. For non-degenerate carrier gas, where the Fermi level is below the conduction band edge, Eqn. (3.8) is simplified as:

$$f_o(\vec{p}) = C.\exp\left(-\frac{\varepsilon(\vec{p}) + \mu}{k_B T}\right) \tag{3.10}$$

The normalized constant C is expressed as:

$$C = \frac{d_1 d_2 n_o}{2a_o I_o(k_1) I_o(k_2)}\exp\left(\frac{D-\mu}{k_B T}\right) \tag{3.11}$$

where n_o is the surface carriers concentration, a_o is the graphene sheet width, $I_o(x)$ modified Bessel function, $k_1 = \frac{\Delta_x}{k_B T}$ and $k_2 = \frac{\Delta_y}{k_B T}$

(Refer to Appendix B).

The miniband velocity of electron along the x-direction is obtained as:

$$\vec{v}_x(\vec{p}) = \frac{\partial \varepsilon(\vec{p})}{\partial \vec{p}_x} = \frac{\Delta_x d_1}{\hbar} \sin \frac{\vec{p}_x d_1}{\hbar}$$

Making the transformation $\left(\vec{p} - e \int_{t-t'}^{t'} \left[\vec{E}_o + \vec{E}_1 \cos(\omega t") \right] dt" \right) \to \vec{p}$

$$\vec{v}_x \left(\vec{p} - e \int_{t-t'}^{t'} \left[\vec{E}_o + \vec{E}_1 \cos(\omega t") \right] dt" \right) = \frac{\Delta_x d_1}{\hbar} \sin \frac{d_1}{\hbar} \left(\vec{p} - e \int_{t-t'}^{t'} \left[\vec{E}_o + \vec{E}_1 \cos(\omega t") \right] dt" \right) \quad (3.12)$$

(Refer to Appendix B)

The current density along the x-coordinate becomes:

$$\vec{J}_x = e\tau^{-1} \int_0^{\infty} dt \exp(-t/\tau) \sum_p v_x \left(\vec{p} - e \int_{t-t'}^{t'} \left[\vec{E}_o + \vec{E}_1 \cos(\omega t") \right] dt" \right) f_o(\vec{p})$$
$$+ e\tau^{-1} \int_0^{\infty} dt \exp(-t/\tau) \sum_p v(\vec{p}) \left\{ \left[\varepsilon(\vec{p}) - \mu \right] \frac{\nabla_x T}{T} + \nabla_x \mu \right\}$$
$$\times \vec{v} \left(\vec{p} - e \int_{t-t'}^{t'} \left[\vec{E}_o + \vec{E}_1 \cos(\omega t") \right] dt" \right) \frac{\partial f_o}{\partial \varepsilon} \vec{v}_x(\vec{p}) \quad (3.13)$$

Using the transformation $\sum_p \to \frac{2}{(2\pi\hbar)^2} \int_{-\pi/d_1}^{\pi/d_1} d\vec{p}_x \int_{-\pi/d_2}^{\pi/d_2} d\vec{p}_y$ (3.13) becomes

$$\vec{J}_x = \frac{2e\tau^{-1}}{(2\pi\hbar)^2} \int_0^{\infty} dt \exp(-t/\tau) \int_{-\pi/d_1}^{\pi/d_1} d\vec{p}_x \int_{-\pi/d_2}^{\pi/d_2} d\vec{p}_y \vec{v}_x \left(\vec{p} - e \int_{t-t'}^{t'} \left[\vec{E}_o + \vec{E}_1 \cos(\omega t") \right] dt" \right) f_o(\vec{p})$$
$$+ \frac{2e\tau^{-1}}{(2\pi\hbar)^2} \int_0^{\infty} dt \exp(-t/\tau) \int_{-\pi/d_1}^{\pi/d_1} d\vec{p}_x \int_{-\pi/d_2}^{\pi/d_2} d\vec{p}_y \left\{ \left[\varepsilon(\vec{p}) - \mu \right] \frac{\nabla_x T}{T} + \nabla_x \right\}$$
$$\times \vec{v} \left(\vec{p} - e \int_{t-t'}^{t'} \left[\vec{E}_o + \vec{E}_1 \cos(\omega t") \right] dt" \right) \frac{\partial f_o}{\partial \varepsilon} \vec{v}_x(\vec{p}) \quad (3.14)$$

where the integration is carried out within the first Brillouin zone $-\hbar\pi/d_1 \le dp_x \le \hbar\pi/d_1$ and $-\hbar\pi/d_2 \le dp_y \le \hbar\pi/d_2$, respectively. Eqn. (3.14) is solved explicitly and the current density is obtained as:

$$\vec{J}_x = -\sigma_x(\vec{E})\left(\vec{E}_n + \frac{\nabla_x \mu}{e}\right) - \sigma_x(\vec{E})\frac{k_B}{e}\left\{\left[\frac{D-\mu}{k_B T}\right] - k_1\frac{I_o(k_1)}{I_1(k_1)} + \frac{1}{2} - k_2\frac{I_1(k_2)}{I_o(k_2)}\right\}\nabla_x T \quad (3.15)$$

where $k_1 = \Delta_x / k_B T$ and $k_2 = \Delta_y / k_B T$. Hence

$$\vec{J}_x = -\sigma_x(\vec{E})\vec{E}'_{xn} - \sigma_x(\vec{E})\frac{k_B}{e}\left\{\left[\frac{D-\mu}{k_B T}\right] - k_1\frac{I_o(k_1)}{I_1(k_1)} + \frac{1}{2} - k_2\frac{I_1(k_2)}{I_o(k_2)}\right\}\nabla_x \quad (3.16)$$

where $\vec{E}'_{xn}$ is the external electric field along the x-direction given as $\vec{E}'_{xn} = \vec{E}_{xn} + \nabla_x \mu / e$ (Refer to Appendix D).

The electrical conductivity $\sigma_x(\vec{E})$ and electrical resistivity $\rho_x(\vec{E})$ are respectively obtained as:

$$\sigma_x(\vec{E}) = -\frac{e^2\tau\Delta_x d_1^2}{a_o\hbar^2}\frac{n_o I_1(k_1)}{I_o(k_1)}\sum_{n=-\infty}^{\infty}\left[\frac{J_n^2(\chi)}{1+(\Omega_x + n\omega\hbar)^2\tau^2}\right] \quad (3.17)$$

$$\rho_x(\vec{E}) = -\frac{1}{\frac{e^2\tau\Delta_x d_1^2}{a_o\hbar^2}\frac{n_o I_1(k_1)}{I_o(k_1)}\sum_{n=-\infty}^{\infty} J_n^2(\chi)\left[\frac{1}{1+(d_1 eE_o/\hbar + n\omega\hbar)^2\tau^2}\right]} \quad (3.18)$$

where Ω_x and χ are respectively the Bloch frequency and Bessel function along the x direction, and are given as $\Omega_x = d_1 eE_o/\hbar$ and $\chi = d_1 e\vec{E}_x/\hbar\omega$. (See to Appendix C).

In an open circuit, the differential thermo-power is defined as the ratio $\left|\frac{\vec{E}_{xn}}{\nabla_x T}\right|$.

Thus setting $\vec{J}_x = 0$ to zero in Eqn. (3.16), the thermo-power α_x along the x-direction is obtained as:

$$\alpha_x = \left|\frac{\vec{E}_{xn}}{\nabla_x T}\right| = -\frac{k_B}{e}\left\{\left[\frac{D-\mu}{k_B T}\right] - k_1 \frac{I_o(k_1)}{I_1(k_1)} + \frac{1}{2} - k_2 \frac{I_1(k_2)}{I_o(k_2)}\right\} \quad (3.19)$$

(Refer to Appendix D)

When the ac source is switched off, that is, if $\vec{E}_x = 0$ and $\omega = 0$, the electrical conductivity in Eqn. (3.17) reduces to:

$$\sigma_x(\vec{E}) = -\frac{e^2 \tau \Delta_x d_1^{\,2}}{a_o \hbar^2} \frac{n_o I_1(k_1)}{I_o(k_1)} \sum_{n=-\infty}^{\infty}\left[\frac{J_n^{\,2}(\chi)}{1+(\Omega_x \tau)^2}\right] \quad (3.20)$$

The electrical power factor along the x-direction of the GSL is given as:

$$P_x = \alpha_x^{\,2} \sigma_x \quad (3.21)$$

Therefore,

$$P_x = \left(\frac{k_B}{e}\left[\left(\frac{D-\mu}{k_B T}\right) - k_1 \frac{I_o(k_1)}{I_1(k_1)} + \frac{1}{2} - k_2 \frac{I_1(k_2)}{I_o(k_2)}\right]\right)^2$$

$$\times \frac{e^2 \tau \Delta_x d_1^{\,2} n_o}{\hbar^2 a_o} \frac{I_1(k_1)}{I_o(k_1)} \sum_{n=-\infty}^{\infty} J_n^{\,2}(\chi)\left[\frac{1}{1+(d_1 e E_o/\hbar + n\omega\hbar)^2 \tau^2}\right] \quad (3.22)$$

(See Appendix D)

Chapter Summary

In summary, analytical expressions have been derived for the carrier current density $\vec{J}$, electrical resistivity ρ_x, thermoelectrical power α_x, and electrical power factor P_x of graphene superlattice. These analytical

expressions were derived using the semiclassical Boltzmann's Transport Equation. It can be seen from these equations that ρ_x, α_x and P_x depend on the temperature T, carrier concentration n_o, and the overlapping integrals for jumps along the x and y directions.

CHAPTER FOUR

RESULTS AND DISCUSSION

Introduction

Expressions for the electrical resistivity ρ_x, thermoelectrical power α_x, and electrical power factor P_x of GSL were derived in chapter three using a tractable analytical approach. These derivations were carried out by solving the semi-classical BTE together with the energy dispersion relation of GSL obtained in the tight-binding approximation.

In this chapter, graphical representations of the analytical equations obtained for ρ_x, α_x and P_x in chapter three will be analyzed numerically using MATLAB (219b version). With appropriate values for d_1, a_o, ω , and τ, the dependence of ρ_x, α_x and P_x on temperature T, the dc field E_o, ac field intensity E_x, the material's carrier concentration n_o and the overlapping integrals for jumps $(\Delta_1 \text{and } \Delta_2)$ are investigated.

Electrical Resistivity of Graphene Superlattice

The relationship between the electrical resistivity of GSL and temperature given in Eqn. (3.18) is presented numerically as shown in Figures (12 — 18). With varying values of the of *dc* field intensity E_o, the dopant carrier concentration n_o, the ac field intensity E_x and the real overlapping integrals for jumps $(\Delta_{1,2})$.

Figure 12 represents the relationship between the electrical resistivity ρ_x and temperature T of GSL for different values of the dc field intensity E_0.

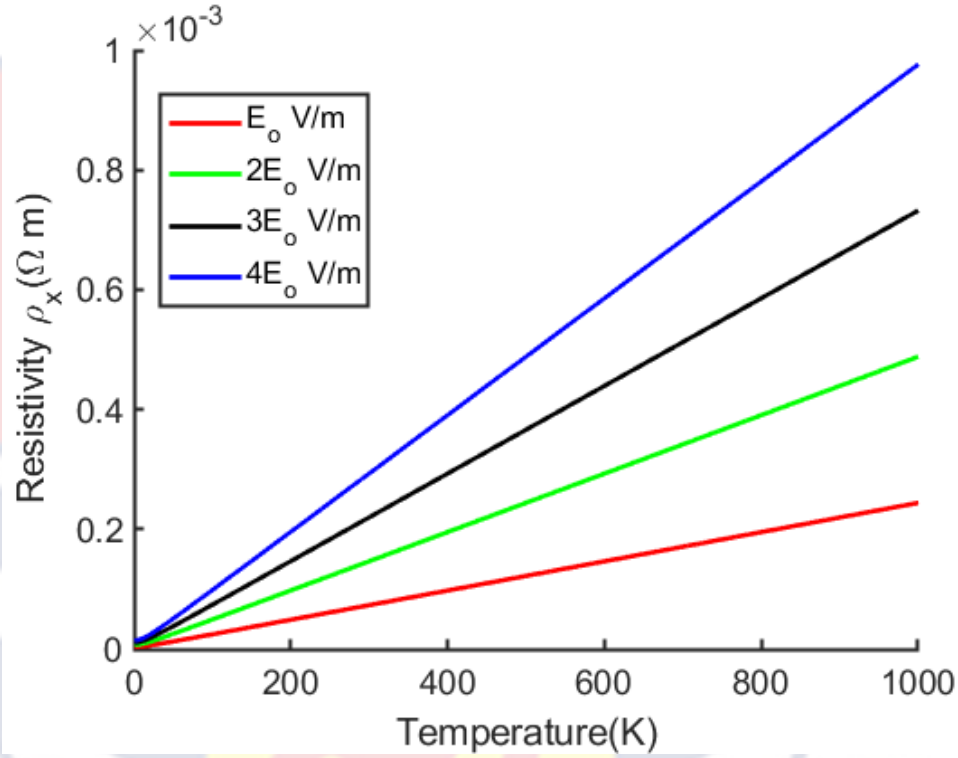

Figure 12: Dependence of resistivity of graphene superlattice on temperature for various values of E_o with $\Delta_2 = 0.024$ eV, $\Delta_1 = 0.012$ eV, $n_o = 10^{13}$ cm^{-3} and $E_x = 10^2$ V/m.

It is observed from Figure 12 that in the presence of the ac source, increasing the *dc* field from E_o to $4E_o$ increases the resistivity narrowly at low temperatures up to about 100 K and then increases marginally with increasing temperature. This behavior is as a result of the interactions of electrons and phonons which scatter the charge carriers in the GSL as temperature increases. This is to be expected because in high fields, interaction of carriers with the

lattice and other impurities increases, and this, increases the resistivity. Increasing the dc field energizes the electrons in the GSL to undergo intraminiband transport, resulting in low intramimniband current and low conductivity and thus high electrical resistivity.

Figure 13 displays the plot of the resistivity of GSL against temperature for a range of values of Δ_1 in the presents of combined dc-ac field.

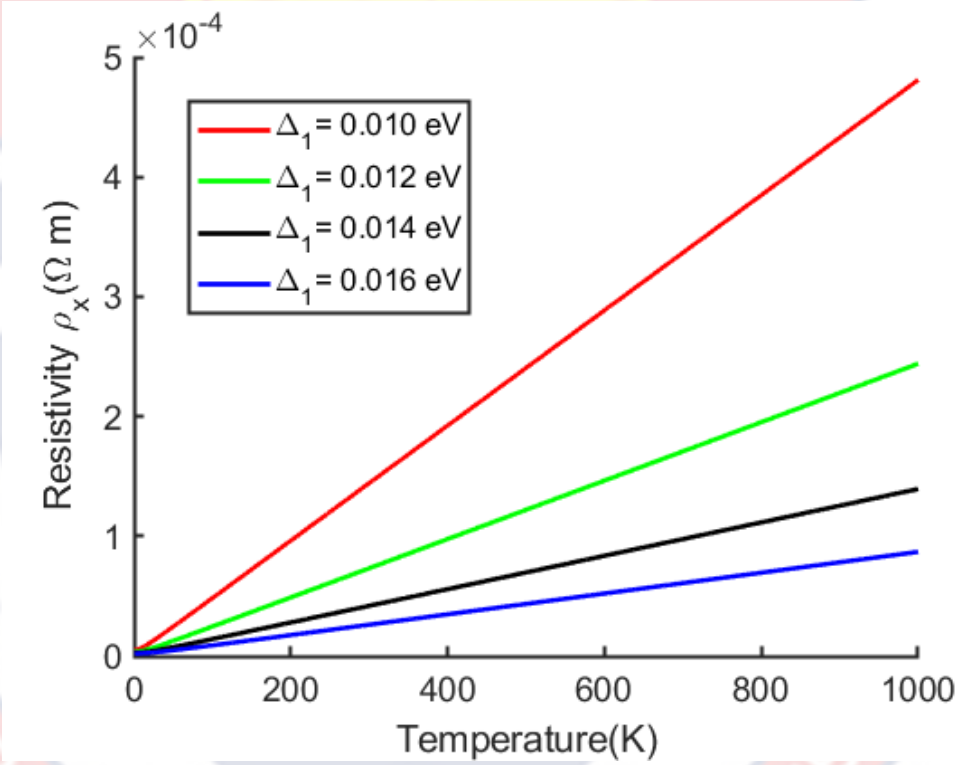

Figure 13: Dependence of resistivity of graphene superlattice on temperature for various values of Δ_1 with $\Delta_2 = 0.024$ eV, $n_o = 10^{13}$ cm^{-3}, $E_o = 10^7$ V/m, and $E_x = 10^2$ V/m.

From Figure 13, a significant decrease of the resistivity is observed for increasing Δ_1 while keeping Δ_2 constant. The plot shows that as Δ_1 increases,

the resistivity decreases. This is because increasing Δ_1 reduces the carrier scattering and so the differential conductivity increases and this decreases the resistivity.

Figure 14 illustrates the dependence of the resistivity of GSL on temperature for various values of Δ_2 with $\Delta_1 = 0.012$ eV, $n_o = 10^{13}$ cm^{-3}, $E_o = 10^7$ V/m, and $E_x = 10^2$ V/m.

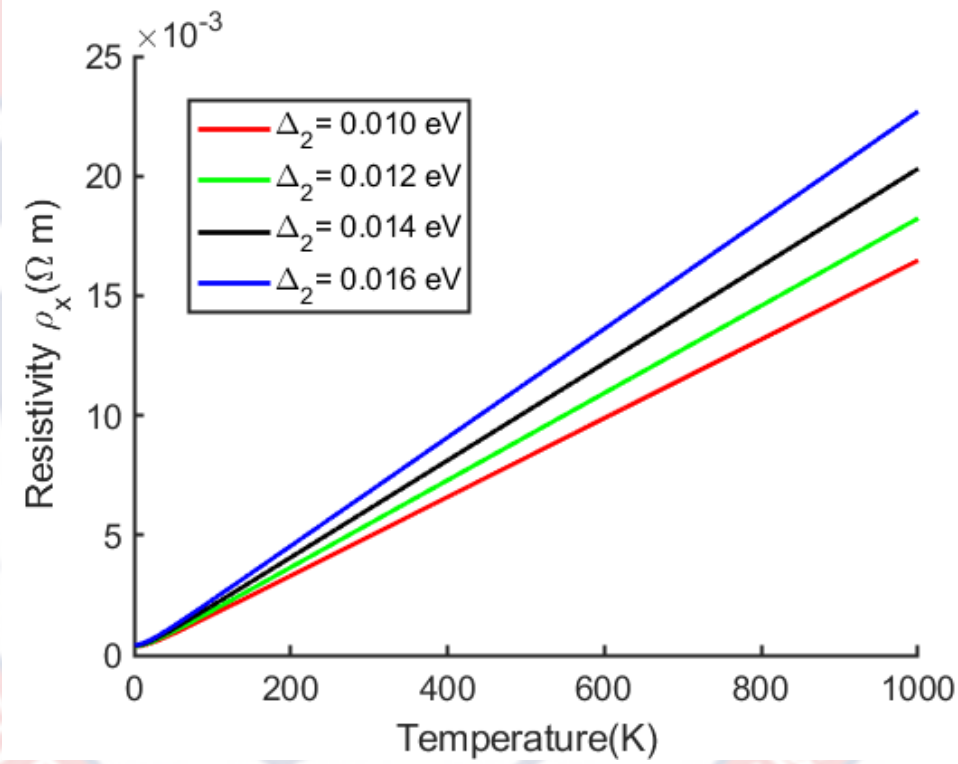

Figure 14: Dependence of resistivity on temperature for various values of Δ_2 with $\Delta_1 = 0.012$ eV, $n_o = 10^{13}$ cm^{-3}, $E_o = 10^7$ V/m, and $E_x = 10^2$ V/m

It is observed that increasing Δ_2 has very little effect on the ρ_x at temperatures below 100 K. However, above 100 K there is a marked increase in resistivity as Δ_2 increases but in marginally smaller increments as shown in Figure 14. This is due to the strong carrier scattering along y-direction of the GSL.

Figure 15 depicts a plot of the resistivity against temperature with various values of carrier concentration.

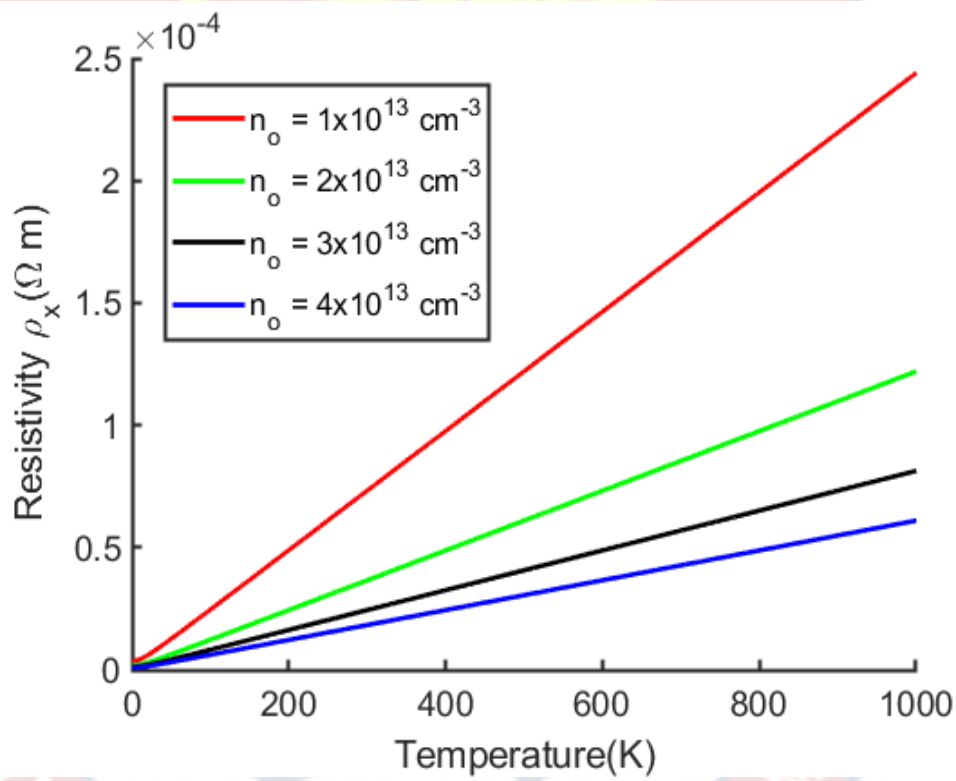

Figure 15: Dependence of resistivity of graphene superlattice on temperature for various values of n_o with $\Delta_2 = 0.024$ eV, $\Delta_1 = 0.012$ eV, $E_o = 10^7$ V/m, and $E_x = 10^2$ V/m

It can clearly be seen from Figure 15 that the resistivity of the GSL decreases with increasing carrier concentration. This is due to the drop-in carrier

scattering in the material along the direction where carrier-carrier interaction is minimal.

The dependence of resistivity of GSL on temperature for varying values of the amplitude of the external electric is depicted in Figure 16.

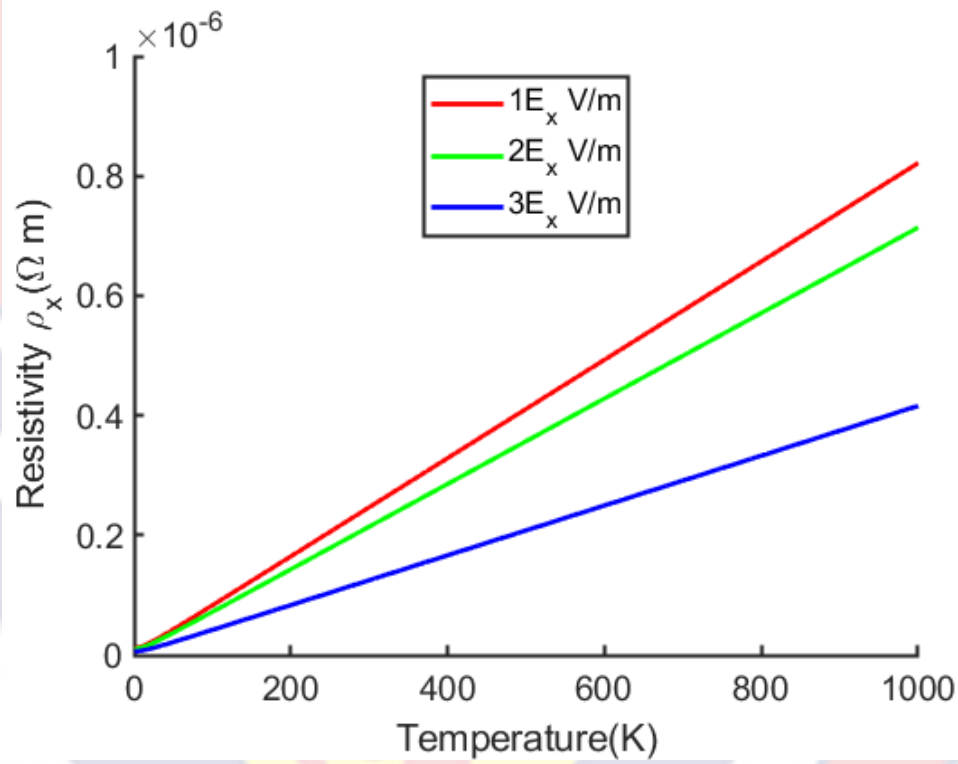

Figure 16: Dependence of resistivity of graphene superlattice on temperature for various values of E_x with $\Delta_2 = 0.012$ eV, $\Delta_1 = 0.012$ eV, $n_o = 10^{13}$ cm^{-3} and $E_o = 10^7$ V/m.

The Figure 16 indicates that the electrical resistivity ρ_x of the GSL decreases with increasing E_x. The low resistivity observed is attributed to the

influence of charge velocity by the electric field. The resistivity values observed in this study are very low as compared to those of other known low-dimensional materials [99] which shows clearly that GSL has metallic properties.

Thermoelectric Power of Graphene Superlattice

The differential thermoelectric power of GSL is analyzed using the approach developed in [100]. An analytical expression (Eqn. (3.19)) was derived for the current density in the presence of combined dc-ac field and a temperature gradient ∇T. From this relation, expressions were obtained for the differential electrical conductivity σ_x (Eqn. (3.17)) and the thermoelectric power α_x (Eqn. (3.19)). The thermoelectric power is highly anisotropic, depending on temperature *T*, the real overlapping integrals for jumps along the respective coordinates. To better understand the analytical expression obtained in Eqn. (3.19), graphical representations of the variation of the thermoelectric power on temperature for different values of Δ_1 and Δ_2 (measured in electron volts) have been investigated and results shown in Figures 17 and 18.

Figure 17 illustrates the dependence of thermoelectric power of the GSL (α_x) on temperature T for a fixed value of Δ_2 and a range of values of Δ_1.

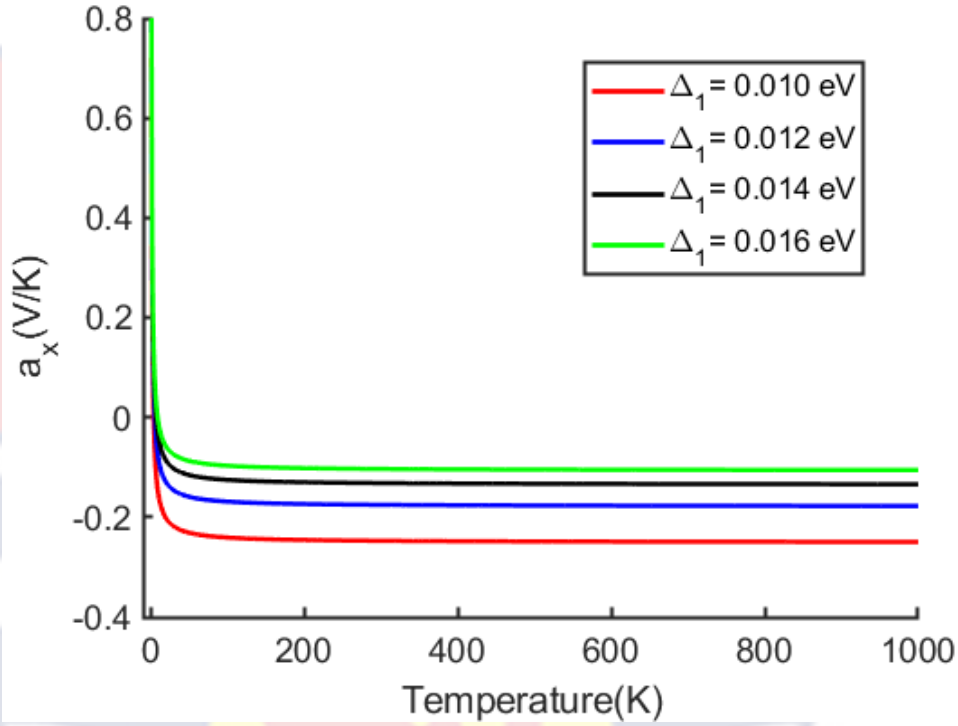

Figure 17: Dependence of thermoelectric power on temperature for various values of Δ_1 with $\Delta_2 = 0.024$ eV.

It is noted that, the differential thermoelectric power is high at low temperatures, but rapidly decreases as the temperature increases switching from a p-type to n-type semiconductor. At high temperatures, it slowly tends to a lower constant value. This is to be expected for semiconducting nanostructures which in general exhibit the behavior $\alpha_x \approx T^{-1}$ [101]. This is attributed to the mirror symmetry of the coexisting electrons and holes in the overlapping π-bands.

Figure 18 displays the variation of thermoelectrical power of GSL with temperature for various values of Δ_2.

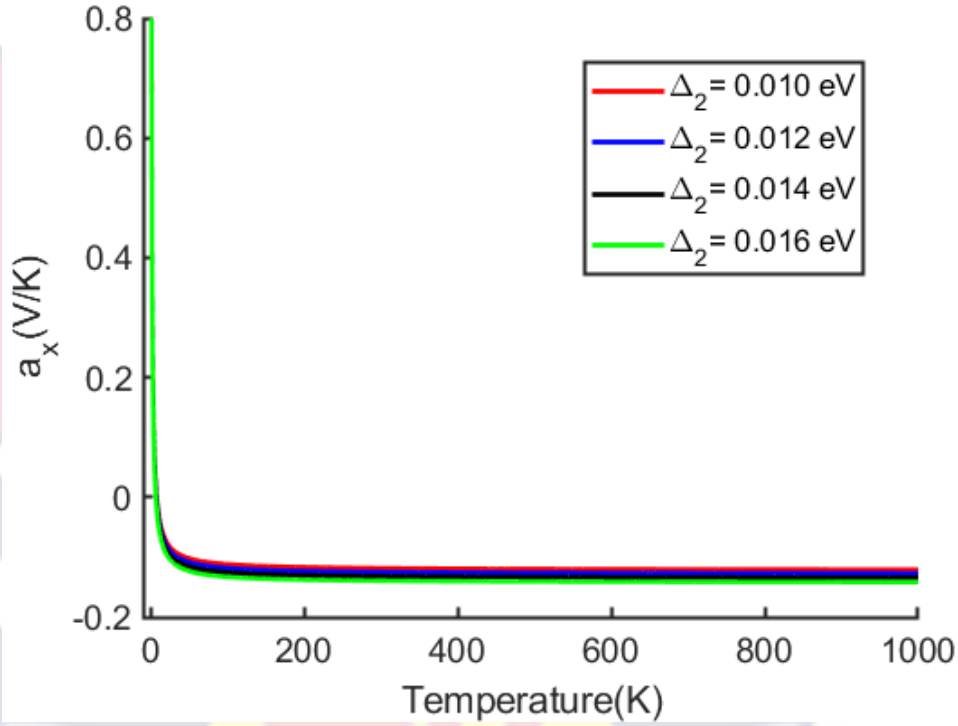

Figure 18: Dependence of thermoelectric power on temperature for various values of Δ_2 with $\Delta_1 = 0.012$ eV.

From Figure 18, the GSL behaves completely as a p-type semiconductor at low temperature, the thermoelectric power decreases rapidly, up to lowest (minimum) and then decreases slowly to a constant value. The turning point occurs at about 50 K. A similar observation was noted in [101] but at 100 K, where the thermoelectric power of a single walled-carbon nanotube (SWCNT) was measured. It is obvious that the material, under these conditions is behaving as a semimetal. One also notes that there exists a threshold temperature of 50 K for which hole conductivity switches over to electron conductivity, i.e. positive

α_x becomes negative. This can be explained by the fact that graphite has a pair of weakly overlapping electron and hole sp^2 or π-bands with near mirror symmetry about the Fermi energy E_F. The number of electrons and holes are approximately equal in these symmetric π-bands which is consistent with the negative thermoelectric power observed in [102]. The threshold value for the temperature shifts towards lower temperature as Δ_2 increases.

Electrical Power Factor in Graphene Superlattice

The electrical power factor of the GSL was calculated using a tractable mathematical technique as shown in Eqn. (3.22), which is extremely nonlinear in terms of career concentration n_o, external dc field E_o, temperature T and real overlapping integrals for jumps Δ_1 and Δ_2. To visualize the result of Eqn. (3.22) graphically, a numerical analysis was done using MATLAB (219b version).

Figure 19 illustrates the dependence of electrical power factor P_x of the GSL on temperature T for dc field E_o strength varied from E_o to $4E_o$.

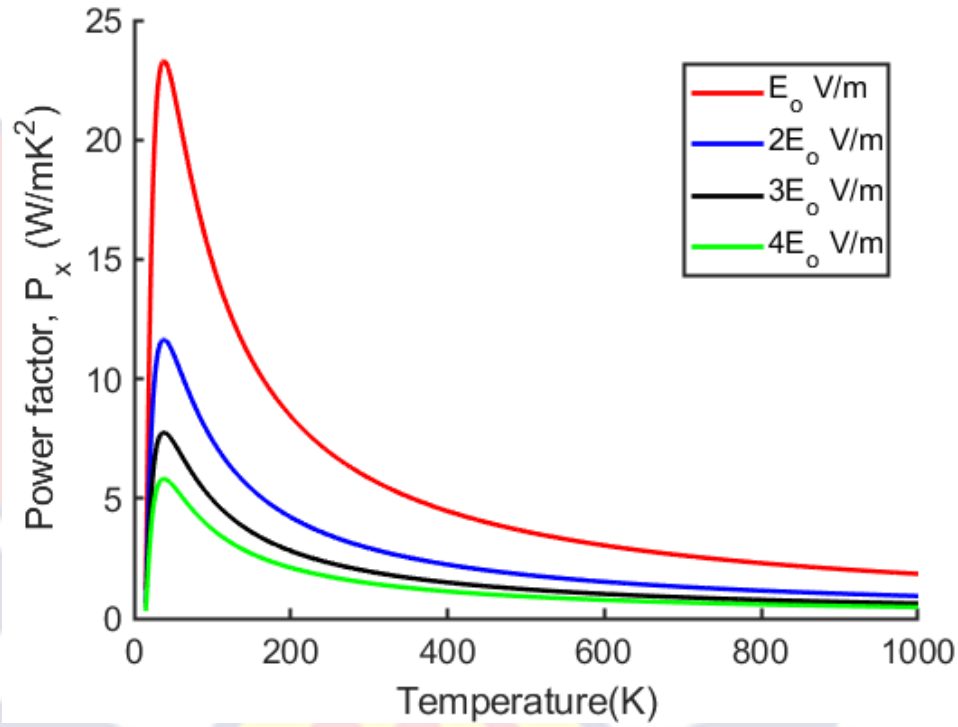

Figure 19: Dependence of electrical power factor of graphene superlattice on temperature for various values of E_o with $\Delta_2 = 0.012$ eV, $\Delta_1 = 0.012$ eV, $n_o = 10^{13}$ cm^{-3} and $E_x = 10^2$ V/m.

It is observed that the relationship between P_x and T is nonlinear. The curves in Figure 19 indicate that the power factor P_x initially increases sharply and attains maximum for all the four cases considered. With further increment in the temperature T, P_x experiences exponential decrease and then becomes independent of T at large values of T. The maximum value of the power factor attained varies inversely as the electric field E_o is increased. The peak values of

P_x decrease as E_o is increased from E_o to $4E_o$. Thus, the maximum value of P_x is higher for E_o than that for $2E_o$,$3E_o$ and has the least value in the case of $4E_o$.

Figure 20 depicts a plot of GSL against temperature for various values of Δ_1 ranging from 0.010 eV to 0.016 eV with a constant value of Δ_2.

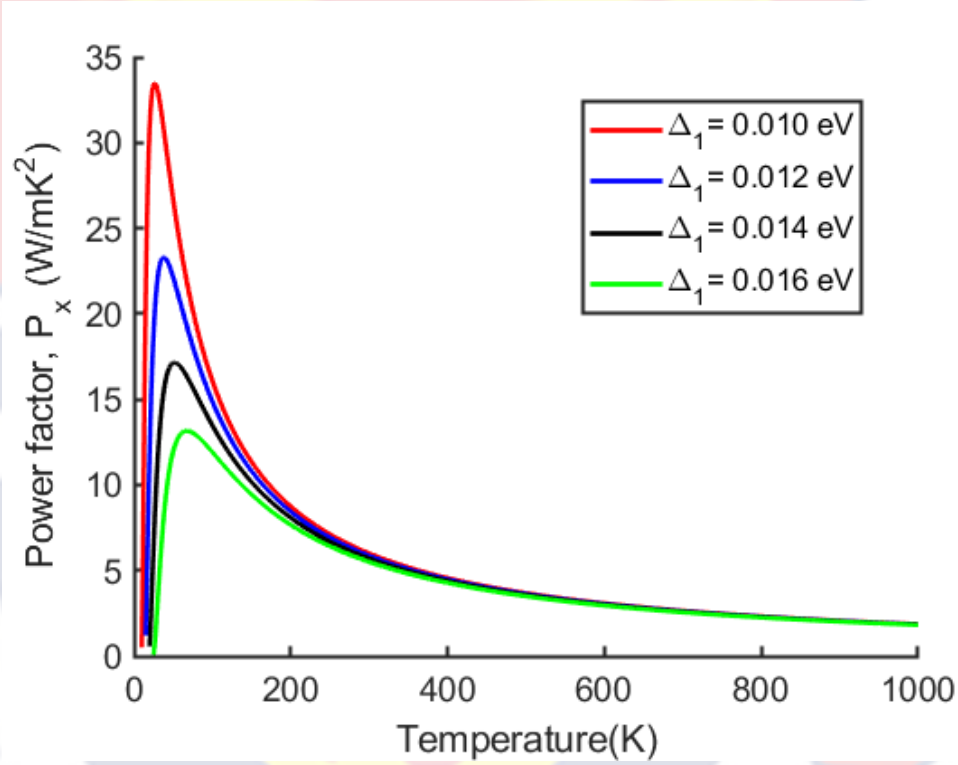

Figure 20: Dependence of electrical power factor of graphene superlattice on temperature for various values of Δ_1 with $\Delta_2 = 0.024$ eV, $n_o = 10^{13}$ cm^{-3} $E_o = 10^7$ V/m, and $E_x = 10^2$ V/m.

It is observed that in general P_x increases sharply and attains a maximum peak at low value of Δ_1= 0.010 eV and then reduces as the value of Δ_1 increases from 0.012 eV to 0.016 eV at a resistivity low temperature (~50 K). However, at high temperatures, i.e., about 400 K and above, the electrical

power factor assumes a lower constant exponential decay for all the values of Δ_1. This is because the majority of the carriers that contribute to the P_x are electrons.

Figure 21 displays variation of thermoelectrical power factor of GSL with temperature for several values of Δ_2.

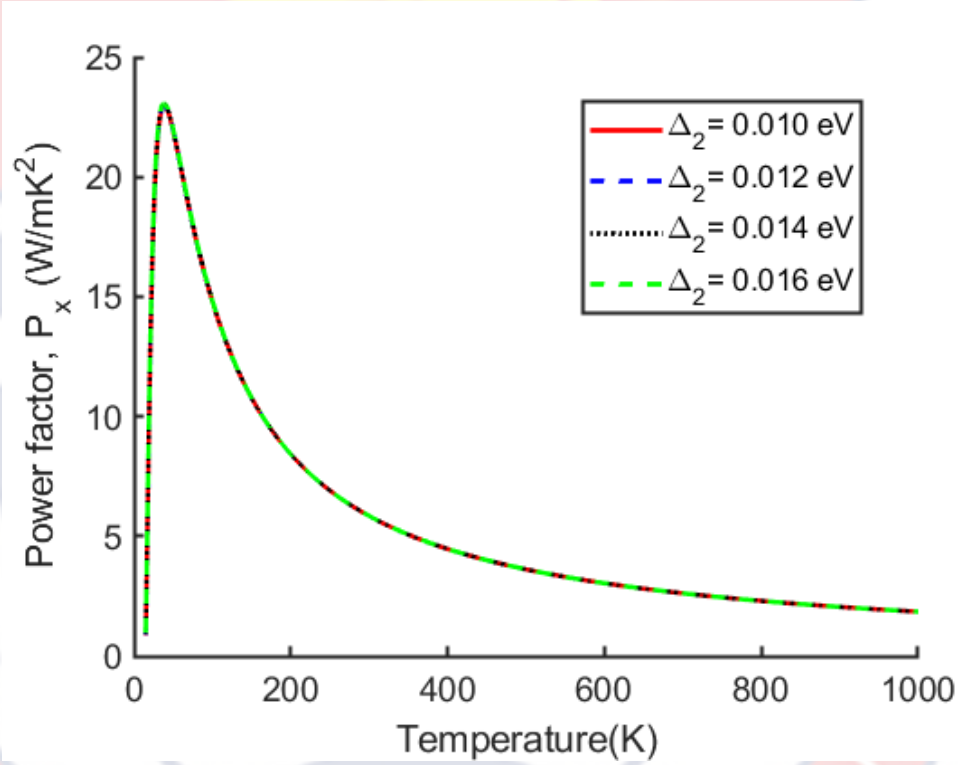

Figure 21: Dependence of electrical power factor on temperature for various values of Δ_2 with $\Delta_1 = 0.012$ eV, $n_o = 10^{13}$ cm^{-3}, $E_o = 10^7$ V/m, and $E_x = 10^2$ V/m.

As clearly seen in Figure 21, the electrical power factor is independent Δ_2.

Comparing the material response to the variation of Δ_1 and Δ_2 under the combined dc-ac field, it clearly shows that Δ_1 results in higher peak value of electrical power factor than Δ_2. Again, increasing Δ_1 affects the electrical power factor of GSL but Δ_2 does not have any obvious effect on the power factor.

Figure 22, shows the plot of thermoelectrical power factor of GSL against temperature for different values of n_o .

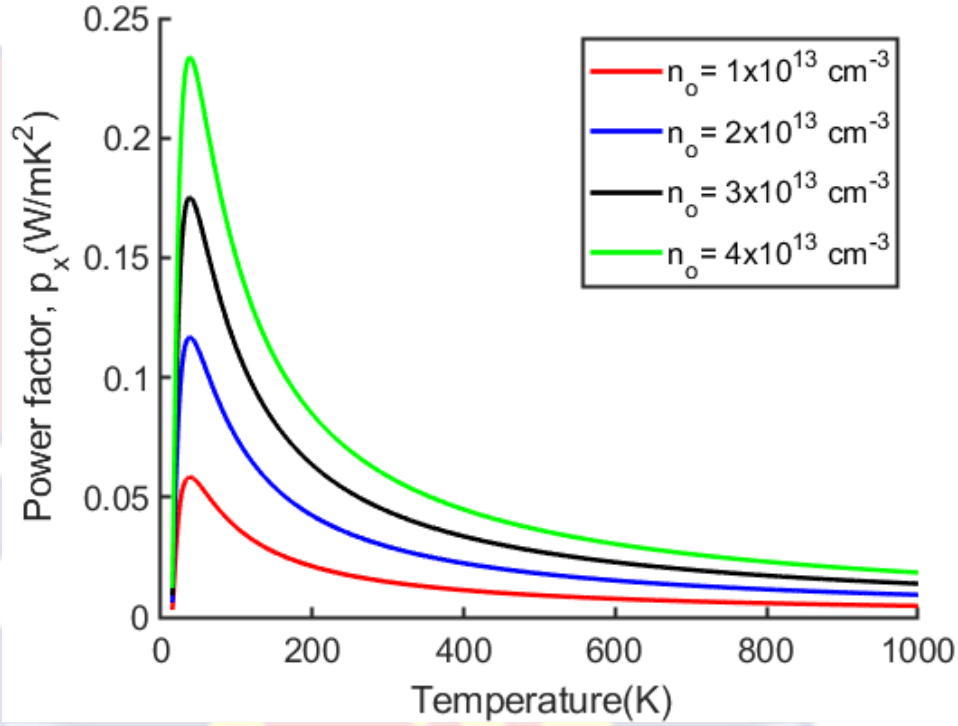

Figure 22: Dependence of electrical power factor of graphene superlattice on temperature for various values of n_o with $\Delta_2 = 0.024$ eV, $\Delta_1 = 0.012$ eV, $E_o = 10^7$ V/m, and $E_x = 10^2$ V/m.

It can be clearly observed from Figure 22 that at low temperatures increasing n_o increases P_x to peak values correspond to approximately 50 K. However, as the temperature increases beyond this threshold value, P_x decreases exponentially. The highest peak value of P_x occurs at $n_o = 4\times10^{13}$ cm^{-3}, but decreases with decreasing n_o. This is because increasing the carrier concentration increases the mobile electrons and so does the power

factor. The negative slopes of the curves at high temperatures show that electrons are the dominant carriers. Comparing P_x of GSL with Bi_2Te which is currently the preferred material, the P_x of GSL is about 5 times higher than P_x of Bi_2Te [103]. Therefore, the results of the present study will provide the theoretical basis for the synthesis of high-performance GSL thermoelectric materials.

Chapter Summary

The chapter presented an analysis of the results of resistivity, electrical power and the electrical power factor of GSL. The results of the study were visualized graphically and their trends were discussed to make an informed decision on electrical properties of GSL. The low resistivity and high thermoelectric power factor produced indicate that GSL has a high normalized figure of merit ($ZT = \alpha^2 \sigma T / \kappa$) since it is a direct function of the Seebeck coefficient, and inversely related to resistivity.

CHAPTER FIVE

SUMMARY, CONCLUSIONS, AND RECOMMENDATIONS

Overview

The thermoelectric properties of graphene superlattice were studied using the semiclassical Boltzmann transport equation, where the effective scattering time, τ was assumed to be constant. This chapter gives the summary and conclusions drawn from the study. It also provides suggestions for further research in this field.

Summary

This study employed the Boltzmann's Transport Equation (BTE) in the semi-classical regime to investigate the thermoelectric properties of h-BN/SiO_2 graphene superlattice using combined dc-ac fields.

The study reviewed the relevant theory on the transport properties of graphene superlattice as well as thermoelectric materials. The theoretical formulation made use of the BTE in the semi-classical regime to derive an analytical expression for the Electric resistivity, thermoelectric power and thermoelectrical power factor of h-BN/SiO_2 GSL using combined dc-ac fields. Numerical analysis was performed to visualize the results graphically to better understand the variation of these derived quantities with temperature, the material parameters as well as the dc-ac field intensities.

The Electric resistivity of h-BN/SiO_2 GSL was plotted as a function of temperature for varying the values of the dc-ac field intensities, the dopant carrier concentration as well as the real overlapping integrals for jumps (along the material's axes respectively).

The thermoelectric power which is the Seebeck coefficient of h-BN/SiO_2 GSL was plotted as a function of temperature for varying the values of the real overlapping integrals for jumps.

Electrical power factor of GSL as a function of temperature for varying values of the intensities of dc field, ac fields, carrier density as well as the real overlapping integrals for jumps.

Conclusions

The thermoelectric properties of GSL were investigated using the semiclassical Boltzmann Transport Equation. The results of the study show that the electrical resistivity, thermoelectric power, as well as thermoelectric power factor of h-BN/SiO_2 GSL are influenced by material parameters such as overlapping integrals, carrier density, and intensities of the dc-ac fields. The low resistivity in our findings show that h-BN/SiO_2 GSL is a good conductor of electricity and hence exhibit metallic properties. The results reveal that an increase in Δ_1, n_o, and E_x causes a decrease in resistivity which will in turn enhances normalized ZT.

In the case of TE power, the results show that the h-BN/SiO_2 GSL exhibit semiconductor properties. It indicates that as temperature increases beyond 50 K, the h-BN/SiO_2 GSL switches from a p-type to an n-type semiconductor material. Varying the overlapping integrals could be used to tune the h-BN/SiO_2 GSL to ascertain which carriers contributed to the thermoelectric power.

The results obtained from the TE power factor was also found to be influenced by the GSL parameters, Δ_1 , n_o and dc-field. The high normalized ZT value obtained at low temperatures shows that h-BN/SiO_2 GSL is a good conductor of electricity, therefore exhibits metallic properties. Hence, h-BN/SiO_2 GSL could be suitable for thermoelectric applications. The results obtained from this research will serve as a guide for synthesis of h-BN/SiO_2 GSL and other materials of high thermoelectric performance. The insights gained from this research have the potential to guide the designing and development of graphene-based materials for efficient thermoelectric applications.

Recommendation(s)

The following are some recommendations for further study:

i. Similar research could be carried out using the same material (h-BN/SiO_2 GSL) under the influence of combined magnetic and electric field.

ii. A similar study could also be used to investigate the effect of laser on acoustoelectric effects in h-BN/SiO_2 GSL in the quantum regime.

REFERENCES

[1]. Alam, Hilaal, and Seeram Ramakrishna. "A review on the enhancement of figure of merit from bulk to nano-thermoelectric materials." *Nano energy* 2, no. 2 (2013): 190-212.

[2]. Alsaleh, Najebah M., Elvis Shoko, and Udo Schwingenschlögl. "Pressure-induced conduction band convergence in the thermoelectric ternary chalcogenide CuBiS 2." *Physical Chemistry Chemical Physics* 21, no. 2 (2019): 662-673.

[3]. Bulusu, A., and D. G. Walker. "Review of electronic transport models for thermoelectric materials." *Superlattices and Microstructures* 44, no. 1 (2008): 1-36.

[4]. Bourgeois, Olivier, Dimitri Tainoff, Adib Tavakoli, Yanqing Liu, Christophe Blanc, Mustapha Boukhari, André Barski, and Emmanuel Hadji. "Reduction of phonon mean free path: From low-temperature physics to room temperature applications in thermoelectricity." *Comptes Rendus Physique* 17, no. 10 (2016): 1154-1160.

[5]. Iotti, Rita Claudia, and Fausto Rossi. "Simulation of Electronic Quantum Devices: Failure of Semiclassical Models." *Applied Sciences* 10, no. 3 (2020): 1114.

[6]. Geim, Andrey K., and Allan H. MacDonald. "Graphene: exploring carbon flatland." *Physics today* 60, no. 8 (2007): 35-41.

[7]. Wang, Li-Gang, and Shi-Yao Zhu. "Electronic band gaps and transport properties in graphene superlattices with one-dimensional periodic potentials of square barriers." *Physical Review B* 81, no. 20 (2010): 205444.

[8]. Li, Changan, Hemeng Cheng, Ruofan Chen, Tianxing Ma, Li-Gang Wang, Yun Song, and Hai-Qing Lin. "Electronic band gaps and transport properties in aperiodic bilayer graphenes uperlattices of Thue-Morse sequence." *Applied Physics Letters* 103, no. 17 (2013).

[9]. Novoselov, K. S. "Nobel lecture: Graphene: Materials in the flatland." *Reviews of modern physics* 83, no. 3 (2011): 837.

[10]. Novoselov, Kostya S., Andre K. Geim, Sergei Vladimirovich Morozov, Dingde Jiang, Michail I. Katsnelson, Irina V. Grigorieva, SVb Dubonos, and and AA Firsov. "Two-dimensional gas of massless Dirac fermions in graphene." *nature* 438, no. 7065 (2005): 197-200.

[11]. Prezhdo, Oleg V. "Graphene—The ultimate surface material." *Surface Science* 605, no. 17-18 (2011): 1607-1610.

[12]. Sharafat Hossain, Md, Feras Al-Dirini, Faruque M. Hossain, and Efstratios Skafidas. "High performance graphene nano-ribbon thermoelectric devices by incorporation and dimensional tuning of nanopores." *Scientific reports* 5, no. 1 (2015): 11297.

[13]. Novoselov, Kostya S., Da Jiang, F. Schedin, T. J. Booth, V. V. Khotkevich, S. V. Morozov, and Andre K. Geim. "Two-dimensional

atomic crystals." *Proceedings of the National Academy of Sciences* 102, no. 30 (2005): 10451-10453.

[14]. Zhang, Yuanbo, Yan-Wen Tan, Horst L. Stormer, and Philip Kim. "Experimental observation of the quantum Hall effect and Berry's phase in graphene." *nature* 438, no. 7065 (2005): 201-204.

[15]. Muniz, Andre R., and Dimitrios Maroudas. "Opening and tuning of band gap by the formation of diamond superlattices in twisted bilayer graphene." *Physical Review B* 86, no. 7 (2012): 075404.

[16]. Venkatasubramanian, R., T. Colpitts, E. Watko, and J. Hutchby. "Experimental evidence of high-power factors and low thermal conductivity in Bi 2 Te 3/Sb 2 Te 3 superlattice thin-films." In *Fifteenth International Conference on Thermoelectrics. Proceedings ICT'96*, pp. 454-458. IEEE, 1996.

[17]. Döhler, Gottfried H. "Solid-state superlattices." *Scientific American* 249, no. 5 (1983): 144-151.

[18]. Lee, Joo-Hyoung, and Jeffrey C. Grossman. "Energy gap of Kronig-Penney-type hydrogenated graphene superlattices." *Physical Review B* 84, no. 11 (2011): 113413.

[19]. Rowe, D. M., Gao Min, and L. Kuznestsov. "Electrical resistivity and Seebeck coefficient of hot-pressed YbAl3 over the temperature range 150-700K." *Philosophical magazine letters* 77, no. 2 (1998): 105-108.

[20]. Mensah, S. Y., F. K. A. Allotey, N. G. Mensah, and V. W. Elloh. "Laser induced amplification of hypersound in nondegenerate semiconductor superlattices." *Superlattices and microstructures* 33, no. 1-2 (2003): 41-52.

[21]. Sugihara, Ko. "Thermoelectric power of graphite intercalation compounds." *Physical Review B* 28, no. 4 (1983): 2157.

[22]. Khitun, A., and K. L. Wang. "Effect of Electron and Phonon Confinement on the Thermoelectric Figure of Merit of Semiconductor Quantum Wires." *Physics of Low-Dimensional Structures* 2000, no. 5-6 (2000): 11-22.

[23]. Heinz, Peter D. "First Principles Study of Thermoelectric Properties of Zinc-Oxide Nanowires." (2010).

[24]. Hu, Lin, and Dimitrios Maroudas. "Thermal transport properties of graphene nanomeshes." *Journal of Applied Physics* 116, no. 18 (2014).

[25]. Twombly, Chris. *A study of thermoelectric properties of graphene materials*. Colorado School of Mines, 2015.

[26]. Klyshko, A., M. Balucani, and A. Ferrari. "Mechanical strength of porous silicon and its possible applications." *Superlattices and Microstructures* 44, no. 4-5 (2008): 374-377.

[27]. Snyder, G. Jeffrey, and Eric S. Toberer. "Complex thermoelectric materials." *Nature materials* 7, no. 2 (2008): 105-114.

[28]. Venkatasubramanian, Rama, Edward Siivola, Thomas Colpitts, and Brooks O'quinn. "Thin-film thermoelectric devices with high room-temperature figures of merit." *Nature* 413, no. 6856 (2001): 597-602.

[29]. DiSalvo, Francis J. "Thermoelectric cooling and power generation." *Science* 285, no. 5428 (1999): 703-706.

[29]. Sakyi-Arthur, D., S. Y. Mensah, N. G. Mensah, K. W. Adu, K. A. Dompreh, and R. Edziah. "Tunable power factor in fluorine-doped single-walled carbon nanotubes." *Journal of Applied Physics* 128, no. 24 (2020).

[30]. Boukai, Akram I., Yuri Bunimovich, Jamil Tahir-Kheli, Jen-Kan Yu, William A. Goddard Iii, and James R. Heath. "Silicon nanowires as efficient thermoelectric materials." *nature* 451, no. 7175 (2008): 168-171.

[31]. Böttner, Harald, Gang Chen, and Rama Venkatasubramanian. "Aspects of thin-film superlattice thermoelectric materials, devices, and applications." *MRS bulletin* 31, no. 3 (2006): 211-217.

[32]. Dresselhaus, M. S. *Nanostructures and energy conversion*. 2003.

[33]. Novoselov, Kostya S., Andre K. Geim, Sergei V. Morozov, De-eng Jiang, Yanshui Zhang, Sergey V. Dubonos, Irina V. Grigorieva, and Alexandr A. Firsov. "Electric field effect in atomically thin carbon films." *science* 306, no. 5696 (2004): 666-669.

[34]. Geim, Andre K., and Irina V. Grigorieva. "Van der Waals heterostructures." *Nature* 499, no. 7459 (2013): 419-425.

[35]. Hochbaum, Allon I., Renkun Chen, Raul Diaz Delgado, Wenjie Liang, Erik C. Garnett, Mark Najarian, Arun Majumdar, and Peidong Yang. "Enhanced thermoelectric performance of rough silicon nanowires." *Nature* 451, no. 7175 (2008): 163-167.

[36]. Hicks, Lyndon D., and Mildred S. Dresselhaus. "Effect of quantum-well structures on the thermoelectric figure of merit." *Physical Review B* 47, no. 19 (1993): 12727.

[37]. Hicks, Lyndon D., and Mildred S. Dresselhaus. "Thermoelectric figure of merit of a one-dimensional conductor." *Physical review B* 47, no. 24 (1993): 16631.

[38]. Mensah, S. Y., and G. K. Kangah. "The thermoelectric effect in a semiconductor superlattice in a non-quantized electric field." *Journal of Physics: Condensed Matter* 4, no. 3 (1992): 919.

[39]. Geim, A. K., and K. S. Novoselov. "The rise of graphene, Nanosci." *Technol. A Collect. Rev.. from Nat. Journals* (2009): 11-19.

[40]. Boehm, Hans Peter, Ralph Setton, and Eberhard Stumpp. "Nomenclature and terminology of graphite intercalation compounds (IUPAC Recommendations 1994)." *Pure and Applied Chemistry* 66, no. 9 (1994): 1893-1901.

[41]. Yang, Shaowu, Yuxin Hao, Wei Zhang, Li Yang, and Lingtao Liu. "Nonlinear vibration of functionally graded graphene platelet-reinforced composite truncated conical shell using first-order shear deformation theory." *Applied Mathematics and Mechanics* 42, no. 7 (2021): 981-998.

[42]. Novoselov, K. S., Artem Mishchenko, Alexandra Carvalho, and A. H. Castro Neto. "2D materials and van der Waals heterostructures." *Science* 353, no. 6298 (2016): aac9439.

[43]. Geim, Andre K., and Irina V. Grigorieva."Van der Waals heterostructures." *Nature* 499, no. 7459 (2013): 419-425.

[44]. Morozov, S. V., K. S. Novoselov, F. Schedin, D. Jiang, A. A. Firsov, and A. K. Geim. "Two-dimensional electron and hole gases at the surface of graphite." *Physical Review B* 72, no. 20 (2005): 201401.

[45]. Zhao, Shaoyu, Zhan Zhao, Zhicheng Yang, LiaoLiang Ke, Sritawat Kitipornchai, and Jie Yang. "Functionally graded graphene reinforced composite structures: A review." *Engineering Structures* 210 (2020): 110339.

[46]. Haldane, F. D. M. "Many-particle translational symmetries of two-dimensional electrons at rational Landau-level filling." *Physical review letters* 55, no. 20 (1985): 2095.

[47]. Kuzmenko, Alexey B., Erik Van Heumen, Fabrizio Carbone, and Dirk Van Der Marel. "Universal optical conductance of graphite." *Physical review letters* 100, no. 11 (2008): 117401.

[48]. uzmenko, Alexey B., Erik Van Heumen, Fabrizio Carbone, and Dirk Van Der Marel. "Universal optical conductance of graphite." *Physical review letters* 100, no. 11 (2008): 117401.

[49]. Seibert, K., G. C. Cho, W. Kütt, H. Kurz, D. H. Reitze, J. I. Dadap, H. Ahn, M. C. Downer, and A. M. Malvezzi. "Femtosecond carrier dynamics in graphite." *Physical Review B* 42, no. 5 (1990): 2842.

[50]. Kauling, Alan P., Andressa T. Seefeldt, Diego P. Pisoni, Roshini C. Pradeep, Ricardo Bentini, Ricardo VB Oliveira, Konstantin S. Novoselov, and Antonio H. Castro Neto. "The worldwide graphene flake production." *Advanced Materials* 30, no. 44 (2018): 1803784.

[51]. Hernandez, Yenny, Valeria Nicolosi, Mustafa Lotya, Fiona M. Blighe, Zhenyu Sun, Sukanta De, Ignatius T. McGovern et al. "High-yield production of graphene by liquid-phase exfoliation of graphite." *Nature nanotechnology* 3, no. 9 (2008): 563-568.

[52]. Tite, Teddy, Christophe Donnet, A-S. Loir, Stéphanie Reynaud, J-Y. Michalon, Francis Vocanson, and Florence Garrelie. "Graphene-based textured surface by pulsed laser deposition as a robust platform for surface enhanced Raman scattering applications." *Applied Physics Letters* 104, no. 4 (2014).

[53]. Brownson, Dale AC, and Craig E. Banks. "The electrochemistry of CVD graphene: progress and prospects." *Physical Chemistry Chemical Physics* 14, no. 23 (2012): 8264-8281.

[54]. Tsu, Raphael. *Superlattice to nanoelectronics*. Elsevier, 2010.

[55]. Pereira, Vitor M., and AH Castro Neto. "Strain engineering of graphene's electronic structure." *Physical review letters* 103, no. 4 (2009): 046801.

[56]. Neto, AH Castro, Francisco Guinea, Nuno MR Peres, Kostya S. Novoselov, and Andre K. Geim. "The electronic properties of graphene." *Reviews of modern physics* 81, no. 1 (2009): 109.

[57]. Zhou, J., Q. Wang, Q. Sun, X. S. Chen, Y. Kawazoe, and P. Jena. "Ferromagnetism in semihydrogenated graphene sheet." *Nano letters* 9, no. 11 (2009): 3867-3870.

[58]. Pereira, Vitor M., and AH Castro Neto. "Strain engineering of graphene's electronic structure." *Physical review letters* 103, no. 4 (2009): 046801.

[59]. Khabashesku, Valery N., W. Edward Billups, and John L. Margrave. "Fluorination of single-wall carbon nanotubes and subsequent derivatization reactions." *Accounts of chemical research* 35, no. 12 (2002): 1087-1095.

[60]. Dettlaff-Weglikowska, Urszula, Viera Skakalova, Jannik Meyer, Jiri Cech, Bernd G. Mueller, and Siegmar Roth. "Effect of fluorination on

electrical properties of single walled carbon nanotubes and C60 peapods in networks." *Current Applied Physics* 7, no. 1 (2007): 42-46.

[61]. Geim, Andre K. "Nobel Lecture: Random walk to graphene." *Reviews of Modern Physics* 83, no. 3 (2011): 851.

[62]. Kryuchkov, Sergey V., and Constantine A. Popov. "Transport properties of the two-dimentional graphene superlattice effect of the constant and alternating electric field." In *2017 IEEE 7th International Conference Nanomaterials: Application & Properties (NAP)*, pp. 03CBN09-1. IEEE, 2017.

[63]. Seifert, Gotthard, Thomas Köhler, and Thomas Frauenheim. "Molecular wires, solenoids, and capacitors by sidewall functionalization of carbon nanotubes." *Applied Physics Letters* 77, no. 9 (2000): 1313-1315.

[64]. Haddon, R. C., A. F. Hebard, M. J. Rosseinsky, D. W. Murphy, S. J. Duclos, K. B. Lyons, B. Miller et al. "Conducting films of C60 and C70 by alkali-metal doping." *Nature* 350, no. 6316 (1991): 320-322.

[65]. Aghabozorg, H. R., R. Mousavi, S. Asckari, and H. Aghabozorg. "Effects of synthesis methods of vanadium oxide nanotubes on the inter layer distances." *Journal of Nanoparticle Research* 9 (2007): 497-500.

[66]. Wu, Xiaosong, Yike Hu, Ming Ruan, Nerasoa K. Madiomanana, John Hankinson, Mike Sprinkle, Claire Berger, and Walt A. De Heer. "Half

integer quantum Hall effect in high mobility single layer epitaxial graphene." *Applied Physics Letters* 95, no. 22 (2009).

[67]. Winters, Michael. *Electron transport studies in epitaxial graphene on SiC*. Chalmers Tekniska Hogskola (Sweden), 2013.

[68]. Tanabe, Shinichi, Yoshiaki Sekine, Hiroyuki Kageshima, Masao Nagase, and Hiroki Hibino. "Half-integer quantum Hall effect in gate-controlled epitaxial graphene devices." *Applied physics express* 3, no. 7 (2010): 075102.

[69]. Wang, Jingang, Fengcai Ma, and Mengtao Sun. "Graphene, hexagonal boron nitride, and their heterostructures: properties and applications." *RSC advances* 7, no. 27 (2017): 16801-16822.

[70]. Wallace, Philip Richard. "The band theory of graphite." *Physical review* 71, no. 9 (1947): 622.

[71]. Hass, J., R. Feng, J. E. Millán-Otoya, X. Li, M. Sprinkle, Ph N. First, W. A. De Heer, E. H. Conrad, and C. Berger. "Structural properties of the multilayer graphene/4 H− Si C (000 1¯) system as determined by surface x-ray diffraction." *Physical Review B* 75, no. 21 (2007): 214109.

[72]. Srednicki, Mark. *Quantum field theory*. Cambridge University Press, 2007.

[73]. Griffith, D. "Introduction to Quantum Mechanics 2014." *Essex: Pearson*.

[74]. Sarma, S. Das, Shaffique Adam, E. H. Hwang, and Enrico Rossi. "Electronic transport in two-dimensional graphene." *Reviews of modern physics* 83, no. 2 (2011): 407.

[75]. Bena, Cristina, and Gilles Montambaux. "Remarks on the tight-binding model of graphene." *New Journal of Physics* 11, no. 9 (2009): 095003.

[76]. Hayashi, T., M. Terrones, C. Scheu, Y. A. Kim, M. Rühle, T. Nakajima, and M. Endo. "NanoTeflons: structure and EELS characterization of fluorinated carbon nanotubes and nanofibers." *Nano letters* 2, no. 5 (2002): 491-496.

[77]. Kittel, Charles. *Introduction to solid state physics*. John Wiley & sons, inc, 2005.

[78]. Houssa, Michel, Geoffrey Pourtois, V. V. Afanas'Ev, and Andre Stesmans. "Can silicon behave like graphene? A first-principles study." *Applied Physics Letters* 97, no. 11 (2010).

[79]. Reich, Stephanie, Janina Maultzsch, Christian Thomsen, and Pablo Ordejon. "Tight-binding description of graphene." *Physical Review B* 66, no. 3 (2002): 035412.

[80]. Metin, Önder, Emine Kayhan, Saim Özkar, and Jörg J. Schneider. "Palladium nanoparticles supported on chemically derived graphene: An efficient and reusable catalyst for the dehydrogenation of ammonia

borane." *International Journal of Hydrogen Energy* 37, no. 10 (2012): 8161-8169.

[81]. Nguyen, Phuong Hoa, Karl R. Hofmann, and Gernot Paasch. "Comparative full-band Monte Carlo study of Si and Ge with screened pseudopotential-based phonon scattering rates." *Journal of applied physics* 94, no. 1 (2003): 375-386.

[82]. Joshi, Rakesh K., Humberto Gomez, Farah Alvi, and Ashok Kumar. "Graphene films and ribbons for sensing of O2, and 100 ppm of CO and NO2 in practical conditions." *The Journal of Physical Chemistry C* 114, no. 14 (2010): 6610-6613.

[83]. Kikuchi, Makoto, Hisao Hayakawa, and Yutaka Abe. "Acoustoelectric current oscillation in InSb and its dependence on the transverse magnetic field." *Japanese Journal of Applied Physics* 5, no. 12 (1966): 1259.

[84]. Mueller, Thomas, Fengnian Xia, and Phaedon Avouris. "Graphene photodetectors for high-speed optical communications." *Nature photonics* 4, no. 5 (2010): 297-301.

[85]. Davisson, J. W., and J. Pasternak. "Chapter V conduction phenomena in solid dielectrics." *Digest of Literature on Dielectrics* 25 (1961): 147-226.

[86]. Nguyen, Phuong Hoa, Karl R. Hofmann, and Gernot Paasch. "Full-band Monte Carlo model with screened pseudo-potential based phonon

scattering rates for a lattice with basis." *Journal of applied physics* 92, no. 9 (2002): 5359-5370.

[87]. Jacoboni, Carlo, and Lino Reggiani. "The Monte Carlo method for the solution of charge transport in semiconductors with applications to covalent materials." *Reviews of modern Physics* 55, no. 3 (1983): 645.

[88]. Bao, Qiaoliang, and Kian Ping Loh. "Graphene photonics, plasmonics, and broadband optoelectronic devices." *ACS nano* 6, no. 5 (2012): 3677-3694.

[89]. Kunikiyo, T., M. Takenaka, Y. Kamakura, M. Yamaji, H. Mizuno, M. Morifuji, K. Taniguchi, and C. Hamaguchi. "A Monte Carlo simulation of anisotropic electron transport in silicon including full band structure and anisotropic impact-ionization model." *Journal of Applied Physics* 75, no. 1 (1994): 297-312.

[90]. Yoder, P. D., J. M. Higman, J. Bude, and K. Hess. "Monte Carlo simulation of hot electron transport in Si using a unified pseudopotential description of the crystal." *Semiconductor Science and Technology* 7, no. 3B (1992): B357.

[91]. Abeygunasekara, Waranatha L., Pritesh Hiralal, Lilantha Samaranayake, Chih-Tao Chien, Abhishek Kumar, Andrew J. Flewitt, Veranja Karunaratne, and Gehan AJ Amaratunga. "Incorporating semiconducting single-walled carbon nanotubes as efficient charge extractors in organic solar cells." *Applied Physics Letters* 106, no. 12 (2015).

[92]. Dompreh, Kwadwo A., Natalia G. Mensah, and Samuel Y. Mensah. "Amplification of Hypersound in Graphene with degenerate energy dispersion." *arXiv preprint arXiv:1503.07360* (2015).

[93]. Bau, Nguyen Quang, Le Dinh, and Tran Cong Phong. "Absorption coefficient of weak electromagnetic waves caused by confined electrons in quantum wires." *JOURNAL-KOREAN PHYSICAL SOCIETY* 51, no. 4 (2007): 1325.

[94]. Mason, Warren P. "Physical acoustics and the properties of solids." *The Journal of the Acoustical Society of America* 28, no. 6 (1956): 1197-1206.

[95]. Dresselhaus, Mildred S., Gene Dresselhaus, P. C. Eklund, and A. M. Rao. *Carbon nanotubes*. Springer Netherlands, 2000.

[96]. Dresselhaus, M. S., G. Dresselhaus, P. Eklund, and A. Rao. "The physics of fullerene-based and fullerene-related materials." *Phys. Chem. Mater. Low-Dimens. Struct.* 23 (2000): 331- 379.

[97]. Mensah, S. Y., F. K. A. Allotey, and S. K. Adjepong. "Acoustomagnetoelectric effect in a superlattice." *Journal of Physics: Condensed Matter* 8, no. 9 (1996): 1235.

[98]. Blatt, J. *Thermoelectric power of metals*. Springer Science & Business Media, 2012.

[99]. Gelbstein, Yaniv, Zinovi Dashevsky, and Moshe P. Dariel. "Highly efficient bismuth telluride doped p-type Pb0. 13Ge0. 87Te for thermoelectric applications." *physica status solidi (RRL)–Rapid Research Letters* 1, no. 6 (2007): 232-234.

[100]. Mensah, S. Y., F. K. A. Allotey, N. G. Mensah, and G. Nkrumah. "Giant electrical power factor in single-walled chiral carbon nanotube." *Superlattices and microstructures* 33, no. 3 (2003): 173-180.

[101]. Hone, J., I. Ellwood, M. Muno, Ari Mizel, Marvin L. Cohen, A. Zettl, Andrew G. Rinzler, and R. E. Smalley. "Thermoelectric power of single-walled carbon nanotubes." *Physical Review Letters* 80, no. 5 (1998): 1042.

[102]. Grigorian, L., G. U. Sumanasekera, A. L. Loper, S. L. Fang, J. L. Allen, and P. C. Eklund. "Giant thermopower in carbon nanotubes: A one-dimensional Kondo system." *Physical Review B* 60, no. 16 (1999): R11309.

[103]. Zhou, Yang, Liangliang Li, Qing Tan, and Jing-Feng Li. "Thermoelectric properties of Pb-doped bismuth telluride thin films deposited by magnetron sputtering." *Journal of Alloys and Compounds* 590 (2014): 362-367.

APPENDICES

APPENDIX A

SOLUTION OF THE BOLTZMANN TRANSPORT EQUATION

The Boltzmann transport Eqn. is expressed as:

$$\frac{df}{dt}+\vec{v}(p)\frac{\partial f(\vec{r},\vec{p},t)}{\partial r}+e\vec{E}\frac{\partial f(\vec{r},\vec{p},t)}{dp}=-\frac{f(\vec{r},\vec{p},t)-f_o(\vec{p})}{\tau} \quad \text{(A1)}$$

where $\vec{E}(t)=\vec{E}_o+\vec{E}_1 cos\omega t$

At equilibrium, the distribution function of an electron is defined by the Fermi-Dirac statistics as:

$$f_o(\vec{r},\vec{p},t)=\frac{1}{1+e^{\left(\frac{E_C(\vec{r},t)+E(\vec{p})-F_n(\vec{r},t)}{k_BT}\right)}} \quad \text{(A2)}$$

where $E_c(\vec{r},t)$ is the conduction band edge, $E(\vec{p})$ is the carrier band structure $F_n(\vec{r},t)$ is the quasi-Fermi level

Let

$$\phi=\frac{E_c(\vec{r},t)+E(\vec{p})-F_n(\vec{r},t)}{k_BT} \quad \text{(A3)}$$

And suppose that $f(\vec{r},\vec{p},t)=f_o(\vec{r},\vec{p},t)+f_1(\vec{r},\vec{p},t)+f'(\vec{r},\vec{p},t)$, where $f_1(\vec{r},\vec{p},t)$ is a small perturbation and f' is the hot electron source distribution function.

For $f'(\vec{r},\vec{p},t)=0$ and $\nabla_t(f_o+f_1)$ is time independent.

Eqn. (A1) is expressed as:

$$\nabla_t(f_o+f_1)+\vec{v}.\nabla_r(f_o+f_1)+e\vec{E}.\nabla_p(f_o+f_1)=-\frac{f_o+f_1-f_o}{\tau}$$

$$\vec{v}.\nabla_r(f_o+f_1)+e\vec{E}.\nabla_p(f_o+f_1)=-\frac{f_1}{\tau} \quad \text{(A4)}$$

Also, if $f_o(\vec{r},\vec{p},t)>>f_1(\vec{r},\vec{p},t)$ and $\nabla_r f_o>>f_1$

$$\vec{v}.\nabla_r f_o(\vec{r},\vec{p},t)+e\vec{E}.\nabla_p f_o(\vec{r},\vec{p},t)=-\frac{f_1(\vec{r},\vec{p},t)}{\tau} \quad \text{(A5)}$$

Applying the chain rule Eqn. (A5) is expressed as:

$$\vec{v}.\frac{\partial f_o(\vec{r},\vec{p},t)}{\partial\phi}.\nabla_r\phi+e\vec{E}.\frac{\partial f_o(\vec{r},\vec{p},t)}{\partial\phi}.\nabla_p\phi=-\frac{f_1(\vec{r},\vec{p},t)}{\tau} \quad \text{(A6)}$$

Differentiating $\nabla_r\phi$ and $\nabla_p\phi$ in Eqn. (A6) with respect to position and momentum respectively yields:

$$\nabla_r\phi=\frac{[\nabla_r E_c(\vec{r})-\nabla_r F_n(\vec{r})]}{k_BT}+[E_c(\vec{r})+E(\vec{p})-F_n(\vec{r})]\nabla_r\left(\frac{1}{k_BT(\vec{r})}\right) \quad \text{(A7)}$$

$$\nabla_p\phi=\frac{\vec{v}}{k_BT(\vec{r})} \quad \text{(A8)}$$

Substituting Eqn. (A7) and Eqn. (A8) into Eqn. (A6) and simplified gives:

$$\vec{v}.\frac{\partial f_o(\vec{r},\vec{p},t)}{\partial\phi}\left\{\frac{[\nabla_r E_c(\vec{r})-\nabla_r F_n(\vec{r})]}{k_BT}+[E_c(\vec{r})+E(\vec{p})-F_n(\vec{r})]\nabla_r\left(\frac{1}{k_BT(\vec{r})}\right)\right\}$$
$$+e\vec{E}.\frac{\partial f_o(\vec{r},\vec{p},t)}{\partial\phi}\frac{\vec{v}}{k_BT(\vec{r})}=-\frac{f_1(\vec{r},\vec{p},t)}{\tau}$$

$$\vec{v}.\frac{\partial f_o(\vec{r},\vec{p},t)}{\partial\phi}\left\{\frac{[\nabla_r E_c(\vec{r})-\nabla_r F_n(\vec{r})]}{k_BT}+[E_c(\vec{r})-F_n(\vec{r})]\nabla_r\left(\frac{1}{k_BT(\vec{r})}\right)\right\}$$
$$+\frac{e\vec{E}}{k_BT(\vec{r})}=\frac{f_1(\vec{r},\vec{p},t)}{\tau} \quad \text{(A9)}$$

Also, differentiating the electric field potential with respect to r in Eqn. (A9) gives:

$$\nabla_r E_c(\vec{r})=-e\vec{E} \quad \text{(A10)}$$

Substituting Eqn. (A10) into Eqn. (A9) and simplified further yields:

$$f_1(\vec{r},\vec{p},t) = -\frac{\vec{v}\tau}{k_B T}.\frac{\partial f_o(\vec{r},\vec{p},t)}{\partial\phi}\left\{-\frac{e\vec{E}}{k_B T(\vec{r})} - \nabla_r F_n(\vec{r}) + \left[E_c(\vec{r}) + E(\vec{p}) - F_n(\vec{r})\right]\nabla_r\left(\frac{1}{k_B T(\vec{r})}\right) + \frac{e\vec{E}}{k_B T(\vec{r})}\right\}$$

$$f_1(\vec{r},\vec{p},t) = -\frac{\vec{v}\tau}{k_B T}.\frac{\partial f_o}{\partial\phi}\left\{\left[E_c(\vec{r}) + E(\vec{p}) - F_n(\vec{r})\right]\nabla_r\left(\frac{1}{k_B T(\vec{r})}\right) - \nabla_r F_n(\vec{r})\right\}$$

$$f_1 = -\frac{\vec{v}\tau}{k_B T}.\frac{\partial f_o}{\partial\phi}\left\{k_B T\left[E_c(\vec{r}) + E(\vec{p}) - F_n(\vec{r})\right]\nabla_r\left(\frac{1}{T(\vec{r})}\right) - \nabla_r F_n(\vec{r})\right\}$$

$$f_1 = -\frac{\vec{v}\tau}{k_B T}.\frac{\partial f_o}{\partial\phi}\left\{k_B T\left[E_c(\vec{r}) + E(\vec{p}) - F_n(\vec{r})\right]\left(\frac{\nabla_r T}{T}\right) - \nabla_r F_n(\vec{r})\right\}$$

$$f_1 = \frac{\tau}{k_B T}\left(-\frac{\partial f_o}{\partial\phi}\right)\vec{v}.\Theta \qquad \text{(A11)}$$

where $\Theta = -\nabla_r F_n(\vec{r}) + \left[E_c(\vec{r}) + E(\vec{p}) - F_n(\vec{r})\right](\nabla_r T / T)$ is the generalized force

Substituting Eqn. (A10) into the expression $f = f_o + f_1$ yields:

$$f = f_o(\vec{p}) + \frac{\vec{v}\tau}{k_B T}.\frac{\partial f_o}{\partial\phi}\left\{k_B T\left[E_c(\vec{r}) + E(\vec{p}) - F_n(\vec{r})\right]\left(\frac{\nabla_r T}{T}\right) - \nabla_r F_n(\vec{r})\right\} \qquad \text{(A12)}$$

From Eqn. (A3)

$$E_c(\vec{r},t) + E(\vec{p}) - F_n(\vec{r},t) = k_B T\phi = \varepsilon(p)$$

Therefore; $$\partial\phi = \frac{\partial\varepsilon(p)}{k_B T} \qquad \text{(A13)}$$

Substitute Eqn. (A13) into Eqn. (A12) gives:

$$f(\vec{r},\vec{p},t) = f_o(\vec{r},\vec{p},t) + \frac{\vec{v}\tau}{k_B T}.k_B T\frac{\partial f_o(\vec{p})}{\partial\varepsilon(\vec{p})}\left\{\left[E_c(\vec{r}) + E(\vec{p}) - F_n(\vec{r})\right]\frac{\nabla_r T}{T} - \nabla_r F_n(\vec{r})\right\} \qquad \text{(A14)}$$

Simplifying Eqn. (A14) further

$$f(\vec{r},\vec{p},t) = \tau^{-1}\int_0^{-\infty}\exp(-t/\tau)\,dt\; f_o(\vec{r},\vec{p},t) + \frac{\vec{v}\tau}{k_B T}.k_B T\frac{\partial f_o(\vec{p})}{\partial\varepsilon(\vec{p})}\int_0^{-\infty}\exp(-t/\tau)dt\left\{\left[E_c(\vec{r}) + E(\vec{p}) - F_n(\vec{r})\right]\frac{\nabla_r T}{T} - \nabla_r F_n(\vec{r})\right\}$$

$$f(\vec{r},\vec{p},t)=\tau^{-1}\int_{0}^{-\infty}\exp(-t/\tau)\,dtf_o(\vec{r},\vec{p},t)$$
$$+\tau\int_{0}^{-\infty}\exp(-t/\tau)dt\left\{\left[E_c(\vec{r})+E(\vec{p})-F_n(\vec{r})\right]\frac{\nabla_r T}{T}-\nabla_r F_n(\vec{r})\right\}.\vec{v}\frac{\partial f_o(\vec{p})}{\partial\varepsilon(\vec{p})} \quad \text{(A15)}$$

If $E_c(\vec{r})<<E(\vec{p})$ and the quasi-fermi level $\nabla_r F_n=\nabla_r\mu$, where μ is the electrochemical potential, then Eqn. (A15) becomes;

$$f(\vec{r},\vec{p},t)=\tau^{-1}\int_{0}^{-\infty}\exp(-t/\tau)\,dtf_o(\vec{p})$$
$$+\tau\int_{0}^{-\infty}\exp(-t/\tau)dt\left\{\left[E(\vec{p})-\mu\right]\frac{\nabla_r T}{T}-\nabla_r\mu\right\}.\vec{v}\frac{\partial f_o(\vec{p})}{\partial\varepsilon(\vec{p})} \quad \text{(A16)}$$

Making the transformation $p\rightarrow\vec{p}-e\int_{t-t'}^{t}\left[E_o+E_1\cos\omega t'\right]dt'$

$$f(\vec{r},\vec{p},t)=\tau^{-1}\int_{0}^{-\infty}\exp(-t/\tau)\,dt\;f_o\left(p\rightarrow\vec{p}-e\int_{t-t'}^{t'}\left[E_o+E_1\cos\omega t''\right]dt''\right)$$
$$+\tau\int_{0}^{-\infty}\exp(-t/\tau)dt\left\{\left[E(\vec{p})-\mu\right]\frac{\nabla_r T}{T}-\nabla_r\mu\right\}$$
$$\times\vec{v}\frac{\partial f_o}{\partial\varepsilon(\vec{p})}(p\rightarrow\vec{p}-e\int_{t-t'}^{t'}\left[E_o+E_1\cos\omega t''\right]dt'') \quad \text{(A17)}$$

In the linear approximation of $\nabla\mu$ and ∇T, the solution to the Boltzmann Transport Equation (BTE) for an electron is given as:

$$f(\vec{p})=\tau^{-1}\int_{0}^{\infty}dt\exp(-t/\tau)f_o\left(p\rightarrow\vec{p}-e\int_{t-t'}^{t'}\left[E_o+E_1\cos\omega t''\right]dt''\right)$$
$$+\tau^{-1}\int_{0}^{\infty}dt\exp(-t/\tau)\left\{\left[\varepsilon\left(p\rightarrow\vec{p}-e\int_{t-t'}^{t'}\left[E_o+E_1\cos\omega t''\right]dt''\right)\right]\frac{\nabla T}{T}+\nabla\mu\right\}$$
$$\times v\left(p\rightarrow\vec{p}-e\int_{t-t'}^{t'}\left[E_o+E_1\cos\omega t''\right]dt''dt'\right)$$
$$\times\frac{\partial f_o}{\partial\varepsilon}\left(p\rightarrow\vec{p}-e\int_{t-t'}^{t'}\left[E_o+E_1\cos\omega t''\right]dt''\right) \quad \text{(A18)}$$

APPENDIX B

DERIVATION OF CURRENT DENSITY OF GSL

The current density is defined as;

$$\vec{J} = -e\sum_{p} v(\vec{p}) f(\vec{p}) \tag{B1}$$

Substituting Eqn. (A18) into Eqn. (B1) yields:

$$\vec{J} = e\tau^{-1}\sum_{p} v(\vec{p})\int_{0}^{\infty} dt \exp(-t/\tau) f_o\left(p \to \vec{p} - e\int_{t-t'}^{t'} [E_o + E_1 \cos\omega t"]dt"\right)$$
$$+ e\tau^{-1}\int_{0}^{\infty} dt \exp(-t/\tau)\sum_{p} v(\vec{p})\left\{\left[\varepsilon\left(\vec{p} - e\int_{t-t'}^{t'} [E_o + E_1\cos(\omega t") - \mu]dt"\right)\right]\frac{\nabla T}{T} + \nabla\mu\right\}$$
$$\times v\left(p \to \vec{p} - e\int_{t-t'}^{t'} [E_o + E_1\cos\omega t"]dt"\right)\frac{\partial f_o}{\partial\varepsilon}\left(p \to \vec{p} - e\int_{t-t'}^{t'} [E_o + E_1\cos\omega t"]dt"\right) \tag{B2}$$

Making the transformation $p \to p \to \vec{p} - e\int_{t-t'}^{t'} [E_o + E_1\cos\omega t"]dt"$

Eqn.(B2) becomes

$$\vec{J} = e\tau^{-1}\int_{0}^{\infty} dt \exp(-t/\tau)\sum_{p} v\left(p \to \vec{p} - e\int_{t-t'}^{t'} [E_o + E_1\cos\omega t"]dt"\right) f_o(\vec{p})$$
$$+ e\tau^{-1}\int_{0}^{\infty} dt \exp(-t/\tau)\sum_{p} v(\vec{p})\left\{[\varepsilon(\vec{p}) - \mu]\frac{\nabla T}{T} + \nabla\mu\right\}$$
$$\times v\left(p \to \vec{p} - e\int_{t-t'}^{t'} [E_o + E_1\cos\omega t"]dt"\right)\frac{\partial f_o}{\partial\varepsilon} v(\vec{p}) \tag{B3}$$

If the current is traversing along only the x-component of the sheet, the current density is obtained to be as;

$$\vec{J}_x = e\tau^{-1}\int_{0}^{\infty} dt \exp(-t/\tau)\sum_{p} v_x\left(p \to \vec{p} - e\int_{t-t'}^{t'} [E_o + E_1\cos\omega t"]dt"\right) f_o(\vec{p})$$
$$+ e\tau^{-1}\int_{0}^{\infty} dt \exp(-t/\tau)\sum_{p} v(\vec{p})\left\{[\varepsilon(\vec{p}) - \mu]\frac{\nabla_x T}{T} + \nabla_x\mu\right\}$$
$$\times \vec{v}\left(p \to \vec{p} - e\int_{t-t'}^{t'} [E_o + E_1\cos\omega t"]dt"\right)\frac{\partial f_o}{\partial\varepsilon}\vec{v}_x(\vec{p}) \tag{B4}$$

$$\vec{J}_x = \frac{2e\tau^{-1}}{(2\pi\hbar)^2}\int_0^{\infty} dt \exp(-t/\tau) \int_{-\pi/d_1}^{\pi/d_1} d\vec{p}_x \int_{-\pi/d_2}^{\pi/d_2} d\vec{p}_y \vec{v}_x f_o(\vec{p})$$

$$\times\left(p \to \vec{p} - e\int_{t-t'}^{t'} \left[E_o + E_1 \cos\omega t''\right] dt'' \right)$$

$$+ \frac{2e\tau^{-1}}{(2\pi\hbar)^2}\int_0^{\infty} dt \exp(-t/\tau) \int_{-\pi/d_1}^{\pi/d_1} d\vec{p}_x \int_{-\pi/d_2}^{\pi/d_2} d\vec{p}_y \left\{ \left[\varepsilon(\vec{p}) - \mu\right] \frac{\nabla_x T}{T} + \nabla_x \mu \right\}$$

$$\times\vec{v}\left(p \to \vec{p} - e\int_{t-t'}^{t'} \left[E_o + E_1 \cos\omega t''\right] dt'' \right) \frac{\partial f_o}{\partial \varepsilon} \vec{v}_x(\vec{p}) \qquad \text{(B5)}$$

where the integration is carried out within the first Brillouin zone $-\hbar\pi/d_1 \le dp_x \le \hbar\pi/d_1$ and $-\hbar\pi/d_2 \le dp_y \le \hbar\pi/d_2$

The energy dispersion relation of graphene superlattice in the conduction band is based on the tight-binding approximation and is found to be:

$$\varepsilon(\vec{p}) = \sqrt{\Delta^2 + {\Delta_1}^2\left(1 - \cos\frac{p_x d_1}{\hbar}\right) + {\Delta_1}^2\left(1 - \cos\frac{p_y d_2}{\hbar}\right)} \qquad \text{(B6)}$$

Expanding Eqn. (B6) gives:

$$\varepsilon(\vec{p}) = \sqrt{\Delta^2 + {\Delta_1}^2 + {\Delta_1}^2 - {\Delta_1}^2\cos\frac{p_x d_1}{\hbar} - {\Delta_2}^2\cos\frac{p_y d_2}{\hbar}}$$

$$\varepsilon(\vec{p}) = D\left(1 - \frac{{\Delta_1}^2}{D^2}\cos\frac{p_x d_1}{\hbar} + \frac{{\Delta_2}^2}{D^2}\cos\frac{p_y d_2}{\hbar}\right)^{\frac{1}{2}} \qquad \text{(B7)}$$

where $D = \sqrt{\Delta^2 + {\Delta_1}^2 + {\Delta_2}^2}$

Eqn. (B7) is linearized using the Binomial theorem of half-integers as:

$$(1+x)^n = 1 + nx + \frac{1}{2!}nx^2 + \ldots$$

$$\varepsilon(\vec{p}) = D\left\{1 - \frac{1}{2}\left(\frac{{\Delta_1}^2}{D^2}\cos\frac{p_x d_1}{\hbar} + \frac{{\Delta_2}^2}{D^2}\cos\frac{p_y d_2}{\hbar}\right)\right\}$$

$$\varepsilon(\vec{p}) = D - \Delta_x\cos\frac{p_x d_1}{\hbar} - \Delta_y\cos\frac{p_y d_2}{\hbar} \qquad \text{(B8)}$$

where $\Delta_x = \frac{{\Delta_1}^2}{2D}$ and $\Delta_y = \frac{{\Delta_1}^2}{2D}$

Employing the transformation, Eqn. (B7) becomes

$$\varepsilon\left(p \to \vec{p} - e\int_{t-t'}^{t'} \left[E_o + E_1 \cos\omega t''\right] dt'' \right) =$$

$$D - \Delta_x\cos\left(p \to \vec{p} - e\int_{t-t'}^{t'} \left[E_o + E_1 \cos\omega t''\right] dt'' \right)\frac{d_1}{\hbar}$$

$$-\Delta_y\cos\left(p \to \vec{p} - e\int_{t-t'}^{t'} \left[E_o + E_1 \cos\omega t''\right] dt'' \right)\frac{d_2}{\hbar} \qquad \text{(B9)}$$

and

$$\vec{v}_x(\vec{p}) = \frac{\partial\varepsilon(\vec{p})}{\partial\vec{p}_x} = \frac{\Delta_x d_1}{\hbar}\sin\frac{\vec{p}_x d_1}{\hbar}$$

$$\vec{v}_x\left(D - \Delta_x\cos\left(p \to \vec{p} - e\int_{t-t'}^{t'}\left[E_o + E_1\cos\omega t''\right]dt''\right)\frac{d_1}{\hbar}\right) =$$

$$\frac{\Delta_x d_1}{\hbar}\sin\frac{d_1}{\hbar}\left(D - \Delta_x\cos\left(p \to \vec{p} - e\int_{t-t'}^{t'}\left[E_o + E_1\cos\omega t''\right]dt''\right)\frac{d_1}{\hbar}\right) \tag{B10}$$

Expanding the right-hand expression in Eqn. (B10) using the trigonometry identity yields:

$$\vec{v}_x\left(D - \Delta_x\cos\left(p \to \vec{p} - e\int_{t-t'}^{t'}\left[E_o + E_1\cos\omega t''\right]dt''\right)\frac{d_1}{\hbar}\right) =$$

$$\frac{\Delta_x d_1}{\hbar}\left\{\sin\frac{\vec{p}_x d_1}{\hbar}\cos\left(\frac{d_1 e}{\hbar}\int_{t-t'}^{t'}\left[E_o + E_1\cos\omega t''\right]dt''\right)\right\}$$

$$-\frac{\Delta_x d_1}{\hbar}\left\{\cos\frac{\vec{p}_x d_1}{\hbar}\sin\left(\frac{d_1 e}{\hbar}\int_{t-t'}^{t}\left[\vec{E}_o + \vec{E}_x\cos(\omega t')\right]dt'\right)\right\} \tag{B11}$$

Substituting Eqn. (B11) into Eqn. (B4) gives

$$\vec{J}_x = \frac{2e\tau^{-1}}{(2\pi\hbar)^2}\frac{\Delta_x d_1}{\hbar}\int_0^\infty dt\exp(-t/\tau)\int_{-\pi/d_1}^{\pi/d_1}d\vec{p}_x\int_{-\pi/d_2}^{\pi/d_2}d\vec{p}_y$$

$$\times\left\{\sin\frac{\vec{p}_x d_1}{\hbar}\cos\left(\frac{d_1 e}{\hbar}\int_{t-t'}^{t'}\left[\vec{E}_o + \left[\vec{E}_o + \vec{E}_x\cos(\omega t'')\right]\right]dt''\right)\right.$$

$$\left.-\cos\frac{\vec{p}_x d_1}{\hbar}\sin\left(\frac{d_1 e}{\hbar}\int_{t-t'}^{t'}\left[\vec{E}_o + \left[\vec{E}_o + \vec{E}_x\cos(\omega t'')\right]\right]dt''\right)\right\}f_o(\vec{p})$$

$$-\frac{2e\tau^{-1}}{(2\pi\hbar)^2}\left(\frac{\Delta_x d_1}{\hbar}\right)^2\int_0^\infty dt\exp(-t/\tau)\int_{-\pi/d_1}^{\pi/d_1}d\vec{p}_x\int_{-\pi/d_2}^{\pi/d_2}d\vec{p}_y\left\{\left[\varepsilon(\vec{p}) - \mu\right]\frac{\nabla_x T}{T} + \nabla_x\mu\right\}$$

$$\times\sin\frac{\vec{p}_x d_1}{\hbar}\left\{\sin\frac{\vec{p}_x d_1}{\hbar}\cos\left(\frac{d_1 e}{\hbar}\int_{t-t'}^{t'}\left[\vec{E}_o + \left[\vec{E}_o + \vec{E}_x\cos(\omega t'')\right]\right]dt''\right)\right.$$

$$\left.-\cos\frac{\vec{p}_x d_1}{\hbar}\sin\left(\frac{d_1 e}{\hbar}\int_{t-t'}^{t'}\left[\vec{E}_o + \left[\vec{E}_o + \vec{E}_x\cos(\omega t'')\right]\right]dt''\right)\right\}\frac{\partial f_o(\vec{p})}{\partial\varepsilon} \tag{B12}$$

Eqn. (B12) is difficult to solve analytically. Therefore, it can be expressed as $\vec{J}_x = \vec{J}_1 + \vec{J}_2$ without loss of generality.

Therefore;

$$\vec{J}_1 = \frac{2e\tau^{-1}}{(2\pi\hbar)^2}\frac{\Delta_x d_1}{\hbar}\int_0^{\infty} dt\exp(-t/\tau)\int_{-\pi/d_1}^{\pi/d_1} d\vec{p}_x \int_{-\pi/d_2}^{\pi/d_2} d\vec{p}_y$$
$$\times\left\{\sin\frac{\vec{p}_x d_1}{\hbar}\cos\left(\frac{d_1 e}{\hbar}\int_{t-t'}^{t'}\left[\vec{E}_o + \vec{E}_x\cos(wt")\right]dt"\right)\right.$$
$$\left. -\cos\frac{\vec{p}_x d_1}{\hbar}\sin\left(\frac{d_1 e}{\hbar}\int_{t-t'}^{t'}\left[\vec{E}_o + \vec{E}_x\cos(wt")\right]dt"\right)\right\} f_o(\vec{p}) \quad \text{(B13)}$$

and

$$\vec{J}_2 = \frac{2e\tau^{-1}}{(2\pi\hbar)^2}\left(\frac{\Delta_x d_1}{\hbar}\right)^2\int_0^{\infty} dt\exp(-t/\tau)\int_{-\pi/d_1}^{\pi/d_1} d\vec{p}_x \int_{-\pi/d_2}^{\pi/d_2} d\vec{p}_y \left\{\left[\varepsilon(\vec{p})-\mu\right]\frac{\nabla_x T}{T} + \nabla_x\mu\right\}$$
$$\times\sin\frac{\vec{p}_x d_1}{\hbar}\left\{\sin\frac{\vec{p}_x d_1}{\hbar}\cos\left(\frac{d_1 e}{\hbar}\int_{t-t'}^{t'}\left[\vec{E}_o + \vec{E}_x\cos(wt")\right]dt"\right)\right.$$
$$\left. -\cos\frac{\vec{p}_x d_1}{\hbar}\sin\left(\frac{d_1 e}{\hbar}\int_{t-t'}^{t'}\left[\vec{E}_o + \vec{E}_x\cos(wt")\right]dt"\right)\right\}\frac{\partial f_o(\vec{p})}{\partial\varepsilon} \quad \text{(B14)}$$

Considering $\vec{J}_1$ in Eqn. (B13), $f_o(\vec{p})$ is given by:

$$f_o(\vec{p}) = C.\exp\left(-\frac{\varepsilon(\vec{p})+\mu}{k_B T}\right) \quad \text{(B15)}$$

Substituting the expression of the energy dispersion relation of GSL in Eqn. (B7) into Eqn. (B14) and simplifying gives

$$f_o(\vec{p}) = C.\exp\left(-\frac{D - \Delta_x\cos\frac{p_x d_1}{\hbar} - \Delta_y\cos\frac{p_y d_2}{\hbar} - \mu}{k_B T}\right)$$

$$f_o(\vec{p}) = C.\exp\left(-\frac{1}{k_B T}\left[D - \Delta_x\cos\frac{p_x d_1}{\hbar} - \Delta_y\cos\frac{p_y d_2}{\hbar} - \mu\right]\right) \quad \text{(B16)}$$

where C is the normalization constant which is to be calculated from the condition

Therefore,

$$n_o = \frac{2a_o}{(2\pi\hbar)^2}\int_{-\pi/d_1}^{\pi/d_1} d\vec{p}_x \int_{-\pi/d_2}^{\pi/d_2} d\vec{p}_y f_o(\vec{p})$$
$$= \frac{2a_o C}{(2\pi\hbar)^2}\int_{-\pi/d_1}^{\pi/d_1} d\vec{p}_x \int_{-\pi/d_2}^{\pi/d_2} d\vec{p}_y \exp\left(-\frac{1}{k_B T}\left[D - \Delta_x\cos\frac{p_x d_1}{\hbar} - \Delta_y\cos\frac{p_y d_2}{\hbar} - \mu\right]\right)$$
$$= \frac{2a_o C}{(2\pi\hbar)^2}\exp\left(\frac{\mu - D}{k_B T}\right)\int_{-\pi/d_1}^{\pi/d_1} d\vec{p}_x \int_{-\pi/d_2}^{\pi/d_2} d\vec{p}_y \exp\left(\left[\frac{\Delta_x}{k_B T}\cos\frac{p_x d_1}{\hbar} + \frac{\Delta_y}{k_B T}\cos\frac{p_y d_2}{\hbar}\right]\right)$$

$$n_o = \frac{2a_o C}{(2\pi\hbar)^2}\exp\left(\frac{\mu - D}{k_B T}\right)\int_{-\pi/d_1}^{\pi/d_1} d\vec{p}_x \exp\left(k_1 \cos\frac{p_x d_1}{\hbar}\right)\int_{-\pi/d_2}^{\pi/d_2} d\vec{p}_y \exp\left(k_2 \cos\frac{p_y d_2}{\hbar}\right) \tag{B17}$$

where $k_1 = \frac{\Delta_x}{k_B T}$ and $k_2 = \frac{\Delta_y}{k_B T}$

To change the path of integration, let $\vec{p}_x d_1 = \theta_1 \quad \Rightarrow d\vec{p}_x = \frac{d\theta_1}{d_1}$

Whenever $d\vec{p}_x = \frac{\pi}{d_1};\ d\theta_1 = \pi$ and $d\vec{p}_x = -\frac{\pi}{d_1};\ d\theta_1 = -\pi$

Similarly, $\vec{p}_y d_2 = \theta_2 \Rightarrow d\vec{p}_y = \frac{d\theta_2}{d_2}$

For $d\vec{p}_y = \frac{\pi}{d_2};\ d\theta_2 = \pi \quad d\vec{p}_y = -\frac{\pi}{d_2};\ d\theta_2 = -\pi$

Therefore,

$$n_o = \frac{8a_o c}{(2\pi\hbar)^2 d_1 d_2}\exp\left(\frac{\mu - D}{k_B T}\right)\int_0^{\pi} d\theta_1 \exp\left(k_1 \cos\frac{\theta_1}{\hbar}\right)\int_0^{\pi} d\theta_2 \exp\left(k_2 \cos\frac{\theta_2}{\hbar}\right) \tag{B18}$$

Using the zeroth order modified Bessel function

$$I_n(x) = \frac{1}{\pi}\int_0^{\pi} d\theta \cos n\theta \exp(x\cos\theta)$$

$$\left.\begin{aligned} I_o(k_1) &= \frac{1}{\pi}\int_0^{\pi} d\theta_1 \exp(x\cos\theta) \\ I_o(k_2) &= \frac{1}{\pi}\int_0^{\pi} d\theta_2 \exp(x\cos\theta) \end{aligned}\right\}$$

Eqn.(B18) becomes

$$n_o = \frac{8a_o c}{(2\pi)^2 d_1 d_2}\exp\left(\frac{\mu - D}{k_B T}\right)\hbar^2 \pi I_o(k_1)\pi I_o(k_2)$$

Making C the subject gives

$$C = \frac{d_1 d_2 n_o}{2a_o I_o(k_1) I_o(k_2)}\exp\left(\frac{D - u}{k_B T}\right) \tag{B19}$$

Substitute Eqn. (B19) into Eqn. (B16) and simplify yields

$$f_o(\vec{p}) = \frac{\hbar^2 d_1 d_2 n_o}{2a_o I_o(k_1) I_o(k_2)}\exp\left(\frac{D - \mu}{k_B T}\right)$$

$$\times\exp\left(-\frac{1}{k_B T}\left[D - \Delta_x \cos\frac{p_x d_1}{\hbar} - \Delta_y \cos\frac{p_y d_2}{\hbar} - \mu\right]\right)$$

$$f_o(\vec{p}) = \frac{d_1 d_2 n_o}{2a_o I_o(k_1) I_o(k_2)}.\exp\left(k_1 \cos\frac{p_x d_1}{\hbar} + k_2 \cos\frac{p_y d_2}{\hbar}\right) \tag{B20}$$

APPENDIX C

DERIVATION OF THE ELECTRICAL RESISTIVITY OF GRAPHENE SUPERLATTICE

Substitute Eqn. (B20) into Eqn. (B13) gives

$$\vec{J}_1 = \frac{2e\tau^{-1}}{(2\pi\hbar)^3}\frac{\Delta_x d_1 d_1 d_2 n_o}{2a_o I_o(k_1) I_o(k_2)}\int_{-\pi/d_1}^{\pi/d_1} d\vec{p}_x \int_{-\pi/d_2}^{\pi/d_2} d\vec{p}_y \exp\left(k_1\cos\frac{p_x d_1}{\hbar} + k_2\cos\frac{p_y d_2}{\hbar}\right)$$
$$\times\int_0^{\infty} dt\exp(-t/\tau)\left\{\sin\frac{\vec{p}_x d_1}{\hbar}\cos\left(\frac{d_1 e}{\hbar}\int_{t-t'}^{t'}\left[\vec{E}_o + \vec{E}_x\cos(wt")\right]dt"\right)\right.$$
$$\left. -\cos\frac{\vec{p}_x d_1}{\hbar}\sin\left(\frac{d_1 e}{\hbar}\int_{t-t'}^{t'}\left[\vec{E}_o + \vec{E}_x\cos(wt")\right]dt"\right)\right\}$$

$$= \frac{2e\tau^{-1}}{(2\pi\hbar)^2}\frac{\Delta_x d_1}{\hbar}\frac{d_1 d_2 n_o}{2a_o I_o(k_1) I_o(k_2)}\int_0^{\infty} dt\exp(-t/\tau)\int_{-\pi/d_1}^{\pi/d_1} d\vec{p}_x \int_{-\pi/d_2}^{\pi/d_2} d\vec{p}_y$$
$$\times\left\{\sin\frac{\vec{p}_x d_1}{\hbar}\cos\left(\frac{d_1 e}{\hbar}\int_{t-t'}^{t'}\left[\vec{E}_o + \vec{E}_x\cos(wt")\right]dt"\right)\times\exp\left(k_1\cos\frac{p_x d_1}{\hbar} + k_2\cos\frac{p_y d_2}{\hbar}\right)\right.$$
$$\left. -\cos\frac{\vec{p}_x d_1}{\hbar}\sin\left(\frac{d_1 e}{\hbar}\int_{t-t'}^{t'}\left[\vec{E}_o + \vec{E}_x\cos(wt")\right]dt"\right)\times\exp\left(k_1\cos\frac{p_x d_1}{\hbar} + k_2\cos\frac{p_y d_2}{\hbar}\right)\right\} \quad (C1)$$

Integrating Eqn. (C1) causes the odd functions to vanish in the first Brillouin zone, $-\pi/d_1 < p_x < \pi/d_1$.

$$\vec{J}_1 = -\frac{2e\tau^{-1}}{(2\pi\hbar)^2}\frac{\Delta_x d_1}{\hbar}\frac{d_1 d_2 n_o}{2a_o I_o(k_1) I_o(k_2)}\int_0^{\infty} dt\exp(-t/\tau)\int_{-\pi/d_1}^{\pi/d_1} d\vec{p}_x \int_{-\pi/d_2}^{\pi/d_2} d\vec{p}_y$$
$$\times\left\{\cos\frac{\vec{p}_x d_1}{\hbar}\sin\left(\frac{d_1 e}{\hbar}\int_{t-t'}^{t'}\left[\vec{E}_o + \vec{E}_x\cos(wt")\right]dt"\right)\times\exp\left(k_1\cos\frac{p_x d_1}{\hbar} + k_2\cos\frac{p_y d_2}{\hbar}\right)\right\} \quad (C2)$$

Rearranging the terms gives:

$$\vec{J}_1 = -\frac{2e\tau^{-1}}{(2\pi\hbar)^2}\frac{\Delta_x d_1}{\hbar}\frac{d_1 d_2 n_o}{2a_o I_o(k_1) I_o(k_2)}$$
$$\times\left\{\int_0^{\infty} dt\exp(-t/\tau)\sin\left(\frac{d_1 e}{\hbar}\int_{t-t'}^{t'}\left[\vec{E}_o + \vec{E}_x\cos(wt")\right]dt"\right)\right.$$
$$\left.\times\int_{-\pi/d_1}^{\pi/d_1}\left[\cos\frac{\vec{p}_x d_1}{\hbar}\right]\exp\left(k_1\cos\frac{p_x d_1}{\hbar}\right)d\vec{p}_x \int_{-\pi/d_2}^{\pi/d_2} d\vec{p}_y\exp\left(k_2\cos\frac{p_y d_2}{\hbar}\right)\right\} \quad (C3)$$

Changing the path of the integration becomes

$$\vec{J}_1 = -\frac{e\tau^{-1}}{4(\pi\hbar)^2}\frac{\Delta_x d_1}{\hbar}\frac{d_1 d_2 n_o}{a_o I_o(k_1) I_o(k_2)} \times\left\{\int_0^{\infty} dt \exp(-t/\tau)\sin\left(\frac{d_1 e}{\hbar}\int_{t-t'}^{t'}\left[\vec{E}_o + \vec{E}_x\cos(wt")\right]dt"\right) \times\frac{1}{d_1}\int_{-\pi/d_1}^{\pi/d_1} d\theta_1\left[\cos\frac{\theta_1}{\hbar}\right]\exp\left(k_1\cos\frac{\theta_1}{\hbar}\right)\frac{1}{d_2}\int_{-\pi/d_2}^{\pi/d_2} d\theta_2\exp\left(k_2\cos\frac{\theta_2}{\hbar}\right)\right\} \quad \text{(C4)}$$

$$\vec{J}_1 = -\frac{e\tau^{-1}}{4(\pi\hbar)^2}\frac{\Delta_x d_1}{\hbar}\frac{d_1 d_2 n_o}{a_o I_o(k_1) I_o(k_2)} \times\left\{\int_0^{\infty} dt \exp(-t/\tau)\sin\left(\frac{d_1 e}{\hbar}\int_{t-t'}^{t'}\left[\vec{E}_o + \vec{E}_x\cos(wt")\right]dt"\right) \times\frac{1}{d_1}\int_{-\pi/d_1}^{\pi/d_1} d\theta_1\left[\cos\frac{\theta_1}{\hbar}\right]\exp\left(k_1\cos\frac{\theta_1}{\hbar}\right)\frac{1}{d_2}\int_{-\pi/d_2}^{\pi/d_2} d\theta_2\exp\left(k_2\cos\frac{\theta_2}{\hbar}\right)\right\} \quad \text{(C5)}$$

Simplifying Eqn. (C5) further gives

$$\vec{J}_1 = -\frac{e\tau^{-1}}{(\pi\hbar)^2}\frac{\Delta_x d_1}{\hbar}\frac{n_o}{a_o I_o(k_1) I_o(k_2)} \times\left\{\int_0^{\infty} dt \exp(-t/\tau)\sin\left(\frac{d_1 e}{\hbar}\int_{t-t'}^{t'}\left[\vec{E}_o + \vec{E}_x\cos(wt")\right]dt"\right) \times\frac{1}{\pi}\int_0^{\pi} d\theta_1\left[\cos\frac{\theta_1}{\hbar}\right]\exp\left(k_1\cos\frac{\theta_1}{\hbar}\right)\frac{1}{\pi}\int_0^{\pi} d\theta_2\exp\left(k_2\cos\frac{\theta_2}{\hbar}\right)\right\} \quad \text{(C6)}$$

By definition

$$I_o(k_1) = \frac{1}{\pi}\int_0^{\pi}\frac{d\theta_1}{\hbar}\exp(x\cos\theta) \quad \text{(C7)}$$

and

$$I_o(k_2) = \frac{1}{\pi}\int_0^{\pi}\frac{d\theta_2}{\hbar}\exp(x\cos\theta) \quad \text{(C8)}$$

Substituting Eqn. (C7) and Eqn. (C8) into Eqn. (C6) yields

$$\vec{J}_1 = -\frac{e\tau^{-1}\Delta_x d_1}{\hbar^2}\frac{n_o I_1(k_1)}{a_o I_o(k_1)}\left\{\int_0^{\infty} dt \exp(-t/\tau)\sin\left(\frac{d_1 e}{\hbar}\int_{t-t'}^{t'}\left[\vec{E}_o + \vec{E}_x\cos(wt")\right]dt"\right)\right\} \quad \text{(C9)}$$

Making use of the identity

$$\int_0^{\infty} \exp(-t/\tau)\sin\left(\frac{d_1 e}{\hbar}\int_{t-t'}^{t'}\left[\vec{E}_o + \vec{E}_x\cos(wt")\right]dt"\right)dt$$

$$= \sum_{n=-\infty}^{\infty} J_n{}^2(\chi)\left[\frac{(d_1 eE_o/\hbar + n\omega\hbar)\tau^2}{1+(d_1 eE_o/\hbar + n\omega\hbar)^2\tau^2}\right]$$

Eqn. (C9) becomes;

$$\vec{J}_1 = -\frac{e\tau^{-1}\Delta_x d_1}{\hbar^2}\frac{n_o I_1(k_1)}{a_o I_o(k_1)}\sum_{n=-\infty}^{\infty} J_n{}^2(\chi)\left[\frac{(d_1 eE_o/\hbar + n\omega\hbar)\tau^2}{1+(d_1 eE_o/\hbar + n\omega\hbar)^2\tau^2}\right]$$

$$= -\frac{e^2\tau\Delta_x d_1{}^2}{a_o\hbar^2}\frac{n_o I_1(k_1)}{I_o(k_1)}\sum_{n=-\infty}^{\infty} J_n{}^2(\chi)\left[\frac{1}{1+(d_1 eE_o/\hbar + n\omega\hbar)^2\tau^2}\right]\times\left(E_o + \frac{n\omega\hbar^2}{d_1 e}\right) \quad \text{(C10)}$$

Let $\sigma_x(\vec{E})$ be the conductivity of GSL along the x direction

$$\sigma_x(\vec{E}) = -\frac{e^2\tau\Delta_x d_1{}^2}{a_o\hbar^2}\frac{n_o I_1(k_1)}{I_o(k_1)}\sum_{n=-\infty}^{\infty} J_n{}^2(\chi)\left[\frac{1}{1+(d_1 eE_o/\hbar + n\omega\hbar)^2\tau^2}\right] \quad \text{(C11)}$$

The resistivity of the material is therefore

$$\rho_x(\vec{E}) = \frac{1}{\sigma_x(\vec{E})}$$

$$= -\frac{1}{\frac{e^2\tau\Delta_x d_1{}^2}{a_o\hbar^2}\frac{n_o I_1(k_1)}{I_o(k_1)}\sum_{n=-\infty}^{\infty} J_n{}^2(\chi)\left[\frac{1}{1+(d_1 eE_o/\hbar + n\omega\hbar)^2\tau^2}\right]} \quad \text{(C12)}$$

Let

$$\vec{E}_n = \vec{E}_o + \frac{n\omega\hbar^2}{d_1 e}$$

$$\vec{J}_1 = -\sigma_x(\vec{E})\left(E_o + \frac{n\omega\hbar^2}{d_1 e}\right)$$

$$\vec{J}_1 = -\sigma_x(\vec{E})\vec{E}_n$$

APPENDIX D

DERIVATION OF THE THERMOELECTRIC POWER OF GRAPHENE SUPERLATTICE

Solving for $\vec{J}_2$ in Eqn. (B13)

$$\vec{J}_2 = -\frac{2e\tau^{-1}}{(2\pi\hbar)^2}\left(\frac{\Delta_x d_1}{\hbar}\right)^2 \int_0^{\infty} dt \exp(-t/\tau) \int_{-\pi/d_1}^{\pi/d_1} d\vec{p}_x \int_{-\pi/d_2}^{\pi/d_2} d\vec{p}_y$$
$$\times\left\{\left[D - \Delta_x \cos\frac{\vec{p}_x d_1}{\hbar} - \Delta_y \cos\frac{\vec{p}_y d_2}{\hbar} - \mu\right]\frac{\nabla_x T}{T} + \nabla_x \mu\right\} \times \sin\frac{\vec{p}_x d_1}{\hbar}\frac{\partial f_o(\vec{p})}{\partial\varepsilon}$$
$$\times\left\{\sin\frac{\vec{p}_x d_1}{\hbar}\cos\left(\frac{d_1 e}{\hbar}\int_{t-t'}^{t'}\left[\vec{E}_o + \vec{E}_x\cos(wt")\right]dt"\right)\right.$$
$$\left. -\cos\frac{\vec{p}_x d_1}{\hbar}\sin\left(\frac{d_1 e}{\hbar}\int_{t-t'}^{t'}\left[\vec{E}_o + \vec{E}_x\cos(wt")\right]dt"\right)\right\} \quad \text{(D1)}$$

Differentiating Eqn. (B19), with respect to the energy dispersion relation gives

$$\frac{\partial f_o(\vec{p})}{\partial\varepsilon(\vec{p}_x)} = \frac{d_1 d_2 n_o}{2a_o I_o(k_1) I_o(k_2) k_B T}\exp\left(k_1\cos\frac{p_x d_1}{\hbar} + k_2\cos\frac{p_y d_2}{\hbar}\right) \quad \text{(D2)}$$

Substitute Eqn. (D2) into Eqn. (D1) and expand to obtain

$$\vec{J}_2 = -\frac{2e\tau^{-1}}{(2\pi\hbar)^2}\left(\frac{\Delta_x d_1}{\hbar}\right)^2 \frac{d_1 d_2 n_o}{2a_o I_o(k_1) I_o(k_2) k_B T}\int_0^{\infty} dt \exp(-t/\tau) \int_{-\pi/d_1}^{\pi/d_1} d\vec{p}_x \int_{-\pi/d_2}^{\pi/d_2} d\vec{p}_y$$
$$\times\left\{\left[D - \Delta_x \cos\frac{\vec{p}_x d_1}{\hbar} - \Delta_y \cos\frac{\vec{p}_y d_2}{\hbar} - \mu\right]\frac{\nabla_x T}{T} + \nabla_x \mu\right\}$$
$$\times\sin\frac{\vec{p}_x d_1}{\hbar}\exp\left(k_1\cos\frac{p_x d_1}{\hbar} + k_2\cos\frac{p_y d_2}{\hbar}\right)$$
$$\left\{\sin\frac{\vec{p}_x d_1}{\hbar}\cos\left(\frac{d_1 e}{\hbar}\int_{t-t'}^{t'}\left[\vec{E}_o + \vec{E}_x\cos(wt")\right]dt"\right)\right.$$
$$\left. -\cos\frac{\vec{p}_x d_1}{\hbar}\sin\left(\frac{d_1 e}{\hbar}\int_{t-t'}^{t'}\left[\vec{E}_o + \vec{E}_x\cos(wt")\right]dt"\right)\right\}$$

$$
\begin{aligned}
J_2 = & -\frac{2e\tau^{-1}}{(2\pi\hbar)^2}\left(\frac{\Delta_x d_1}{\hbar}\right)^2 \frac{d_1 d_2 n_o}{2a_o I_o(k_1) I_o(k_2) k_B T}\int_0^\infty dt \exp(-t/\tau) \\
& \times \int_{-\pi/d_1}^{\pi/d_1} d\vec{p}_x \int_{-\pi/d_2}^{\pi/d_2} d\vec{p}_y \cos\left(\frac{d_1 e}{\hbar}\int_{t-t'}^{t'}\left[\vec{E}_o + \vec{E}_x \cos(wt")\right]dt"\right) \\
& \times\left\{\left[D - \Delta_x \cos\frac{\vec{p}_x d_1}{\hbar} - \Delta_y \cos\frac{\vec{p}_y d_2}{\hbar} - \mu\right]\frac{\nabla_x T}{T} + \nabla_x \mu\right\} \\
& \times \sin^2\frac{\vec{p}_x d_1}{\hbar}\exp\left(k_1 \cos\frac{p_x d_1}{\hbar} + k_2 \cos\frac{p_y d_2}{\hbar}\right) \\
& + \frac{2e\tau^{-1}}{(2\pi\hbar)^2}\left(\frac{\Delta_x d_1}{\hbar}\right)^2 \frac{d_1 d_2 n_o}{2a_o I_o(k_1) I_o(k_2) k_B T}\int_0^\infty dt \exp(-t/\tau) \\
& \times \int_{-\pi/d_1}^{\pi/d_1} d\vec{p}_x \int_{-\pi/d_2}^{\pi/d_2} d\vec{p}_y \sin\left(\frac{d_1 e}{\hbar}\int_{t-t'}^{t'}\left[\vec{E}_o + \vec{E}_x \cos(wt")\right]dt"\right) \\
& \times\left\{\left[D - \Delta_x \cos\frac{\vec{p}_x d_1}{\hbar} - \Delta_y \cos\frac{\vec{p}_y d_2}{\hbar} - \mu\right]\frac{\nabla_x T}{T} + \nabla_x \mu\right\}\cos\frac{\vec{p}_x d_1}{\hbar} \\
& \times \sin\frac{\vec{p}_x d_1}{\hbar}\exp\left(k_1 \cos\frac{p_x d_1}{\hbar} + k_2 \cos\frac{p_y d_2}{\hbar}\right)
\end{aligned}
\tag{D3}
$$

Integrating Eqn. (D3) causes the odd functions vanish in the first Brillouin zone,

$-\pi/d_1 < p_x < \pi/d_1$

$$
\begin{aligned}
\vec{J}_2 = & -\frac{2e\tau^{-1}}{(2\pi\hbar)^2}\left(\frac{\Delta_x d_1}{\hbar}\right)^2 \frac{d_1 d_2 n_o}{2a_o I_o(k_1) I_o(k_2) k_B T}\int_0^\infty dt \exp(-t/\tau) \\
& \times \int_{-\pi/d_1}^{\pi/d_1} d\vec{p}_x \int_{-\pi/d_2}^{\pi/d_2} d\vec{p}_y \cos\left(\frac{d_1 e}{\hbar}\int_{t-t'}^{t'}\left[\vec{E}_o + \vec{E}_x \cos(wt")\right]dt"\right) \\
& \times\left\{\left[D - \Delta_x \cos\frac{\vec{p}_x d_1}{\hbar} - \Delta_y \cos\frac{\vec{p}_y d_2}{\hbar} - \mu\right]\frac{\nabla_x T}{T} + \nabla_x \mu\right\} \\
& \times \sin^2\frac{\vec{p}_x d_1}{\hbar}\exp\left(k_1 \cos\frac{p_x d_1}{\hbar} + k_2 \cos\frac{p_y d_2}{\hbar}\right)
\end{aligned}
\tag{D4}
$$

To change the path of integration, let

$$\vec{p}_x d_1 = \theta_1 \quad \Rightarrow d\vec{p}_x = \frac{d\theta_1}{d_1}$$

Whenever $d\vec{p}_x = \frac{\pi}{d_1};\ d\theta_1 = \pi$ and $d\vec{p}_x = -\frac{\pi}{d_1};\ d\theta_1 = -\pi$

Similarly; $\vec{p}_y d_2 = \theta_2 \Rightarrow d\vec{p}_y = \frac{d\theta_2}{d_2}$

For $d\vec{p}_y = \frac{\pi}{d_2};\ d\theta_2 = \pi \quad d\vec{p}_y = -\frac{\pi}{d_2};\ d\theta_2 = -\pi$

$$\vec{J}_2 = -\frac{2e\tau^{-1}}{(2\pi\hbar)^2}\left(\frac{\Delta_x d_1}{\hbar}\right)^2 \frac{d_1 d_2 n_o}{2a_o I_o(k_1) I_o(k_2) k_B T}\frac{4}{d_1 d_2}$$
$$\times \int_0^{\pi} d\theta_1 \int_0^{\pi} d\theta_2 \sin^2\frac{\theta_1}{\hbar}\exp\left(k_1\cos\frac{\theta_1}{\hbar} + k_2\cos\frac{\theta_2}{\hbar}\right)$$
$$\times \int_0^{\infty} dt \exp(-t/\tau)\times\cos\left(\frac{d_1 e}{\hbar}\int_{t-t'}^{t'}\left[\vec{E}_o + \vec{E}_x\cos(wt")\right]dt"\right)$$
$$\times\left\{\left[D - \Delta_x\cos\frac{\theta_1}{\hbar} - \Delta_y\cos\frac{\theta_2}{\hbar} - \mu\right]\frac{\nabla_x T}{T} + \nabla_x\mu\right\} \qquad \text{(D5)}$$

Using the trig identity $\sin^2\theta = \frac{1}{2}(1-\cos 2\theta)$, Eqn. (D5) can be simplified as:

$$\vec{J}_2 = -\frac{2e\tau^{-1}}{(2\pi\hbar)^2}\left(\frac{\Delta_x d_1}{\hbar}\right)^2 \frac{d_1 d_2 n_o}{2a_o I_o(k_1) I_o(k_2) k_B T}\frac{4}{d_1 d_2}\int_0^{\pi} d\theta_1 \int_0^{\pi} d\theta_2$$
$$\times \int_0^{\infty} dt \exp(-t/\tau)\times\cos\left(\frac{d_1 e}{\hbar}\int_{t-t'}^{t'}\left[\vec{E}_o + \vec{E}_x\cos(wt")\right]dt"\right)$$
$$\times\left\{\left[D - \Delta_x\cos\frac{\theta_1}{\hbar} - \Delta_y\cos\frac{\theta_2}{\hbar} - \mu\right]\frac{\nabla_x T}{T} + \nabla_x\mu\right\}$$
$$\times\frac{1}{2}\left(1-\cos\frac{2\theta_1}{\hbar}\right)\exp\left(k_1\cos\frac{\theta_1}{\hbar} + k_2\cos\frac{\theta_2}{\hbar}\right)$$

$$\vec{J}_2 = -\frac{e\tau^{-1}\Delta_x{}^2 d_1{}^2 n_o}{2\pi^2\hbar^4 a_o I_o(k_1) I_o(k_2) k_B T}\int_0^{\pi} d\theta_1 \int_0^{\pi} d\theta_2 \int_0^{\infty} dt \exp(-t/\tau)$$
$$\times\cos\left(\frac{d_1 e}{\hbar}\int_{t-t'}^{t'}\left[\vec{E}_o + \vec{E}_x\cos(wt")\right]dt"\right)$$
$$\times\left\{\left[D - \Delta_x\cos\frac{\theta_1}{\hbar} - \Delta_y\cos\frac{\theta_2}{\hbar} - \mu\right]\frac{\nabla_x T}{T} + \nabla_x\mu\right\}\exp\left(k_1\cos\frac{\theta_1}{\hbar} + k_2\cos\frac{\theta_2}{\hbar}\right)$$
$$+\frac{e\tau^{-1}\Delta_x{}^2 d_1{}^2 n_o}{2\pi^2\hbar^4 a_o I_o(k_1) I_o(k_2) k_B T}\int_0^{\pi}\theta_1\int_0^{\pi}\theta_2\int_0^{\infty} dt\exp(-t/\tau)\times\cos\left(\frac{d_1 e}{\hbar}\int_{t-t'}^{t'}\left[\vec{E}_o + \vec{E}_x\cos(wt")\right]dt"\right)$$
$$\times\left\{\left[D - \Delta_x\cos\frac{\theta_1}{\hbar} - \Delta_y\cos\frac{\theta_2}{\hbar} - \mu\right]\frac{\nabla_x T}{T} + \nabla_x\mu\right\}\cos\frac{2\theta_1}{\hbar}\exp\left(k_1\cos\frac{\theta_1}{\hbar} + k_2\cos\frac{\theta_2}{\hbar}\right) \qquad \text{(D6)}$$

Making use of the identity

$$\int_0^{\infty}\exp(-t/\tau)\cos\left(\frac{d_1 e}{\hbar}\int_{t-t'}^{t'}\left[\vec{E}_o + \vec{E}_x\cos(wt")\right]dt"\right)dt = \sum_{n=-\infty}^{\infty} J_n{}^2(\chi)\left[\frac{\tau^2}{1+(d_1 eE_o/\hbar + n\omega\hbar)^2\tau^2}\right]$$

$$\vec{J}_2 = -\frac{e\tau^{-1}\Delta_x{}^2 d_1{}^2 n_o}{2\pi^2\hbar^4 a_o I_o(k_1) I_o(k_2) k_B T}\int_0^{\pi} d\theta_1 \int_0^{\pi} d\theta_2 \sum_{n-\infty}^{\infty} J_n{}^2(\chi)\left[\frac{\tau^2}{1+\left(d_1 eE_o/\hbar + n\omega\hbar\right)^2\tau^2}\right]$$
$$\times\left\{\left[D-\Delta_x\cos\frac{\theta_1}{\hbar}-\Delta_y\cos\frac{\theta_2}{\hbar}-\mu\right]\frac{\nabla_x T}{T}+\nabla_x\mu\right\}\exp\left(k_1\cos\frac{\theta_1}{\hbar}+k_2\cos\frac{\theta_2}{\hbar}\right)$$
$$-\frac{e\tau^{-1}\Delta_x{}^2 d_1{}^2 n_o}{2\pi^2\hbar^4 a_o I_o(k_1) I_o(k_2) k_B T}\int_0^{\pi} d\theta_1 \int_0^{\pi} d\theta_2 \sum_{n-\infty}^{\infty} J_n{}^2(\chi)\left[\frac{\tau^2}{1+\left(d_1 eE_o/\hbar + n\omega\hbar\right)^2\tau^2}\right]$$
$$\times\left\{\left[D-\Delta_x\cos\frac{\theta_1}{\hbar}-\Delta_y\cos\frac{\theta_2}{\hbar}-\mu\right]\frac{\nabla_x T}{T}+\nabla_x\mu\right\}\cos\frac{2\theta_1}{\hbar}\exp\left(k_1\cos\frac{\theta_1}{\hbar}+k_2\cos\frac{\theta_2}{\hbar}\right) \quad \text{(D7)}$$

$$\vec{J}_2 = -\frac{e\tau\Delta_x{}^2 d_1{}^2 n_o}{2\pi^2\hbar^4 a_o I_o(k_1) I_o(k_2) k_B T}\int_0^{\pi} d\theta_1 \int_0^{\pi} d\theta_2 \sum_{n-\infty}^{\infty} J_n{}^2(\chi)\left[\frac{1}{1+\left(d_1 eE_o/\hbar + n\omega\hbar\right)^2\tau^2}\right]$$
$$\times\left\{\left[(D-\mu)-\Delta_x\cos\frac{\theta_1}{\hbar}-\Delta_y\cos\frac{\theta_2}{\hbar}\right]\frac{\nabla_x T}{T}+\nabla_x\mu\right\}\exp\left(k_1\cos\frac{\theta_1}{\hbar}+k_2\cos\frac{\theta_2}{\hbar}\right)$$
$$+\frac{e\tau\Delta_x{}^2 d_1{}^2 n_o}{2\pi^2\hbar^4 a_o I_o(k_1) I_o(k_2) k_B T}\int_0^{\pi} d\theta_1 \int_0^{\pi} d\theta_2 \sum_{n-\infty}^{\infty} J_n{}^2(\chi)\left[\frac{1}{1+\left(d_1 eE_o/\hbar + n\omega\hbar\right)^2\tau^2}\right]$$
$$\times\left\{\left[D-\Delta_x\cos\frac{\theta_1}{\hbar}-\Delta_y\cos\frac{\theta_2}{\hbar}-\mu\right]\frac{\nabla_x T}{T}+\nabla_x\mu\right\}\cos\frac{2\theta_1}{\hbar}\exp\left(k_1\cos\frac{\theta_1}{\hbar}+k_2\cos\frac{\theta_2}{\hbar}\right) \quad \text{(D8)}$$

Expanding Eqn. (D8) gives

$$\vec{J}_2 = -\frac{e\tau\Delta_x{}^2 d_1{}^2 n_o}{2\pi^2\hbar^4 a_o I_o(k_1) I_o(k_2) k_B T}\times\frac{1}{\pi}\int_0^{\pi} d\theta_1 \frac{1}{\pi}\int_0^{\pi} d\theta_2$$
$$\times\sum_{n-\infty}^{\infty} J_n{}^2(\chi)\left[\frac{1}{1+\left(d_1 eE_o/\hbar + n\omega\hbar\right)^2\tau^2}\right]$$
$$\times\left\{(D-\mu)\frac{\nabla_x T}{T}+\nabla_x\mu\right\}\exp\left(k_1\cos\frac{\theta_1}{\hbar}+k_2\cos\frac{\theta_2}{\hbar}\right)$$
$$+\frac{e\tau\Delta_x{}^2 d_1{}^2 n_o}{2\pi^2\hbar^4 a_o I_o(k_1) I_o(k_2) k_B T}\times\frac{1}{\pi}\int_0^{\pi} d\theta_1 \frac{1}{\pi}\int_0^{\pi} d\theta_2$$
$$\times\sum_{n-\infty}^{\infty} J_n{}^2(\chi)\left[\frac{1}{1+\left(d_1 eE_o/\hbar + n\omega\hbar\right)^2\tau^2}\right]\frac{\nabla T}{T}$$
$$\times\cos\frac{\theta_1}{\hbar}\exp\left(k_1\cos\frac{\theta_1}{\hbar}+k_2\cos\frac{\theta_2}{\hbar}\right)$$

$$+\frac{e\tau\Delta_x{}^2 d_1{}^2 n_o}{2\pi^2\hbar^4 a_o I_o(k_1) I_o(k_2) k_B T}\times\frac{1}{\pi}\int_0^{\pi} d\theta_1 \frac{1}{\pi}\int_0^{\pi} d\theta_2$$

$$\times\sum_{n-\infty}^{\infty} J_n{}^2(\chi)\left[\frac{1}{1+\left(d_1 eE_o/\hbar+n\omega\hbar\right)^2\tau^2}\right]\frac{\nabla T}{T}\times\cos\frac{\theta_2}{\hbar}\exp\left(k_1\cos\frac{\theta_1}{\hbar}+k_2\cos\frac{\theta_2}{\hbar}\right)$$

$$+\frac{e\tau\Delta_x{}^2 d_1{}^2 n_o}{2\pi^2\hbar^4 a_o I_o(k_1) I_o(k_2) k_B T}\frac{1}{\pi}\int_0^{\pi} d\theta_1 \frac{1}{\pi}\int_0^{\pi} d\theta_2$$

$$\times\sum_{n-\infty}^{\infty} J_n{}^2(\chi)\left[\frac{1}{1+\left(d_1 eE_o/\hbar+n\omega\hbar\right)^2\tau^2}\right]\times\left\{(D-\mu)\frac{\nabla_x T}{T}+\nabla_x\mu\right\}$$

$$\times\cos\frac{2\theta_1}{\hbar}\exp\left(k_1\cos\frac{\theta_1}{\hbar}+k_2\cos\frac{\theta_2}{\hbar}\right)$$

$$-\frac{e\tau\Delta_x{}^2 d_1{}^2 n_o}{2\pi^2\hbar^4 a_o I_o(k_1) I_o(k_2) k_B T}\frac{1}{\pi}\int_0^{\pi} d\theta_1 \frac{1}{\pi}\int_0^{\pi} d\theta_2\exp\left(k_1\cos\frac{\theta_1}{\hbar}+k_2\cos\frac{\theta_2}{\hbar}\right)$$

$$\times\cos\frac{\theta_1}{\hbar}\cos\frac{2\theta_1}{\hbar}\sum_{n-\infty}^{\infty} J_n{}^2(\chi)\left[\frac{1}{1+\left(d_1 eE_o/\hbar+n\omega\hbar\right)^2\tau^2}\right]\frac{\nabla_x T}{T}$$

$$-\frac{e\tau\Delta_x{}^2 d_1{}^2 n_o}{2\pi^2\hbar^4 a_o I_o(k_1) I_o(k_2) k_B T}\frac{1}{\pi}\int_0^{\pi} d\theta_1 \frac{1}{\pi}\int_0^{\pi} d\theta_2\cos\frac{\theta_2}{\hbar}\cos\frac{2\theta_1}{\hbar}$$

$$\times\exp\left(k_1\cos\frac{\theta_1}{\hbar}+k_2\cos\frac{\theta_2}{\hbar}\right)\sum_{n-\infty}^{\infty} J_n{}^2(\chi)\left[\frac{1}{1+\left(d_1 eE_o/\hbar+n\omega\hbar\right)^2\tau^2}\right]\frac{\nabla T}{T} \quad \text{(D9)}$$

Eqn. (D9) is broken down into $\vec{J}_2=\vec{J}_{21}+\vec{J}_{22}+\vec{J}_{23}+\vec{J}_{24}+\vec{J}_{25}+\vec{J}_{26}$ and simplified as:

$$\vec{J}_{21}=-\frac{e\tau\Delta_x{}^2 d_1{}^2 n_o}{2\pi^2\hbar^4 a_o I_o(k_1) I_o(k_2) k_B T}\times\frac{1}{\pi^2}\int_0^{\pi} d\theta_1\int_0^{\pi} d\theta_2\sum_{n-\infty}^{\infty} J_n{}^2(\chi)\left[\frac{1}{1+\left(d_1 eE_o/\hbar+n\omega\hbar\right)^2\tau^2}\right]$$

$$\times\left\{(D-\mu)\frac{\nabla_x T}{T}+\nabla_x\mu\right\}\exp\left(k_1\cos\frac{\theta_1}{\hbar}+k_2\cos\frac{\theta_2}{\hbar}\right)$$

$$\vec{J}_{21}=-\frac{e\tau\Delta_x{}^2 d_1{}^2 n_o}{2\pi^2\hbar^4 a_o I_o(k_1) I_o(k_2) k_B T}\times\sum_{n-\infty}^{\infty} J_n{}^2(\chi)\left[\frac{1}{1+\left(d_1 eE_o/\hbar+n\omega\hbar\right)^2\tau^2}\right]$$

$$\times\left\{(D-\mu)\frac{\nabla_x T}{T}+\nabla_x\mu\right\}\frac{1}{\pi}\int_0^{\pi} d\theta_1\exp\left(k_1\cos\frac{\theta_1}{\hbar}\right)\frac{1}{\pi}\int_0^{\pi} d\theta_2\exp\left(k_2\cos\frac{\theta_2}{\hbar}\right)$$

$$\vec{J}_{21} = -\frac{e\tau\Delta_x{}^2 d_1{}^2 n_o}{2\pi^2\hbar^4 a_o I_o(k_1) I_o(k_2) k_B T}\,\pi^2\hbar^2 I_o(k_1) I_o(k_2)\times\left\{(D-\mu)\frac{\nabla_x T}{T}+\nabla_x\mu\right\}$$
$$\times\sum_{n-\infty}^{\infty} J_n{}^2(\chi)\left[\frac{1}{1+\left(d_1 eE_o/\hbar+n\omega\hbar\right)^2\tau^2}\right]$$

$$\vec{J}_{21} = -\frac{e\tau\Delta_x{}^2 d_1{}^2 n_o}{2\pi^2\hbar^4 a_o I_o(k_1) I_o(k_2) k_B T}$$
$$\times\sum_{n-\infty}^{\infty} J_n{}^2(\chi)\left[\frac{1}{1+\left(d_1 eE_o/\hbar+n\omega\hbar\right)^2\tau^2}\right]\times\left\{(D-\mu)\frac{\nabla_x T}{T}+\nabla_x\mu\right\} \quad \text{(D10)}$$

$$\vec{J}_{22} = \frac{e\tau\Delta_x{}^2 d_1{}^2 n_o}{2\pi^2\hbar^4 a_o I_o(k_1) I_o(k_2) k_B T}\times\frac{1}{\pi}\int_0^{\pi} d\theta_1\frac{1}{\pi}\int_0^{\pi} d\theta_2$$
$$\times\sum_{n-\infty}^{\infty} J_n{}^2(\chi)\left[\frac{1}{1+\left(d_1 eE_o/\hbar+n\omega\hbar\right)^2\tau^2}\right]\frac{\nabla T}{T}$$
$$\times\cos\frac{\theta_1}{\hbar}\exp\left(k_1\cos\frac{\theta_1}{\hbar}+k_2\cos\frac{\theta_2}{\hbar}\right)$$

$$=\frac{e\tau\Delta_x{}^2 d_1{}^2 n_o}{2\pi^2\hbar^4 a_o I_o(k_1) I_o(k_2) k_B T}\sum_{n-\infty}^{\infty} J_n{}^2(\chi)\left[\frac{1}{1+\left(d_1 eE_o/\hbar+n\omega\hbar\right)^2\tau^2}\right]\frac{\nabla T}{T}$$
$$\times\frac{1}{\pi}\int_0^{\pi} d\theta_1\frac{1}{\pi}\int_0^{\pi} d\theta_2\cos\frac{\theta_1}{\hbar}\exp\left(k_1\cos\frac{\theta_1}{\hbar}+k_2\cos\frac{\theta_2}{\hbar}\right)$$

$$=\frac{e\tau\Delta_x{}^2 d_1{}^2 n_o}{2\pi^2\hbar^4 a_o I_o(k_1) I_o(k_2) k_B T}\sum_{n=-\infty}^{\infty} J_n{}^2(\chi)\left[\frac{1}{1+\left(d_1 eE_o/\hbar+n\omega\hbar\right)^2\tau^2}\right]\frac{\nabla T}{T}$$
$$\times\frac{1}{\pi}\int_0^{\pi}\cos\frac{\theta_1}{\hbar}\exp\left(k_1\cos\frac{\theta_1}{\hbar}\right)d\theta_1\frac{1}{\pi}\int_0^{\pi} d\theta_2\exp\left(k_2\cos\frac{\theta_2}{\hbar}\right)$$

$$\vec{J}_{22} = \frac{e\tau\Delta_x{}^2 d_1{}^2 n_o}{2\hbar^2 a_o k_B T}\sum_{n=-\infty}^{\infty} J_n{}^2(\chi)\left[\frac{1}{1+\left(d_1 eE_o/\hbar+n\omega\hbar\right)^2\tau^2}\right]\frac{\nabla T}{T}\frac{I_1(k_1)}{I_o(k_1)} \quad \text{(D11)}$$

$$\vec{J}_{23} = \frac{e\tau\Delta_x{}^2 d_1{}^2 n_o}{2\pi^2\hbar^4 a_o I_o(k_1) I_o(k_2) k_B T}\times\frac{1}{\pi}\int_0^{\pi} d\theta_1\frac{1}{\pi}\int_0^{\pi} d\theta_2$$
$$\times\sum_{n=-\infty}^{\infty} J_n{}^2(\chi)\left[\frac{1}{1+\left(d_1 eE_o/\hbar+n\omega\hbar\right)^2\tau^2}\right]\frac{\nabla T}{T}\times\cos\frac{\theta_2}{\hbar}\exp\left(k_1\cos\frac{\theta_1}{\hbar}+k_2\cos\frac{\theta_2}{\hbar}\right)$$

$$= \frac{e\tau\Delta_x{}^2 d_1{}^2 n_o}{2\pi^2\hbar^4 a_o I_o(k_1) I_o(k_2) k_B T} \int_0^{\pi} d\theta_2 \sum_{n=-\infty}^{\infty} J_n{}^2(\chi) \left[\frac{1}{1+\left(d_1 eE_o/\hbar + n\omega\hbar\right)^2 \tau^2} \right] \frac{\nabla T}{T}$$

$$\times \frac{1}{\pi} \int_0^{\pi} d\theta_1 \exp\left(k_1 \cos\frac{\theta_1}{\hbar} \right) \frac{1}{\pi} \int_0^{\pi} d\theta_2 \cos\frac{\theta_2}{\hbar} \exp\left(k_2 \cos\frac{\theta_2}{\hbar} \right)$$

$$= \frac{e\tau\Delta_x{}^2 d_1{}^2 n_o \hbar^2 \pi^2 I_o(k_1) I_1(k_2)}{2\pi^2\hbar^4 a_o I_o(k_1) I_o(k_2) k_B T} \sum_{n=-\infty}^{\infty} J_n{}^2(\chi) \left[\frac{1}{1+\left(d_1 eE_o/\hbar + n\omega\hbar\right)^2 \tau^2} \right] \frac{\nabla T}{T}$$

$$\vec{J}_{23} = \frac{e\tau\Delta_x{}^2 d_1{}^2 n_o}{2\hbar^2 a_o k_B T} \int_0^{\pi} d\theta_2 \sum_{n=-\infty}^{\infty} J_n{}^2(\chi) \left[\frac{1}{1+\left(d_1 eE_o/\hbar + n\omega\hbar\right)^2 \tau^2} \right] \frac{\nabla T}{T} \frac{I_1(k_2)}{I_o(k_2)} \tag{D12}$$

$$\vec{J}_{24} = \frac{e\tau\Delta_x{}^2 d_1{}^2 n_o}{2\pi^2\hbar^4 a_o I_o(k_1) I_o(k_2) k_B T} \sum_{n=-\infty}^{\infty} J_n{}^2(\chi) \left[\frac{1}{1+\left(d_1 eE_o/\hbar + n\omega\hbar\right)^2 \tau^2} \right]$$

$$\times \frac{1}{\pi} \int_0^{\pi} \cos\frac{2\theta_1}{\hbar} \exp\left(k_1 \cos\frac{\theta_1}{\hbar} \right) d\theta_1 \frac{1}{\pi} \int_0^{\pi} \exp\left(k_2 \cos\frac{\theta_2}{\hbar} \right) d\theta_2 \left\{ (D-\mu) \frac{\nabla_x T}{T} + \nabla_x \mu \right\}$$

$$= \frac{e\tau\Delta_x{}^2 d_1{}^2 n_o}{2\pi^2\hbar^4 a_o k_B T} \pi^2\hbar^2 I_2(k_1) I_o(k_2)$$

$$\times \sum_{n=-\infty}^{\infty} J_n{}^2(\chi) \left[\frac{1}{1+\left(d_1 eE_o/\hbar + n\omega\hbar\right)^2 \tau^2} \right] \left\{ (D-\mu) \frac{\nabla_x T}{T} + \nabla_x \mu \right\}$$

$$= \frac{e\tau\Delta_x{}^2 d_1{}^2 n_o}{2\hbar^2 a_o k_B T} \sum_{n-\infty}^{\infty} J_n{}^2(\chi) \left[\frac{1}{1+\left(d_1 eE_o/\hbar + n\omega\hbar\right)^2 \tau^2} \right]$$

$$\times \left\{ (D-\mu) \frac{\nabla_x T}{T} + \nabla_x \mu \right\} \frac{I_2(k_1)}{I_o(k_1)}$$

where $\frac{1}{\pi} \int_0^{\pi} \cos\frac{2\theta_1}{\hbar} \exp\left(k_1 \cos\frac{\theta_1}{\hbar} \right) d\theta_1 = I_2(k_1)$ (D13)

Eqn. (D13) obeys the recurrence relation

$$I_{n+1}(x) = I_{n-1}(x) - \frac{2n}{x} I_n(x)$$

Therefore,

$$I_2(k_1) = I_o(k_1) - \frac{2}{k_1} I_1(k_1)$$

$$= I_o(k_1) - \frac{2}{k_1} I_1(k_1) \tag{D14}$$

$$= \frac{e\tau\Delta_x{}^2 d_1{}^2 n_o}{2\hbar^2 a_o k_B T} \times \sum_{n=-\infty}^{\infty} J_n{}^2(\chi)\left[\frac{1}{1+\left(d_1 eE_o/\hbar + n\omega\hbar\right)^2\tau^2}\right] \times\left\{(D-\mu)\frac{\nabla_x T}{T}+\nabla_x\mu\right\}\left(1-\frac{2}{k_1}\frac{I_1(k_1)}{I_o(k_1)}\right)$$

$$J_{24} = \frac{e\tau\Delta_x{}^2 d_1{}^2 n_o}{2\hbar^2 a_o k_B T} \times \sum_{n=-\infty}^{\infty} J_n{}^2(\chi)\left[\frac{1}{1+\left(d_1 eE_o/\hbar + n\omega\hbar\right)^2\tau^2}\right]\left\{(D-\mu)\frac{\nabla_x T}{T}+\nabla_x\mu\right\}$$

$$-\frac{e\tau\Delta_x{}^2 d_1{}^2 n_o}{2\hbar^2 a_o k_B T}\sum_{n=-\infty}^{\infty} J_n{}^2(\chi)\left[\frac{1}{1+\left(d_1 eE_o/\hbar + n\omega\hbar\right)^2\tau^2}\right]\left\{(D-\mu)\frac{\nabla_x T}{T}+\nabla_x\mu\right\}\frac{2}{k_1}\frac{I_1(k_1)}{I_o(k_1)} \quad \text{(D15)}$$

$$\vec{J}_{25} = \frac{e\tau\Delta_x{}^2 d_1{}^2 n_o}{2\pi^2\hbar^4 a_o I_o(k_1) I_o(k_2) k_B T} \times \sum_{n=-\infty}^{\infty} J_n{}^2(\chi)\left[\frac{1}{1+\left(d_1 eE_o/\hbar + n\omega\hbar\right)^2\tau^2}\right]\frac{\nabla_x T}{T} \times \int_0^{\pi} d\theta_1 \int_0^{\pi} d\theta_2 \times \cos\frac{\theta_1}{\hbar}\cos\frac{2\theta_1}{\hbar}\exp\left(k_1\cos\frac{\theta_1}{\hbar}+k_2\cos\frac{\theta_2}{\hbar}\right)$$

$$= -\frac{e\tau\Delta_x{}^2 d_1{}^2 n_o}{2\pi^2\hbar^4 a_o I_o(k_1) I_o(k_2) k_B T} \times \sum_{n-\infty}^{\infty} J_n{}^2(\chi)\left[\frac{1}{1+\left(d_1 eE_o/\hbar + n\omega\hbar\right)^2\tau^2}\right]\frac{\nabla_x T}{T} \times \frac{1}{\pi}\int_0^{\pi}\cos\frac{\theta_1}{\hbar}\cos\frac{2\theta_1}{\hbar}\exp\left(k_1\cos\frac{\theta_1}{\hbar}\right)d\theta_1 \frac{1}{\pi}\int_0^{\pi}\exp\left(k_2\cos\frac{\theta_2}{\hbar}\right)d\theta_2$$

$$= -\frac{e\tau\Delta_x{}^2 d_1{}^2 n_o}{2\pi^2\hbar^4 a_o I_o(k_1) I_o(k_2) k_B T} \times \sum_{n=-\infty}^{\infty} J_n{}^2(\chi)\left[\frac{1}{1+\left(d_1 eE_o/\hbar + n\omega\hbar\right)^2\tau^2}\right]\frac{\nabla_x T}{T} \times \frac{1}{\pi}\int_0^{\pi}\cos\frac{\theta_1}{\hbar}\cos\frac{2\theta_1}{\hbar}\exp\left(k_1\cos\frac{\theta_1}{\hbar}\right)d\theta_1 \frac{1}{\pi}\int_0^{\pi}\exp\left(k_2\cos\frac{\theta_2}{\hbar}\right)d\theta_2$$

$$= -\frac{e\tau\Delta_x{}^2 d_1{}^2 n_o}{2\pi^2\hbar^4 a_o I_o(k_1) I_o(k_2) k_B T} \times \sum_{n=-\infty}^{\infty} J_n{}^2(\chi)\left[\frac{1}{1+\left(d_1 eE_o/\hbar + n\omega\hbar\right)^2\tau^2}\right]\frac{\nabla_x T}{T} \times \frac{1}{\pi}\int_0^{\pi}\frac{1}{2}\left(\cos\frac{\theta_1}{\hbar}+\cos\frac{3\theta_1}{\hbar}\right)\exp\left(k_1\cos\frac{\theta_1}{\hbar}\right)d\theta_1 \frac{1}{\pi}\int_0^{\pi}\exp\left(k_2\cos\frac{\theta_2}{\hbar}\right)d\theta_2$$

$$= -\frac{e\tau\Delta_x{}^2 d_1{}^2 n_o}{4\pi^2\hbar^4 a_o I_o(k_1) I_o(k_2) k_B T} \times \sum_{n=-\infty}^{\infty} J_n{}^2(\chi)\left[\frac{1}{1+\left(d_1 eE_o/\hbar + n\omega\hbar\right)^2\tau^2}\right]\frac{\nabla_x T}{T} \times \frac{1}{\pi}\int_0^{\pi}\cos\frac{\theta_1}{\hbar}\exp\left(k_1\cos\frac{\theta_1}{\hbar}\right)d\theta_1 \frac{1}{\pi}\int_0^{\pi}\exp\left(k_2\cos\frac{\theta_2}{\hbar}\right)d\theta_2$$

$$-\frac{e\tau\Delta_x{}^2 d_1{}^2 n_o}{4\pi^2\hbar^4 a_o I_o(k_1) I_o(k_2) k_B T} \times \sum_{n=-\infty}^{\infty} J_n{}^2(\chi)\left[\frac{1}{1+\left(d_1 eE_o/\hbar + n\omega\hbar\right)^2\tau^2}\right]\frac{\nabla_x T}{T} \times \frac{1}{\pi}\int_0^{\pi}\cos\frac{3\theta_1}{\hbar}\exp\left(k_1\cos\frac{\theta_1}{\hbar}\right)d\theta_1 \frac{1}{\pi}\int_0^{\pi}\exp\left(k_2\cos\frac{\theta_2}{\hbar}\right)d\theta_2$$

$$= -\frac{e\tau\Delta_x^{\,2} d_1^{\,2} n_o}{4\pi^2\hbar^4 a_o k_B T}\frac{I_1(k_1)I_o(k_2)}{I_o(k_1)I_o(k_2)}\times\sum_{n=-\infty}^{\infty} J_n^{\,2}(\chi)\left[\frac{1}{1+\left(d_1 eE_o/\hbar+n\omega\hbar\right)^2\tau^2}\right]\frac{\nabla_x T}{T}$$

$$-\frac{e\tau\Delta_x^{\,2} d_1^{\,2} n_o}{4\pi^2\hbar^4 a_o k_B T}\frac{I_3(k_1)I_o(k_2)}{I_o(k_1)I_o(k_2)}\times\sum_{n=-\infty}^{\infty} J_n^{\,2}(\chi)\left[\frac{1}{1+\left(d_1 eE_o/\hbar+n\omega\hbar\right)^2\tau^2}\right]\frac{\nabla_x T}{T}$$

$$= -\frac{e\tau\Delta_x^{\,2} d_1^{\,2} n_o}{4\pi^2\hbar^4 a_o k_B T}\frac{I_1(k_1)I_o(k_2)}{I_o(k_1)I_o(k_2)}$$

$$\times\sum_{n=-\infty}^{\infty} J_n^{\,2}(\chi)\left[\frac{1}{1+\left(d_1 eE_o/\hbar+n\omega\hbar\right)^2\tau^2}\right]\frac{\nabla_x T}{T}\left\{\frac{I_1(k_1)+I_3(k_1)}{I_o(k_1)}\right\}$$

where

$$\frac{1}{\pi}\int_0^{\pi}\left(\cos\frac{2\theta_1}{\hbar}\right)\exp\left(k_1\cos\frac{\theta_1}{\hbar}\right)d\theta_1 = I_2(k_1) \qquad \text{(D16)}$$

Eqn. (D16) obeys the recurrence relation of second order modified Bessel's function as;

$$I_{n+1}(x) = I_{n-1}(x) - \frac{2n}{x}I_n(x)$$

Therefore;

$$I_3(k_1) = I_1(k_1) - \frac{4}{k_1}I_2(k_1)$$

$$I_3(k_1) = I_1(k_1) - \frac{4}{k_1}\left[I_o(k_1) - \frac{2}{k_1}I_1(k_1)\right]$$

$$I_3(k_1) = I_1(k_1) - \frac{4}{k_1}I_o(k_1) + \frac{8}{k_1^{\,2}}I_1(k_1)$$

Thus;

$$\frac{I_1(k_1)+I_3(k_1)}{I_o(k_1)} = \frac{I_1(k_1)+I_1(k_1)-\frac{4}{k_1}I_o(k_1)+\frac{8}{k_1^{\,2}}I_1(k_1)}{I_o(k_1)}$$

$$\frac{I_1(k_1)+I_3(k_1)}{I_o(k_1)} = \frac{2I_1(k_1)}{I_o(k_1)} - \frac{4}{k_1}\frac{I_o(k_1)}{I_o(k_1)} + \frac{8}{k_1^{\,2}}\frac{I_1(k_1)}{I_o(k_1)} \qquad \text{(D17)}$$

$$\vec{J}_{25} = -\frac{e\tau\Delta_x^{\,2} d_1^{\,2} n_o\Delta_x}{4\hbar^2 a_o k_B T}\times\sum_{n=-\infty}^{\infty} J_n^{\,2}(\chi)\left[\frac{1}{1+\left(d_1 eE_o/\hbar+n\omega\hbar\right)^2\tau^2}\right]$$

$$\times\frac{\nabla_x T}{T}\left\{\frac{2I_1(k_1)}{I_o(k_1)} - \frac{4}{k_1}\frac{I_o(k_1)}{I_o(k_1)} + \frac{8}{k_1^{\,2}}\frac{I_1(k_1)}{I_o(k_1)}\right\}$$

$$= -\frac{e\tau\Delta_x{}^2 d_1{}^2 n_o \Delta_x}{2\hbar^2 a_o k_B T} \times \sum_{n=-\infty}^{\infty} J_n{}^2(\chi)\left[\frac{1}{1+\left(d_1 eE_o/\hbar + n\omega\hbar\right)^2\tau^2}\right]\frac{\nabla_x T}{T}\frac{I_1(k_1)}{I_o(k_1)}$$

$$+\frac{e\tau\Delta_x{}^2 d_1{}^2 n_o \Delta_x}{\hbar^2 a_o k_B T} \times \sum_{n=-\infty}^{\infty} J_n{}^2(\chi)\left[\frac{1}{1+\left(d_1 eE_o/\hbar + n\omega\hbar\right)^2\tau^2}\right]\frac{\nabla_x T}{T}\frac{1}{k_1}\frac{I_o(k_1)}{I_o(k_1)}$$

$$-\frac{e\tau\Delta_x{}^2 d_1{}^2 n_o \Delta_x}{2\hbar^2 a_o k_B T} \times \sum_{n=-\infty}^{\infty} J_n{}^2(\chi)\left[\frac{1}{1+\left(d_1 eE_o/\hbar + n\omega\hbar\right)^2\tau^2}\right]\frac{\nabla_x T}{T}\frac{1}{k_1{}^2}\frac{I_1(k_1)}{I_o(k_1)} \quad \text{(D18)}$$

$$\vec{J}_{26} = -\frac{e\tau\Delta_x{}^2 d_1{}^2 n_o \Delta_y}{2\pi^2\hbar^4 a_o I_o(k_1) I_o(k_2) k_B T}\int_0^{\pi} d\theta_1 \int_0^{\pi} d\theta_2 \cos\frac{\theta_2}{\hbar}\cos\frac{2\theta_1}{\hbar}\exp\left(k_1\cos\frac{\theta_1}{\hbar} + k_2\cos\frac{\theta_2}{\hbar}\right)$$

$$\times\frac{1}{\pi^2}\sum_{n-\infty}^{\infty} J_n{}^2(\chi)\left[\frac{1}{1+\left(d_1 eE_o/\hbar + n\omega\hbar\right)^2\tau^2}\right]\frac{\nabla T}{T}$$

$$= -\frac{e\tau\Delta_x{}^2 d_1{}^2 n_o \Delta_y}{2\pi^2\hbar^4 a_o I_o(k_1) I_o(k_2) k_B T} \times \sum_{n=-\infty}^{\infty} J_n{}^2(\chi)\left[\frac{1}{1+\left(d_1 eE_o/\hbar + n\omega\hbar\right)^2\tau^2}\right]\frac{\nabla T}{T}$$

$$\times\frac{1}{\pi}\int_0^{\pi} d\theta_1 \cos\frac{2\theta_1}{\hbar}\exp\left(k_1\cos\frac{\theta_1}{\hbar}\right)\frac{1}{\pi}\int_0^{\pi} d\theta_2 \cos\frac{\theta_2}{\hbar}\exp\left(k_2\cos\frac{\theta_2}{\hbar}\right)$$

$$= -\frac{e\tau\Delta_x{}^2 d_1{}^2 n_o \Delta_y I_2(k_1) I_1(k_2)}{2\hbar^2 a_o I_o(k_1) I_o(k_2) k_B T}\sum_{n=-\infty}^{\infty} J_n{}^2(\chi)\left[\frac{1}{1+\left(d_1 eE_o/\hbar + n\omega\hbar\right)^2\tau^2}\right]\frac{\nabla T}{T}$$

$$\frac{I_2(k_1) I_1(k_2)}{I_o(k_1) I_o(k_2)} = \frac{I_1(k_2)}{I_o(k_2)} - \frac{2}{k_1}\frac{I_1(k_1) I_1(k_2)}{I_o(k_1) I_o(k_2)}$$

$$= -\frac{e\tau\Delta_x{}^2 d_1 \Delta_y n_o}{2\hbar^2 d_2 a_o k_B T}$$

$$\times\sum_{n=-\infty}^{\infty} J_n{}^2(\chi)\left[\frac{1}{1+\left(d_1 eE_o/\hbar + n\omega\hbar\right)^2\tau^2}\right]\left\{\frac{I_1(k_2)}{I_o(k_2)} - \frac{2}{k_1}\frac{I_1(k_1) I_1(k_2)}{I_o(k_1) I_o(k_2)}\right\}\frac{\nabla_x T}{T}$$

$$\vec{J}_{26} = -\frac{e\tau\Delta_x{}^2 d_1 \Delta_y n_o}{2\hbar^2 d_2 a_o k_B T} \times \sum_{n=-\infty}^{\infty} J_n{}^2(\chi)\left[\frac{1}{1+\left(d_1 eE_o/\hbar + n\omega\hbar\right)^2\tau^2}\right]\frac{I_1(k_2)}{I_o(k_2)}\frac{\nabla_x T}{T}$$

$$+\frac{e\tau\Delta_x{}^2 d_1 \Delta_y n_o}{\hbar^2 d_2 a_o k_B T}\frac{1}{k_1}\sum_{n=-\infty}^{\infty} J_n{}^2(\chi)\left[\frac{1}{1+\left(d_1 eE_o/\hbar + n\omega\hbar\right)^2\tau^2}\right]\left\{\frac{I_1(k_1) I_1(k_2)}{I_o(k_1) I_o(k_2)}\right\}\frac{\nabla_x T}{T} \quad \text{(D19)}$$

Adding all the terms in $\vec{J}_2$

Thus $\vec{J}_2 = \vec{J}_{21} + \vec{J}_{22} + \vec{J}_{23} + \vec{J}_{24} + \vec{J}_{25} + \vec{J}_{26}$

$$\vec{J}_2 = -\frac{e\tau\Delta_x^{\,2} d_1^{\,2} n_o}{2\hbar^2 a_o k_B T}\sum_{n=-\infty}^{\infty} J_n^{\,2}(\chi)\left[\frac{1}{1+\left(d_1 eE_o/\hbar + n\omega\hbar\right)^2\tau^2}\right]\times\left\{(D-\mu)\frac{\nabla_x T}{T}+\nabla_x\mu\right\}$$

$$+\frac{e\tau\Delta_x^{\,2} d_1^{\,2} n_o\Delta_x}{2\hbar^2 a_o k_B T}\sum_{n=-\infty}^{\infty} J_n^{\,2}(\chi)\left[\frac{1}{1+\left(d_1 eE_o/\hbar + n\omega\hbar\right)^2\tau^2}\right]\frac{\nabla T}{T}\frac{I_1(k_1)}{I_o(k_1)}$$

$$+\frac{e\tau\Delta_x^{\,2} d_1^{\,2} n_o}{2\hbar^2 a_o k_B T}\int_0^{\pi} d\theta_2\sum_{n=-\infty}^{\infty} J_n^{\,2}(\chi)\left[\frac{1}{1+\left(d_1 eE_o/\hbar + n\omega\hbar\right)^2\tau^2}\right]\frac{\nabla T}{T}\frac{I_1(k_2)}{I_o(k_2)}$$

$$+\frac{e\tau\Delta_x^{\,2} d_1^{\,2} n_o}{2\hbar^2 a_o k_B T}\times\sum_{n=-\infty}^{\infty} J_n^{\,2}(\chi)\left[\frac{1}{1+\left(d_1 eE_o/\hbar + n\omega\hbar\right)^2\tau^2}\right]\left\{(D-\mu)\frac{\nabla_x T}{T}+\nabla_x\mu\right\}$$

$$-\frac{e\tau\Delta_x^{\,2} d_1^{\,2} n_o}{2\hbar^2 a_o k_B T}\sum_{n=-\infty}^{\infty} J_n^{\,2}(\chi)\left[\frac{1}{1+\left(d_1 eE_o/\hbar + n\omega\hbar\right)^2\tau^2}\right]\left\{(D-\mu)\frac{\nabla_x T}{T}+\nabla_x\mu\right\}\frac{2}{k_1}\frac{I_1(k_1)}{I_o(k_1)}$$

$$-\frac{e\tau\Delta_x^{\,2} d_1^{\,2} n_o\Delta_x}{2\hbar^2 a_o k_B T}\times\sum_{n=-\infty}^{\infty} J_n^{\,2}(\chi)\left[\frac{1}{1+\left(d_1 eE_o/\hbar + n\omega\hbar\right)^2\tau^2}\right]\frac{\nabla_x T}{T}\frac{I_1(k_1)}{I_o(k_1)}$$

$$+\frac{e\tau\Delta_x^{\,2} d_1^{\,2} n_o\Delta_x}{\hbar^2 a_o k_B T}\times\sum_{n=-\infty}^{\infty} J_n^{\,2}(\chi)\left[\frac{1}{1+\left(d_1 eE_o/\hbar + n\omega\hbar\right)^2\tau^2}\right]\frac{\nabla_x T}{T}\frac{1}{k_1}\frac{I_o(k_1)}{I_o(k_1)}$$

$$-\frac{e\tau\Delta_x^{\,2} d_1^{\,2} n_o\Delta_x}{2\hbar^2 a_o k_B T}\times\sum_{n=-\infty}^{\infty} J_n^{\,2}(\chi)\left[\frac{1}{1+\left(d_1 eE_o/\hbar + n\omega\hbar\right)^2\tau^2}\right]\frac{\nabla_x T}{T}\frac{1}{k_1^{\,2}}\frac{I_1(k_1)}{I_o(k_1)}$$

$$-\frac{e\tau\Delta_x^{\,2} d_1\Delta_y n_o}{2\hbar^2 a_o k_B T}\times\sum_{n=-\infty}^{\infty} J_n^{\,2}(\chi)\left[\frac{1}{1+\left(d_1 eE_o/\hbar + n\omega\hbar\right)^2\tau^2}\right]\frac{I_1(k_2)}{I_o(k_2)}\frac{\nabla_x T}{T}$$

$$+\frac{e\tau\Delta_x^{\,2} d_1\Delta_2^{\,2} n_o\Delta_y}{\hbar^2 a_o k_B T k_1}\sum_{n=-\infty}^{\infty} J_n^{\,2}(\chi)\left[\frac{1}{1+\left(d_1 eE_o/\hbar + n\omega\hbar\right)^2\tau^2}\right]\left\{\frac{I_1(k_1)I_1(k_2)}{I_o(k_1)I_o(k_2)}\right\}\frac{\nabla_x T}{T} \qquad \text{(D20)}$$

Simplifying Eqn. (D20) further,

$$\vec{J}_2 = -\frac{e\tau\Delta_x^{\,2} d_1^{\,2} n_o}{\hbar^2 a_o k_B T}\times\sum_{n=-\infty}^{\infty} J_n^{\,2}(\chi)\left[\frac{1}{1+\left(d_1 eE_o/\hbar + n\omega\hbar\right)^2\tau^2}\right]\left\{(D-\mu)\frac{\nabla_x T}{T}+\nabla_x\mu\right\}\frac{2}{k_1}\frac{I_1(k_1)}{I_o(k_1)}$$

$$+\frac{e\tau\Delta_x^{\,2} d_1^{\,2} n_o}{\hbar^2 a_o}\times\sum_{n=-\infty}^{\infty} J_n^{\,2}(\chi)\left[\frac{1}{1+\left(d_1 eE_o/\hbar + n\omega\hbar\right)^2\tau^2}\right]\frac{\nabla_x T}{T}$$

$$-\frac{e\tau\Delta_x^{\,2} d_1^{\,2} n_o}{2\hbar^2 a_o k_1}\times\sum_{n=-\infty}^{\infty} J_n^{\,2}(\chi)\left[\frac{1}{1+\left(d_1 eE_o/\hbar + n\omega\hbar\right)^2\tau^2}\right]\frac{\nabla_x T}{T}\frac{I_1(k_1)}{I_o(k_1)}$$

$$+\frac{e\tau\Delta_x^{\,2} d_1\Delta_2^{\,2} n_o}{\hbar^2 a_o k_B T}\frac{1}{k_1}\times\sum_{n=-\infty}^{\infty} J_n^{\,2}(\chi)\left[\frac{1}{1+\left(d_1 eE_o/\hbar + n\omega\hbar\right)^2\tau^2}\right]\left\{\frac{I_1(k_1)I_1(k_2)}{I_o(k_1)I_o(k_2)}\right\}\frac{\nabla_x T}{T} \qquad \text{(D21)}$$

$$\vec{J}_2 = -\frac{e\tau\Delta_x{}^2 d_1{}^2 n_o}{4D^2\hbar^2 a_o k_B T}\frac{1}{k_1}\sum_{n=-\infty}^{\infty} J_n{}^2(\chi)\left[\frac{1}{1+\left(d_1 eE_o/\hbar+n\omega\hbar\right)^2\tau^2}\right](D-\mu)\frac{\nabla_x T}{T}\frac{I_1(k_1)}{I_o(k_1)}$$
$$-\frac{e\tau\Delta_x{}^2 d_1{}^2 n_o}{\hbar^2 a_o k_B T}\times\sum_{n=-\infty}^{\infty} J_n{}^2(\chi)\left[\frac{1}{1+\left(d_1 eE_o/\hbar+n\omega\hbar\right)^2\tau^2}\right]\left(\frac{1}{k_1}\frac{I_1(k_1)}{I_o(k_1)}\right)\nabla_x\mu$$
$$+\frac{e\tau^{-1}\Delta_x{}^2 d_1{}^2 n_o}{\hbar^2 a_o}\times\sum_{n=-\infty}^{\infty} J_n{}^2(\chi)\left[\frac{1}{1+\left(d_1 eE_o/\hbar+n\omega\hbar\right)^2\tau^2}\right]\frac{\nabla_x T}{T}$$
$$-\frac{e\tau\Delta_x{}^2 d_1{}^2 n_o}{2\hbar^2 a_o k_1}\times\sum_{n=-\infty}^{\infty} J_n{}^2(\chi)\left[\frac{1}{1+\left(d_1 eE_o/\hbar+n\omega\hbar\right)^2\tau^2}\right]\frac{\nabla_x T}{T}\frac{I_1(k_1)}{I_o(k_1)}$$
$$+\frac{e\tau\Delta_x{}^2 d_1\Delta_y n_o}{\hbar^2 a_o k_B T}\frac{1}{k_1}\times\sum_{n=-\infty}^{\infty} J_n{}^2(\chi)\left[\frac{1}{1+\left(d_1 eE_o/\hbar+n\omega\hbar\right)^2\tau^2}\right]\left\{\frac{I_1(k_1)I_1(k_2)}{I_o(k_1)I_o(k_2)}\right\}\frac{\nabla_x T}{T} \quad \text{(D22)}$$

$$\vec{J}_2 = -\frac{e\tau\Delta_x{}^2 d_1{}^2 n_o}{\hbar^2 a_o k_B T}\frac{1}{k_1}[D-\mu]\frac{\nabla_x T}{T}\frac{I_1(k_1)}{I_o(k_1)}\times\sum_{n=-\infty}^{\infty} J_n{}^2(\chi)\left[\frac{1}{1+\left(d_1 eE_o/\hbar+n\omega\hbar\right)^2\tau^2}\right]$$
$$-\frac{e\tau\Delta_x{}^2 d_1{}^2 n_o}{\hbar^2 a_o k_B T}\left(\frac{1}{k_1}\frac{I_1(k_1)}{I_o(k_1)}\right)\nabla_x\mu\times\sum_{n=-\infty}^{\infty} J_n{}^2(\chi)\left[\frac{1}{1+\left(d_1 eE_o/\hbar+n\omega\hbar\right)^2\tau^2}\right]$$
$$+\frac{e\tau\Delta_x^2 d_1{}^2 n_o}{\hbar^2 a_o}\frac{\nabla_x T}{T}\times\sum_{n=-\infty}^{\infty} J_n{}^2(\chi)\left[\frac{1}{1+\left(d_1 eE_o/\hbar+n\omega\hbar\right)^2\tau^2}\right]$$
$$-\frac{e\tau\Delta_x^2 d_1{}^2 n_o}{2\hbar^2 a_o k_1}\frac{I_1(k_1)}{I_o(k_1)}\frac{\nabla_x T}{T}\times\sum_{n=-\infty}^{\infty} J_n{}^2(\chi)\left[\frac{1}{1+\left(d_1 eE_o/\hbar+n\omega\hbar\right)^2\tau^2}\right]$$
$$+\frac{e\tau\Delta_x d_1\Delta_y n_o}{\hbar^2 a_o k_B T}\frac{1}{k_1}\left\{\frac{I_1(k_1)I_1(k_2)}{I_o(k_1)I_o(k_2)}\right\}\frac{\nabla_x T}{T}\times\sum_{n=-\infty}^{\infty} J_n{}^2(\chi)\left[\frac{1}{1+\left(d_1 eE_o/\hbar+n\omega\hbar\right)^2\tau^2}\right] \quad \text{(D23)}$$

$$\vec{J}_2 = -\frac{e\tau\Delta_x d_1{}^2 n_o}{\hbar^2 a_o}[D-\mu]\frac{\nabla_x T}{T}\frac{I_1(k_1)}{I_o(k_1)}\times\sum_{n-\infty}^{\infty} J_n{}^2(\chi)\left[\frac{1}{1+\left(d_1 eE_o/\hbar+n\omega\hbar\right)^2\tau^2}\right]$$
$$-\frac{e\tau\Delta_x d_1{}^2 n_o}{\hbar^2 a_o}\frac{I_1(k_1)}{I_o(k_1)}\nabla_x\mu\sum_{n=-\infty}^{\infty} J_n{}^2(\chi)\left[\frac{1}{1+\left(d_1 eE_o/\hbar+n\omega\hbar\right)^2\tau^2}\right]$$
$$+\frac{e\tau\Delta_x^2 d_1{}^2 n_o}{\hbar^2 a_o}\frac{\nabla_x T}{T}\times\sum_{n=-\infty}^{\infty} J_n{}^2(\chi)\left[\frac{1}{1+\left(d_1 eE_o/\hbar+n\omega\hbar\right)^2\tau^2}\right]$$

$$-\frac{e\tau\Delta_x^2 d_1^{\,2} n_o}{2\hbar^2 a_o}\frac{1}{k_1}\frac{I_1(k_1)}{I_o(k_1)}\frac{\nabla_x T}{T}\times\sum_{n=-\infty}^{\infty}J_n^{\,2}(\chi)\left[\frac{1}{1+\left(d_1eE_o/\hbar+n\omega\hbar\right)^2\tau^2}\right]$$
$$+\frac{e\tau\Delta_x d_1^{\,2} n_o\Delta_y n_o}{\hbar^2 d_2 a_o}\left\{\frac{I_1(k_1)I_1(k_2)}{I_o(k_1)I_o(k_2)}\right\}\frac{\nabla_x T}{T}\times\sum_{n=-\infty}^{\infty}J_n^{\,2}(\chi)\left[\frac{1}{1+\left(d_1eE_o/\hbar+n\omega\hbar\right)^2\tau^2}\right] \quad \text{(D24)}$$

$$\vec{J}_2=-\frac{e\tau\Delta_x d_1^{\,2} n_o}{\hbar^2 a_o}\frac{I_1(k_1)}{I_o(k_1)}\nabla_x\mu\sum_{n=-\infty}^{\infty}J_n^{\,2}(\chi)\left[\frac{1}{1+\left(d_1eE_o/\hbar+n\omega\hbar\right)^2\tau^2}\right]$$
$$-\frac{e\tau\Delta_x d_1^{\,2} n_o}{\hbar^2 a_o}\frac{I_1(k_1)}{I_o(k_1)}\sum_{n=-\infty}^{\infty}J_n^{\,2}(\chi)\left[\frac{1}{1+\left(d_1eE_o/\hbar+n\omega\hbar\right)^2\tau^2}\right]$$
$$\times\left\{\left[D-\mu\right]-\Delta_x\frac{I_o(k_1)}{I_1(k_1)}+\frac{\Delta_x}{2k_1}-\Delta_y\frac{I_1(k_2)}{I_o(k_2)}\right\}\frac{\nabla_x T}{T} \quad \text{(D25)}$$

$$\vec{J}_2=-\frac{e^2\tau\Delta_x d_1^{\,2} n_o}{\hbar^2 a_o}\frac{I_1(k_1)}{I_o(k_1)}\frac{\nabla_x\mu}{e}\sum_{n=-\infty}^{\infty}J_n^{\,2}(\chi)\left[\frac{1}{1+\left(d_1eE_o/\hbar+n\omega\hbar\right)^2\tau^2}\right]$$
$$-\frac{e^2\tau\Delta_1^{\,2} d_1^{\,2} n_o}{\hbar^2 a_o e}\frac{I_1(k_1)}{I_o(k_1)}\sum_{n=-\infty}^{\infty}J_n^{\,2}(\chi)\left[\frac{1}{1+\left(d_1eE_o/\hbar+n\omega\hbar\right)^2\tau^2}\right]$$
$$\times\left\{\left[D-\mu\right]-\Delta_x\frac{I_o(k_1)}{I_1(k_1)}+\frac{\Delta_x}{2k_1}-\Delta_y\frac{I_1(k_2)}{I_o(k_2)}\right\}\frac{\nabla_x T}{T} \quad \text{(D26)}$$

$$J_2=-\frac{e^2\tau\Delta_x d_1^{\,2} n_o}{\hbar^2 a_o}\frac{I_1(k_1)}{I_o(k_1)}\frac{\nabla_x\mu}{e}\sum_{n=-\infty}^{\infty}J_n^{\,2}(\chi)\left[\frac{1}{1+\left(d_1eE_o/\hbar+n\omega\hbar\right)^2\tau^2}\right]$$
$$-\frac{e^2\tau\Delta_x d_1^{\,2} n_o}{\hbar^2 a_o e}\frac{I_1(k_1)}{I_o(k_1)}\sum_{n=-\infty}^{\infty}J_n^{\,2}(\chi)\left[\frac{1}{1+\left(d_1eE_o/\hbar+n\omega\hbar\right)^2\tau^2}\right]$$
$$\times\left\{\left[\frac{D-\mu}{T}\right]-k_1k_BT\frac{I_o(k_1)}{I_1(k_1)T}+\frac{k_1k_BT}{2T}-\frac{k_2k_BT}{T}\frac{I_1(k_2)}{I_o(k_2)}\right\}\nabla_x T \quad \text{(D27)}$$

$$\vec{J}_2=-\frac{e^2\tau\Delta_x d_1^{\,2} n_o}{\hbar^2 a_o}\frac{I_1(k_1)}{I_o(k_1)}\frac{\nabla_x\mu}{e}\sum_{n=-\infty}^{\infty}J_n^{\,2}(\chi)\left[\frac{1}{1+\left(d_1eE_o/\hbar+n\omega\hbar\right)^2\tau^2}\right]$$
$$-\frac{e^2\tau\Delta_1^{\,2} d_1^{\,2} n_o}{\hbar^2 a_o}\frac{I_1(k_1)}{I_o(k_1)}\sum_{n=-\infty}^{\infty}J_n^{\,2}(\chi)\left[\frac{1}{1+\left(d_1eE_o/\hbar+n\omega\hbar\right)^2\tau^2}\right]$$
$$\times\frac{k_B}{e}\left\{\left[\frac{D-\mu}{k_BT}\right]-k_1\frac{I_o(k_1)}{I_1(k_1)}+\frac{1}{2}-k_2\frac{I_1(k_2)}{I_o(k_2)}\right\}\nabla_x T \quad \text{(D28)}$$

$$\vec{J}_2=-\sigma_x(\vec{E})\frac{\nabla_x u}{e}-\sigma_x(\vec{E})\frac{k_B}{e}\left\{\left[\frac{D-u}{k_BT}\right]-k_1\frac{I_o(k_1)}{I_1(k_1)}+\frac{1}{2}-k_2\frac{I_1(k_2)}{I_o(k_2)}\right\}\nabla_x T \quad \text{(D29)}$$

where $\sigma_x(\vec{E})$ is the conductivity. But $\vec{J}_x = \vec{J}_1 + \vec{J}_2$

$$\vec{J}_x = -\sigma_x(\vec{E})\left(\vec{E}_n + \frac{\nabla_x u}{e}\right) - \sigma_x(\vec{E})\frac{k_B}{e}\left\{\left[\frac{D-u}{k_B T}\right] - k_1\frac{I_o(k_1)}{I_1(k_1)} + \frac{1}{2} - k_2\frac{I_1(k_2)}{I_o(k_2)}\right\}\nabla_x T \quad \text{(D30)}$$

$$\vec{J}_x = -\sigma_x(\vec{E})\vec{E}'_{xn} - \sigma_x(\vec{E})\frac{k_B}{e}\left\{\left[\frac{D-u}{k_B T}\right] - k_1\frac{I_o(k_1)}{I_1(k_1)} + \frac{1}{2} - k_2\frac{I_1(k_2)}{I_o(k_2)}\right\}\nabla_x T \quad \text{(D31)}$$

where $\vec{E}'_{xn} = \vec{E}_{xn} + \nabla_x u / e$

The differential thermoelectric power is defined as the ratio $\left|\frac{\vec{E}_{xn}}{\nabla_x T}\right|$ in an open circuit. Thus setting $\vec{J} = 0$ to zero, the thermoelectric power α_x along the x-direction is obtained as follows:

$$0 = -\sigma_x(\vec{E})\vec{E}'_{xn} - \sigma_x(\vec{E})\frac{k_B}{e}\left\{\left[\frac{D-\mu}{k_B T}\right] - k_1\frac{I_o(k_1)}{I_1(k_1)} + \frac{1}{2} - k_2\frac{I_1(k_2)}{I_o(k_2)}\right\}\nabla_x T \quad \text{(D32)}$$

$$\left|\frac{\vec{E}_{xn}}{\nabla_x T}\right| = -\frac{\sigma_x(\vec{E})}{\sigma_x(\vec{E})}\frac{k_B}{e}\left\{\left[\frac{D-\mu}{k_B T}\right] - \frac{\Delta_x}{k_1}\frac{I_o(k_1)}{I_1(k_1)} + \frac{1}{2\Delta_x} - k_2\frac{I_1(k_2)}{I_o(k_2)}\right\} \quad \text{(D33)}$$

$$\alpha_x = \left|\frac{\vec{E}_{xn}}{\nabla_x T}\right| = -\frac{k_B}{e}\left\{\left[\frac{D-\mu}{k_B T}\right] - k_1\frac{I_o(k_1)}{I_1(k_1)} + \frac{1}{2} - k_2\frac{I_1(k_2)}{I_o(k_2)}\right\} \quad \text{(D34)}$$

The electrical power factor along the x-direction is given as:

$$P_x = \alpha_x{}^2\sigma_x \quad \text{(D35)}$$

Substituting the expressions obtained in Eqn. (C11) and (C34) into Eqn. (D35) gives

$$P_x = \alpha_x{}^2\sigma_x = \left\{\left(\frac{k_B}{e}\left[\left(\frac{D-u}{k_B T}\right) - k_1\frac{I_o(k_1)}{I_1(k_1)} + \frac{1}{2} - k_2\frac{I_1(k_2)}{I_o(k_2)}\right]\right)^2 \times \frac{e^2\tau\Delta_x d_1{}^2 n_o}{\hbar^2 a_o}\frac{I_1(k_1)}{I_o(k_1)}\sum_{n=-\infty}^{\infty} J_n{}^2(\chi)\left[\frac{1}{1+\left(d_1 eE_o/\hbar + n\omega\hbar\right)^2\tau^2}\right] \quad \text{(D36)}$$

APPENDIX E

RESISTIVITY AGAINST TEMPERATURE FOR VARYING E_o

```
clc;
clear;
figure;
T=0:1000;              % Temperature range
 e =1;                 % electronic charge in electron volt
Eo=10^7;               % dc field intensity
Ex=10^2;               % ac field intensity
delta=0.013;           % outer shell energy
delta_1=0.010;         % overlapping integrals for jump along x-axis
delta_2=0.024;         % overlapping integrals for jump along y-axis
no=1e13;               % carrier concentration
ao=0.345e-9;           % graphene sheet width
h=6.582e-16;           % reduced Planck's constant in eV
K=8.617e-5;            % Boltzmann's constant in eV
d1=2e-8 ;              % graphene periodicity along x-axis
w=1e14;                % frequency of the field
t=1e-12;               % relaxation time
D=(sqrt(delta^2+delta_1^2+delta_2^2));
m= (K.*T);
k1=delta_1^2./(2.*D.*m);
k2=delta_2^2./(2.*D.*m);

I1=besseli(1,k1);      % modified Bessel's function of order one
Io=besseli(0,k1);      % modified Bessel's function of order zero
W=d1*e*Eo/h;
p=Io./I1;
jo=-(e^2.*delta_1.^2.*d1.^2.*no.*t)./(2*D*h.^2.*ao);
X=(d1.*e.*Ex./h*w);
jb=0;
for n=-10:10
  y1=jb+sum(besselj(n,X).^2).*(W + n.*w*h)./(1+(W + n.*w*h).^2.*t^2);
end
j2=jo.*y1;
y2=1./j2;
ax=(y2).*p;
plot(T,ax,'r','linewidth',2)
title('Resistivity Against T for Varying Eo')
xlabel('Temperature(K)');
ylabel('Resistivity(Ohm m)');
grid on;
hold on;
T=0:1000;
e=1.6e-19;
Eo=2*10^7;
Ex=10^2;
```

```
delta=0.013;
delta_1=0.012;
delta_2=0.024;
no=1e13;
ao=0.345e-9;
h=6.582e-16;
% h=1;
K=8.617e-5;
d1=2e-8 ;
w=1e14;
t=1e-12;
D=(sqrt(delta^2+delta_1^2+delta_2^2));
m= (K.*T);
k1=delta_1^2./(2.*D.*m);
k2=delta_2^2./(2.*D.*m);
I1=besseli(1,k1);
Io=besseli(0,k1);
W=d1*e*Eo/h;
p=Io./I1;
jo=-(e^2.*delta_1.^2.*d1.^2.*no.*t)./(2*D*h.^2.*ao);
X=(d1.*e.*Ex./h*w);
jb=0;
for n=-10:10 y1=jb+sum(besselj(n,X).^2).*(W+n.*w*h)./(1+(W+
n.*w*h).^2.*t^2);
end
y2=jo.*y1;
ax=(1./y2).*p;
plot(T,ax,'g','linewidth',2)
title('Resistivity Against T for Varying Eo')
xlabel('Temperature(K)');
ylabel('Resistivity(Ohm m)');
grid on;
hold on;
T=0:1000;
eV =1.6e-19;
Eo=3*10^7;
Ex=10^2;
delta=0.013;
delta_1=0.012;
delta_2=0.024;
no=1e13;
ao=0.345e-9;
h=6.582e-16;
% h=1;
K=8.617e-5;
d1=2e-8;
w=1e14;
t=1e-12;
D=(sqrt(delta^2+delta_1^2+delta_2^2));
m= (K.*T);
```

```
k1=delta_1^2./(2.*D.*m);
k2=delta_2^2./(2.*D.*m);
I1=besseli(1,k1);
Io=besseli(0,k1);
W=d1*e*Eo/h;
p=Io./I1;
jo=-(e^2.*delta_1.^2.*d1.^2.*no.*t)./(2*D*h.^2.*ao);
X=(d1.*e.*Ex./h*w);
jb=0;
for n=-10:10y1=jb+sum(besselj(n,X).^2).*(W + n.*w*h)./(1+(W + n.*w*h).^2.*t^2);
end
y2=jo.*y1;
ax=(1./y2).*p;
plot(T,ax,'b','linewidth',2)
% title('Resistivity Against T for Varying Eo')
xlabel('Temperature(K)');
ylabel('Resistivity \rho_{x}(\Omega {m})');
% grid on;
hold on;
T=0:1000;
eV =1.6e-19;
Eo=4*10^7;
Ex=10^2;
delta=0.013;
delta_1=0.012;
delta_2=0.024;
no=1e13;
ao=0.345e-9;
h=6.582e-16;
% h=1;
K=8.617e-5;
d1=2e-8 ;wt=0.1;
w=1e14;
t=1e-12;
D=(sqrt(delta^2+delta_1^2+delta_2^2));
m= (K.*T);
k1=delta_1^2./(2.*D.*m);
k2=delta_2^2./(2.*D.*m);
I1=besseli(1,k1);
Io=besseli(0,k1);
W=d1*e*Eo/h;
p=Io./I1;
jo=-(e^2.*delta_1.^2.*d1.^2.*no.*t)./(2*D*h.^2.*ao);
X=(d1.*e.*Ex./h*w);
jb=0;
for n=-10:10
  y1=jb+sum(besselj(n,X).^2).*(W + n.*w*h)./(1+(W + n.*w*h).^2.*t^2);
end
y2=jo.*y1;
```

```
ax=(1./y2).*p;
plot(T,ax,'b','linewidth',2)
% title('Resistivity Against T for Varying Eo')
xlabel('Temperature(K)');
ylabel('Resistivity \rho_{x}(\Omega {m})');
% grid on;
hold on;
legend('1E_{o}V/m','2E_{o}V/m','3E_{o}V/m', '4E_{o} V/m','location','best')
set(gca, 'Fontsize',14,'linewidth',1.5)
box on
% grid on
hold on
title('')
grid off
```

APPENDIX F

THERMOPOWER AGAINST TEMPERATURE FOR VARYING Δ_1

```
clear;
clc;
figure;
T=(0:1000);
meu=1;          % electrochemical potential in electron volt
delta=0.013; delta_1=0.010;
delta_2=0.0240;
D=(sqrt(delta^2+delta_1^2+delta_2^2));
m1=K.*T;
m2=K./e;
k1=delta_1^2./(2*D.*m1);
k2=delta_2^2./(2*D.*m1);Io=besseli(0,k1); % Bessel's function of zero order
I1=besseli(1,k1); % Bessel's function of first order
p=Io./I1;
y1=besseli(1,k2);
y2=besseli(0,k2);
y=y1./y2;
q=(D-meu)./m1; q2=2.*D.*p.*k1./delta_1^2; q3=D./delta_1^2;q4=k2.*y;
ax=m2.*(q+q3);
plot(T,ax,'r','Linewidth',2)
xlabel('Temperature(K)');
ylabel('a_{zz}(V/K)');
hold on
T=0:1000;
meu=1;
delta=0.013; delta_1=0.012;
delta_2=0.024;
D=(sqrt(delta^2+delta_1^2+delta_2^2));
m1=K.*T;
m2=K./e;
k1=delta_1^2./(2*D.*m1);
k2=delta_2^2./(2*D.*m1);
Io=besseli(0,k1); % Bessel's function of zero order
I1=besseli(1,k1); % Bessel's function of first order
p=Io./I1;
y1=besseli(1,k2);
y2=besseli(0,k2);
y=y1./y2;
q=(D-meu)./m1; q2=2.*D.*p.*k1./delta_1^2; q3=D./delta_1^2;q4=k2.*y;
ax=m2.*(q+q3);
plot(T,ax,'b','Linewidth',2)
xlabel('Temperature(K)');
ylabel('a_{zz}(V/K)');
%title('Temopower against Temperature')
% % grid on
```

```
hold on
T=0:1000;
meu=1;
delta=0.013; delta_1=0.014;
delta_2=0.024;
D=(sqrt(delta^2+delta_1^2+delta_2^2));
m1=K.*T;
m2=K./e;
k1=delta_1^2./(2*D.*m1);
k2=delta_2^2./(2*D.*m1);
Io=besseli(0,k1); % Bessel's function of zero order
I1=besseli(1,k1); % Bessel's function of first order
p=Io./I1;
y1=besseli(1,k2);
y2=besseli(0,k2);
y=y1./y2;
q=(D-meu)./m1; q2=2.*D.*p.*k1./delta_1^2; q3=D./delta_1^2;q4=k2.*y;
ax=m2.*(q+q3);
plot(T,ax,'k','Linewidth',2)
xlabel('Temperature(K)');
ylabel('a_{zz}(V/K)');
%title('Temopower against Temperature')
% % grid on
hold on
T=0:1000;
meu=1;
delta=0.013; delta_1=0.016;
delta_2=0.024;
D=(sqrt(delta^2+delta_1^2+delta_2^2));
m1=K.*T;
m2=K./e;
k1=delta_1^2./(2*D.*m1);
k2=delta_2^2./(2*D.*m1);
Io=besseli(0,k1); % Bessel's function of zero order
I1=besseli(1,k1); % Bessel's function of first order
p=Io./I1;
y1=besseli(1,k2);
y2=besseli(0,k2);
y=y1./y2;
q=(D-meu)./m1; q2=2.*D.*p.*k1./delta_1^2; q3=D./delta_1^2;q4=k2.*y;
ax=m2.*(q+q3);
plot(T,ax,'g','Linewidth',2)
axis([-10 1000 -0.4 0.8])
xlabel('Temperature(K)');
ylabel('a_{x}(V/K)');
title('Temopower against Temperature')
% % grid on
% title('Thermopower vs Temperature for varrying delta1')
set(gca, 'Fontsize',14,'linewidth',1.5)
box on
```

```
% grid on
hold on
legend('\Delta{1}=0.010','\Delta{1}=0.012','\Delta{1}=0.014','\Delta{1}=0.016','location','best')
legend({'\Delta_{1}= 0.010 eV','\Delta_{1}= 0.012 eV','\Delta_{1}= 0.014 eV','\Delta_{1}= 0.016 eV'})
title('')
```

APPENDIX G

POWER FACTOR AGAINST TEMPERATURE FOR VARYING E_o

```
clc;
clear;
figure;
T=0:1:1000;
e=1; meu=1;
Eo=10^7;
Ex=10^2;
delta=0.13;
delta_1=0.012;
delta_2=0.024;
no=1e13;
ao=0.345e-9;
h=6.52e-16;
K=8.617e-5;
d1=2e-8;
w=1e14;
t=1e-12;
D=(sqrt(delta^2+delta_1^2+delta_2^2));
m= (K.*T);
k1=delta_1^2./(2.*D.*m);
k2=delta_2^2./(2.*D.*m);
I1=besseli(1,k1);
Io=besseli(0,k1);
p=I1./Io;
y1=besseli(1,k2);
yo=besseli(0,k2);
y=y1./yo;
W=d1*e*Eo/h;
X=(d1.*e.*Ex./h*w);
jo=(e^2.*delta_1.^2.*d1.^2.*no.*t)./(2.*D.*h.^2.*ao);
jb=0;
for n=-10:10Y=jb+sum(besselj(n,X).^2).*(W + n.*w*h)./(1+(W + n.*w*h).^2.*t^2);
end
Y2=-jo.*Y.*p;
ax=Y2;
m2=K./e;
q=(D-meu)./m; q2=2.*D.*p.*k1./delta_1^2; q3=D./delta_1^2;q4=k2.*y;
a=(-m2.*(q-q2+q3-q4)).^2;
px=a.*ax;
plot(T,(px)./10e2,'r','Linewidth',2);
xlabel('Temperature(K)');
ylabel('power factor(W/K)');
title('power factor against temperature');
hold on
```

```
%%
T=0:1:1000;
e=1; meu=1;
Eo=2*10^7;
Ex=10^2;
delta=0.13;
delta_1=0.012;
delta_2=0.024;
no=1e13;
ao=0.345e-9;
h=6.52e-16;
K=8.617e-5;
d1=2e-8;
w=1e14;
t=1e-12;
D=(sqrt(delta^2+delta_1^2+delta_2^2));
m= (K.*T);
k1=delta_1^2./(2.*D.*m);
k2=delta_2^2./(2.*D.*m);
I1=besseli(1,k1);
Io=besseli(0,k1);
p=I1./Io;
y1=besseli(1,k2);
yo=besseli(0,k2);
y=y1./yo;
W=d1*e*Eo/h;
X=(d1.*e.*Ex./h*w);
jo=(e^2.*delta_1.^2.*d1.^2.*no.*t)./(2.*D.*h.^2.*ao);
jb=0;
for n=-10:10
  Y=jb+sum(besselj(n,X).^2).*(W + n.*w*h)./(1+(W + n.*w*h).^2.*t^2);
end
Y2=-jo.*Y.*p;
ax=Y2;
m2=K./e;
q=(D-meu)./m; q2=2.*D.*p.*k1./delta_1^2; q3=D./delta_1^2;q4=k2.*y;
a=(-m2.*(q-q2+q3-q4)).^2;
px=a.*ax;
plot(T,(px)./10e2,'b','Linewidth',2);
xlabel('Temperature(K)');
ylabel('power factor(W/K)');
title('power factor against temperature');
hold on

T=15:1:1000;
eV =1.6e-19; e=1; meu=1;
Eo=3*10^7;
Ex=10^2;
delta=0.13;
delta_1=0.012;
```

```
delta_2=0.024;
no=1e13;
ao=0.345e-9;
h=6.52e-16;
K=8.617e-5;
d1=2e-8;
w=1e14;
t=1e-12;
D=(sqrt(delta^2+delta_1^2+delta_2^2));
m= (K.*T);
k1=delta_1^2./(2.*D.*m);
k2=delta_2^2./(2.*D.*m);
I1=besseli(1,k1);
Io=besseli(0,k1);
p=I1./Io;
y1=besseli(1,k2);
yo=besseli(0,k2);
y=y1./yo;
W=d1*e*Eo/h;
X=(d1.*e.*Ex./h*w);
jo=(e^2.*delta_1.^2.*d1.^2.*no.*t)./(2.*D.*h.^2.*ao);
jb=0;
for n=-10:10

  Y=jb+sum(besselj(n,X).^2).*(W + n.*w*h)./(1+(W + n.*w*h).^2.*t^2);
end
Y2=-jo.*Y.*p;
ax=Y2;
m2=K./e;
q=(D-meu)./m; q2=2.*D.*p.*k1./delta_1^2; q3=D./delta_1^2;q4=k2.*y;
a=(-m2.*(q-q2+q3-q4)).^2;
px=a.*ax;
plot(T,(px)./10e2,'k','Linewidth',2);
xlabel('Temperature(K)');
ylabel('power factor \P_{x}(W/K)');
title('power factor against temperature');
hold on

T=0:1:1000;
eV =1.6e-19; e=-1; meu=1;
Eo=4*10^7;
Ex=10^2;
delta=0.13;
delta_1=0.012;
delta_2=0.024;
no=1e13;
ao=0.345e-9;
h=6.52e-16;
% h=1;
K=8.617e-5;
```

```
d1=2e-8;
w=1e14;
t=1e-12;
D=(sqrt(delta^2+delta_1^2+delta_2^2));
m= (K.*T);
k1=delta_1^2./(2.*D.*m);
k2=delta_2^2./(2.*D.*m);
I1=besseli(1,k1);
Io=besseli(0,k1);
p=I1./Io;
y1=besseli(1,k2);
yo=besseli(0,k2);
y=y1./yo;
W=d1*e*Eo/h;
X=(d1.*e.*Ex./h*w);
jo=(e^2.*delta_1.^2.*d1.^2.*no.*t)./(2.*D.*h.^2.*ao);
jb=0;
for n=-10:10 Y=jb+sum(besselj(n,X).^2).*(W + n.*w*h)./(1+(W +
n.*w*h).^2.*t^2);
end
Y2=-jo.*Y.*p;
ax=Y2;
m2=K./e;
q=(D-meu)./m; q2=2.*D.*p.*k1./delta_1^2; q3=D./delta_1^2;q4=k2.*y;
a=(-m2.*(q-q2+q3-q4)).^2;
px=a.*ax;
plot(T,(px)./10e2,'g','Linewidth',2);
xlabel('Temperature(K)');
ylabel('Power factor, P_{x} (W/K)');
title('power factor against temperature for varying delta1');
hold on
legend('E_{o} V/m','2E_{o} V/m','3E_{o} V/m','4E_{o} V/m','location','best')
set(gca, 'Fontsize',14,'linewidth',1.5)
box on
% grid on
hold on
 title('')
  grid off
```